# FINAL REPORT

## Acoustic Response of Underwater Munitions near a Sediment Interface: Measurement Model Comparisons and Classification Schemes

SERDP Project MR-2231

APRIL 2015

Steven Kargl
**University of Washington**



SERDP
DOD ▪ EPA ▪ DOE

# REPORT DOCUMENTATION PAGE

*Form Approved*
*OMB No. 0704-0188*



PLEASE DO NOT RETURN YOUR FORM TO THE ABOVE ADDRESS.

| 1. REPORT DATE *(DD-MM-YYYY)* | 2. REPORT TYPE | 3. DATES COVERED *(From - To)* |
|---|---|---|
| 23042015 | Final | 02/01/2012 - 05/01/2015 |

**4. TITLE AND SUBTITLE**

Acoustic Response of Underwater Munitions near a Sediment Interface: Measurement Model Comparisons and Classification Schemes

**5a. CONTRACT NUMBER**

W912HQ-12-C-0016

**5b. GRANT NUMBER**

**5c. PROGRAM ELEMENT NUMBER**

**6. AUTHOR(S)**

Kargl, Steven G. , Applied Physics Laboratory, University of Washington

**5d. PROJECT NUMBER**

MR-2231

**5e. TASK NUMBER**

**5f. WORK UNIT NUMBER**

**7. PERFORMING ORGANIZATION NAME(S) AND ADDRESS(ES)**

Applied Physics Laboratory, University of Washington
1013 NE 45th Street
Seattle, WA 98105-6698

**8. PERFORMING ORGANIZATION REPORT NUMBER**

**9. SPONSORING/MONITORING AGENCY NAME(S) AND ADDRESS(ES)**

SERDP Program Office
Dr. Herb Nelson
4800 Mark Center Drive, Suite 17D08
Arlington, VA 22350-3605

**10. SPONSOR/MONITOR'S ACRONYM(S)**

SERDP

**11. SPONSOR/MONITOR'S REPORT NUMBER(S)**

**12. DISTRIBUTION/AVAILABILITY STATEMENT**

Distribution A: Approved for public release; distribution is unlimited

**13. SUPPLEMENTARY NOTES**

**14. ABSTRACT**

The overall objective is to investigate the use of broadband sonar in the detection, classification, and identification of underwater munitions near a water-sediment interface. The proposed research extends a previous effort (SERDP Project MR-1665) that measured acoustic responses from a collection of underwater targets in a fresh-water pond with a flat sandy bottom and compared some of those measurements to finite-element model predictions. This research effort will collect additional acoustic data from an extended inventory of targets in an oceanic environment and a brackish bay with a mud bottom. Data-model comparisons then will form the basis of classification schemes to discriminate targets from nearby clutter. A central hypothesis is that the environment and the geometry within that environment can alter an acoustic response of a target, so the target-in-the-environment must be taken into account during the development of robust detection, classification, and identification strategies.

**15. SUBJECT TERMS**

Synthetic aperture sonar (SAS), Acoustic template, finite-element (FE) models, UXO

| 16. SECURITY CLASSIFICATION OF: | | | 17. LIMITATION OF ABSTRACT | 18. NUMBER OF PAGES | 19a. NAME OF RESPONSIBLE PERSON |
|---|---|---|---|---|---|
| a. REPORT | b. ABSTRACT | c. THIS PAGE | | | Steven G. Kargl |
| U | U | U | SAR | 109 | 19b. TELEPHONE NUMBER *(Include area code)* 206-685-4677 |

## Table of Contents

## List of Figures

## List of Tables

## Acronyms

| | |
|---|---|
| ADAS | Acoustic data acquisition system |
| APL-UW | Applied Physics Laboratory, University of Washington |
| AUC | Area under the curve |
| BAYEX14 | Bay Experiment 2014 |
| DoD | Department of Defense |
| DOF | Degrees of freedom |
| FE | Finite-element |
| GULFEX12 | Gulf Experiment 2012 |
| HF | High frequency |
| LFM | Linear frequency modulated |
| LF | Low frequency |
| MCS | Motor control system |
| MSO | Marine Species Observer |
| NSWC PCD | Naval Surface Warfare Center, Panama City Division |
| ONR | Office of Naval Research |
| PCB | Pulse-compressed and baseband |
| PC SWAT | Personal Computer Shallow Water Acoustic Toolset |
| PondEx09 | Pond Experiment 2009 |
| PondEx10 | Pond Experiment 2010 |
| ROC | Receiver operating characteristic |
| RVM | Relevance vector machine |
| SAD | Synthetic aperture deconvolution |
| SAS | Synthetic aperture sonar |
| SAX04 | Sediment Acoustic Experiment 2004 |
| TF# | Target field configuration # (where # is 1–6). |
| TIER | Target-in-the-environment-response |
| TREX13 | Target and Reverberation Experiment 2013 |
| TS | Target strength |
| UNOLS | University-National Oceanographic Laboratory System |
| UXO | Unexploded ordnance |
| VMEbus | Versa Module Europa bus |

# Abstract

*Objective:* The overall objective of SERDP MR-2231 is to investigate the use of broadband sonar to detect and classify underwater munitions near a water–sediment interface. The research combined at-sea experiments, target scattering models, and the signal processing required to test binary classification (i.e., target versus non-target). Data–model comparisons provided validation of finite-element (FE) models. Once validated, FE models are executed to obtain free-field scattering amplitudes, which are used by an acoustic ray model to investigate variations in target scattering geometry and environmental properties. Our central hypothesis is that the environment and the geometry within that environment can alter an acoustic response of a target, so the target-in-the-environment-response (TIER) must be taken into account during the development of robust detection and classification strategies.

*Technical Approach:* Until data from at-sea experiments became available, model validation and our efforts in classification leveraged data collected during SERDP MR-1665. Under that effort, scattered acoustic signals were collected from a small set of targets in a freshwater pond with a flattened sand sediment. Some of those measurements were used to validate our FE models. Three at-sea experiments provided additional data from an extended inventory of targets in an oceanic environment with a sand sediment and a brackish bay with a mud layer over sand. The targets included inert unexploded ordnance (UXO), reference targets with well-understood TIER (e.g., a finite cylinder), and a few clutter items (e.g., rocks of comparable size to the UXO and scuba tanks). The first two experiments were conducted in the Gulf of Mexico during 2012 and 2013, and the third experiment was performed in St. Andrew's Bay (Panama City, FL) during 2014. The complexity of the environmental conditions offered by these sites is expected to span conditions in which UXO and munitions are found. Broadband sources and receivers, scanned along a straight rail system, were used to collect scattered acoustic signals suitable for synthetic aperture sonar (SAS) processing and generation of acoustic color templates (i.e., target strength as a function of a target-centered aspect angle and frequency).

The primary frequency band was ~1–30 kHz, but a higher frequency band of ~100–200 kHz was also used during the bay experiment. Targets were placed at horizontal ranges of 5–50 m from the APL-UW rail system. Depending on sediment type and diver manipulations, the burial state of a target could be proud (i.e., on the water–sediment interface), partially buried, or fully buried. To model the interaction of sound with targets and their local environment, FE models were constructed and exercised. Comparisons of FE model predictions with at-sea data provided additional validation, and demonstrated that research carried out under SERDP MR-1665 could be transferred from a pristine pond environment to the ocean.

*Benefits:* This research provided acoustic data on a set of underwater targets under various environmental conditions. These data are the ground truth in the construction of FE models. Once validated, the FE models were exercised to determine free-field scattering amplitudes, which are required by a fast ray model. The combined FE+ray model can provide a cost savings by reducing the number and/or duration of field tests. By providing a capability to simulate sonar performance, SERDP can make informed decisions on the relative merits of existing sonar systems and on proposed modifications to these systems for underwater UXO management.

# I. Background

Although the practice of disposing conventional and chemical munitions in coastal waters was discontinued during the 1970s, the environmental, economical, and even the recreational impact persists [1]. In Overfield and Symons' overview of the Resources and Undersea Threats (RUST) database, they note that over 2100 underwater sites are likely to contain shipwrecks, munitions dumpsites, and radiological waste as well as abandoned pipelines and wellheads [2]. Of those 2100 sites, verification has been completed on only slightly more than 50% with contemporary records (i.e., not through physical survey or assessment). Although not all sites listed in the RUST database contain discarded munitions, the database also may not contain a comprehensive list of current and former DoD training facilities. In any event, there is a clear need for cost-effective physical surveys of possible underwater munitions sites. Schwartz and Brandenburg summarize the current technologies available for underwater UXO applications [3]. Their Table 1 includes metal detection (e.g., magnetometers and electromagnetic induction), chemical sensors (e.g., spectroscopy and fluorescence), and sonar. Metal detection and chemical sensors are typically restricted to short ranges, while the sonar technologies considered are limited in range (e.g., Didson system) or are limited by poor penetration into sediments due to the high frequencies used (e.g., side-scan sonar). Furthermore, Schwartz and Brandenburg note that SAS is still a relatively new technology in UXO detection and that low-frequency SAS systems have demonstrated detection of proud and partially buried objects [4].

Low-frequency SAS systems with a wide bandwidth have several advantages over higher frequency sonar systems. Low frequencies offer greater detection ranges, which permits the rapid surveying of wider areas. In addition, low frequencies attain greater penetration depths into sediments, which allows the detection of partially and completely buried munitions. The range resolution of a SAS system is related to the bandwidth of the transmitted signal, where a wider bandwidth provides higher resolution. Thus, we report here our research on UXO detection and discrimination by a low-frequency wide-bandwidth SAS system.

Our work compliments that of Bucaro et al. [4, 5] and Waters et al. [6] in that they consider isolated UXO in their research. Under SERDP MR-1665, our quick-look experiments conducted during Pond Experiment 2009 (PondEx09) deployed isolated targets, while the experiments during Pond Experiment 2010 (PondEx10) had multiple objects in the field of view of the SAS system with a minimum separation distance approaching ~1.5 m [7]. The techniques developed to isolate the scattering from individual targets allow the deployment of a large collection of targets in our at-sea experiments. This report describes the experiments, data collected, and data processing techniques, and compares model predictions to the field data and investigates a binary classification scheme.

The results of this research can be incorporated into sonar simulation software and can be used to develop and test computer-aided detection and classification software for a sonar designed to search for UXO. Factors that need to be studied are sediment attenuation and dispersion, sediment heterogeneity, sources of variations in target acoustic response (e.g., target or environment induced), and how variations in the acoustic response of a given target affect classification. Our goal is to assess the significance of some of these factors by exercising validated and quantitatively predictive scattering models that include these factors and comparing the predictions to field measurements from a large collection of objects.

A series of monostatic acoustic scattering measurements were conducted to investigate discrimination and classification capabilities based on the acoustic response of targets for UXO remediation. The measurements utilized a straight rail system with a mobile sonar tower. The tower is instrumented with sources and receivers that cover the 1–30 and 100–200 kHz frequency bands, where an emphasis has been placed on the lower band. For PondEx10, 11 targets were deployed at horizontal ranges 5 m and 10 m from the rail. For the at-sea experiments carried out under this effort, up to 30 objects were deployed at various horizontal ranges 5–50 m from the rail. Acoustic data were processed using both time and frequency-domain SAS techniques, and the data were further processed to generate acoustic color templates for the target strength as a function of frequency and target-centered aspect angle. After applying processing techniques to isolate the acoustic response of individual targets, the isolated signals are used in a binary classification study, where we attempt to separate the objects into target versus non-target categories.

## II. Materials and Methods

Three at-sea experiments were performed under SERDP MR-2231: Gulf Experiment 2012 (GULFEX12), Target and Reverberation Experiment 2013 (TREX13), and Bay Experiment 2014 (BAYEX14). GULFEX12 and TREX13 were multi-institutional efforts, which included target scattering and reverberation components. SERDP MR-2231 (this effort), SERDP MR-2232 under NSWC PCD, and a mine countermeasure (MCM) program funded by ONR formed the target scattering component. APL-UW and NSWC PCD were responsible for the target scattering component of these experiments. Researchers from APL-UW and other organizations performed environmental and reverberation measurements. BAYEX14 was solely a target scattering experiment funded jointly by SERDP and ONR, where the experiment was again carried out by APL-UW and NSWC PCD. The target scattering experiments have the general structure of pre-experiment planning and maintenance, mobilization, on-site experiment, and demobilization. In addition, the experimental protocol implemented during GULFEX12 was followed in TREX13 and BAYEX14, where refinements to the experimental protocol were made as knowledge was gained from previous measurements.

### A. Gulf Experiment 2012

The research plan for the target scattering component of GULFEX12 followed the technical approach and methods of Kargl et al. [7, 8] used in PondEx09 and PondEx10 under SERDP MR-1665. SAS data were collected with the APL-UW tower-rail system, where several inert UXO, scientific targets, and clutter items were deployed in the littoral waters southeast of Panama City, FL. Prior to the start of SERDP MR-2231, two acoustic sources from NSWC PCD were integrated onto the APL-UW sonar tower under an ONR-funded MCM program. The two new transducers cover the 1–10 and 10–50-kHz frequency bands. During the 16-day at-sea engineering field test (16 April–2 May 2012), only the NSWC PCD 10–50-kHz source and the APL-UW 1–30-kHz source were used. Although the frequency bands of these sources have a large overlap, the larger frequency band of the NSWC PCD transducer gives nominally 40 kHz of bandwidth. For SAS processing, the bandwidth of an acoustic signal determines the horizontal range resolution, where the horizontal range is measured perpendicular to path of the SAS platform (i.e., perpendicular to the APL-UW rail). Although GULFEX12 was primarily an engineering field test of the newly integrated system and experimental protocols in preparation

for TREX13, the testing offered an opportunity to collect additional data from a set of UXO, scientific targets, and clutter items.

Extensive planning for GULFEX12 occurred prior to the start of SERDP MR-2231 under an ONR-funded MCM program [e.g., logistics, reserving the R/V *Sharp* (a UNOLS vessel), and maintenance of equipment]. This planning is not reviewed here. The mobilization stage occurred during 7–18 April 2012, and included the following tasks:

- Unpack shipped equipment and retrieve equipment stored at NSWC PCD at the completion of PondEx10
- Build up and perform routine maintenance of structures to be deployed (e.g., rail sections, tower, and target alignment frames)
- Deploy anchors for the four-point moor and three rail sections
- Transfer equipment from the NSWC PCD dock to the experiment site using R/V *Sharp* (three deployments).
- Build up laboratory equipment, test electronics dock-side, and stow equipment aboard the R/V *Sharp*

In addition to these tasks, all APL-UW personnel took Marine Species Observer (MSO) training and received certification. MSO training was required by the environmental assessment statement for transmitting sound in the open ocean.

The on-site experiment stage spanned 18–30 April 2012. On the morning of 18 April 2012, the R/V *Sharp* went into a four-point moor to provide a stable platform for diver operations, which were required to deploy equipment and manipulate targets. The APL-UW tower–rail system was deployed on 20 April 2012. The rail consists of three 7-m sections, which divers leveled and joined into a single 21-m rail. The tower with the subsurface STMS-2 electronics package was then lowered over the side of the R/V *Sharp* and placed by divers onto the rail. The divers then surveyed and laid a grid of light-weight cord to mark lines parallel to the rail at 5, 10, 15, 20, and 40-m horizontal ranges. Once the grid was in place, a solid 2:1 aluminum cylinder (2-ft long and 1-ft diameter) was placed at the 10-m horizontal range and centered on the rail. SAS data were collected from the cylinder in a broadside orientation. Linear frequency-modulated (LFM) pulses were transmitted from the two sources. Sequence 0 corresponds to a transmission from the NSWC PCD 10–50-kHz source, and sequence 1 is a transmission from the APL-UW 1–30-kHz source. A sequence is the set of pings that are collected during one run of the tower along the rail (~750 individual pings). A SAS image was formed from sequence 1 and compared to historic SAS images collected during PondEx10. This initial image provided immediate feedback on whether the APL-UW tower–rail was performing as expected. The divers then deployed target configuration 1 (see Appendix A), consisting of eight targets at ranges of 10, 15, 20, and 40 m. Collection of SAS data from target configuration 1 was then initiated. A major weather event was expected to occur during 22–23 April 2012, so the R/V *Sharp* left the four-point moor on the afternoon of 21 April 2012 and returned to the dock. Inspection of SAS images generated from sequences 6–10 (Table A1) revealed potential problems in the hardware modifications or in the experimental protocol.

The R/V *Sharp* returned to the four-point moor on 24 April 2012. Dive operations commenced with the deployment of five additional target configurations (Appendix A). The final target

configuration contained 14 targets, and is referred to as target configuration 6. The targets included 155-mm howitzer shells proud on the surface or embedded in the surface at an oblique angle with the nose buried and its tail up in the water, a 105-mm UXO with a bullet shape, 105-mm UXO with fins, a Mark 82 500-lb bomb (MK82), a diver evaluation unit (DEU), a solid 2:1 aluminum cylinder, and solid aluminum replicas of a 100-mm UXO. The 100-mm UXO was deployed during PondEx09 and PondEx10. Dive operations were conducted to rotate the targets through a set of angles with respect to the APL-UW rail. A total of 114 sequences were collected. Appendix A contains illustrations of the target configurations (Figs. A1–A3). Tables A1–A7 contain specific information for each recorded sequence. In these tables, the "+" direction denotes a movement of the APL-UW tower from west-to-east while the "–" direction is east-to-west. If a direction is not indicated, the tower remained stationary. The third column lists the depression angle for the tilt of the sources and receivers. This angle then corresponds to the incident grazing angle for the acoustic axes of the transducers. The columns labeled by 5, 7, 10, 15, and 20 m are the horizontal ranges to deployed targets, and the listed angle is a rotation angle. Rotation angles are in a clockwise direction when looking down on the target with north at 90º and south at –90º. The final column is a comment concerning the specific sequence.

The final demobilization stage occurred during 1–5 May 2012. Demobilization included the retrieval of deployed equipment and targets, the breakdown of equipment, and packing of equipment for shipment to APL-UW or storage at NSWC PCD.

Inspection of SAS images created from data collected during GulfEx12 revealed two major issues. First, many of the SAS images showed "ghost images" of targets, where the "ghost images" were always to the same side and displaced by roughly the same distance from the true target images. Second, the presence of fish schools caused a degradation in the transmitted and received signals. Each issue is discussed below, and the recommended modification to the original experimental protocol is described.

The "ghost images" appeared when the APL-UW source transmitted the 1–30-kHz LFM chirp. This source is a four-element linear array, where active elements depend on the frequency band such that the horizontal beamwidth of the projected sound is maintained across the frequency band. Figure 1 shows SAS images constructed from sequence 49 for (a) the 2:1 aluminum cylinder and (b) a 155-mm howitzer shell. For the aluminum cylinder, the "ghost image" is the feature that appears between 12.5 and 13.5 m in cross range, while the "ghost images" for the howitzer shell appears near 13 m in cross range. The lower panels in Fig. 1(c, d) were created from sequence 518, and clearly show that once the cause of the "ghost images" was identified, the "ghost images" were removed. Several possible causes of the "ghost images" were investigated including misconfigured array cabling, damage to the array, and problems with the cables, electronics, and water leaks.

Initial speculation was that the "ghost images" may be related to misconfigured array cabling or damage to the APL-UW source. Oscilloscope traces of the input signals and output signals of the four power amplifiers that drive the individual elements of the array were inspected. The duration and phases of the input signals and amplifier outputs were as expected, and no discernible distortions were observed. The ~1 m offset of the "ghost images" corresponds to a ~0.6 ms delay, so if the source projected a second, delayed LFM chirp, then the output signals should be distorted. In addition, the "ghost images" would appear shifted in the horizontal

direction whereas the shift is observed to be in the cross-range direction. It was also determined that the electronics involved in the signal generation functioned correctly. Next, the tower was positioned on the rail to align the solid 2:1 aluminum cylinder on the acoustic axis of the source. The signal generation was configured to transmit a 0.5–15-kHz LFM chirp from only a single element at a time and the scattered signal recorded. The recorded signals revealed that the transmitted signals had the proper phase and that each element was functioning properly. Thus, it was determined that the signal generation and source were not the cause of the "ghost images."

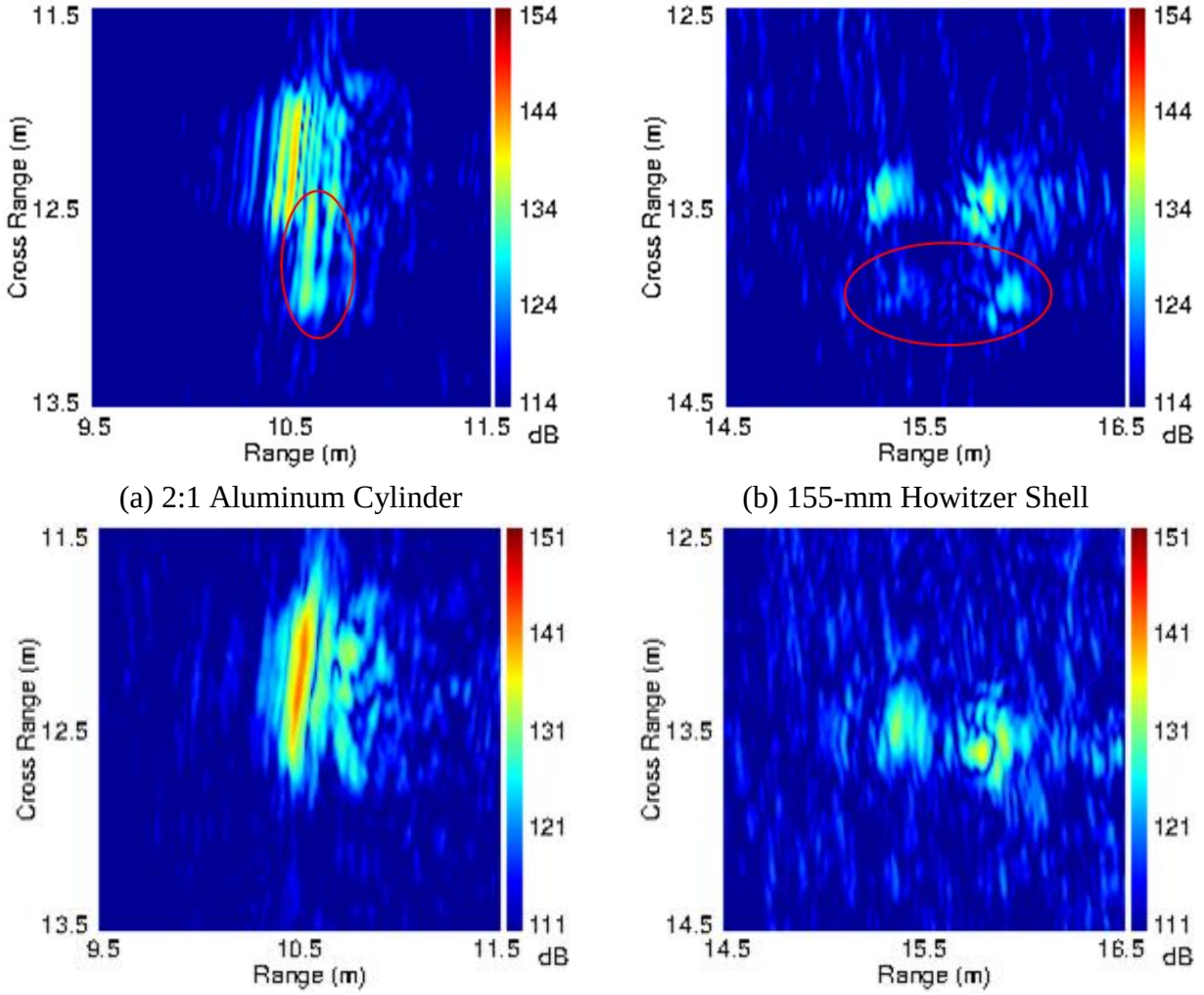


(a) 2:1 Aluminum Cylinder (b) 155-mm Howitzer Shell

(c) 2:1 Aluminum Cylinder (d) 155-mm Howitzer Shell

Figure 1. *SAS images produced from GULFEX12 sequences 49 (top row) and 518 (bottom row). The "ghost image" appears below the true image and is enclosed in a red oval. Once the cause of the "ghost image" was identified, SAS images show no "ghost images" in (c) and (d).*

For TREX13, the planned deployment called for a 42-m long rail. This required 100-m long cable extensions to accommodate a full-length SAS run along the rail. The cable extensions were new and the underwater junction box had not been used since 2004. The extension cables and junction box were inserted for testing during GULFEX12. With the increased cable lengths and junction box, the underwater STMS-2 electronics experience increased electrical cable

impedance at its input connectors. This may cause a portion of an applied signal to reflect within the cable, and feedback into the power amplifier. The cable extensions and junction box were removed such that the cabling to the STMS-2 electronics was identical to the cabling used in PondEx09 and PondEx10. The "ghost images" were still observed. The cables and connectors were inspected visually for damage and tested for electrical conductance. The cables were found to be in good condition, and thus likely not related to the "ghost images." In addition, the cables have waterproof underwater-mateable connectors. The connectors were reseated at the junction box and at the underwater STMS-2 electronics to ensure proper connections. The underwater STMS-2 electronics is equipped with leak detectors; these were monitored throughout the deployment and no leaks were detected. Thus, the cables and underwater electronics were no longer suspected of causing the "ghost images."

The cables from the STMS-2 electronics package to the shipboard electronics are collected into two vinyl sleeves near the tower. These sleeves organize the cables and are intended to prevent tangling and damage due to abrasion as the cables drag across the sea floor. It was proposed that as the cables dragged across the sediment the increased tension caused an intermittent electrical issue. Sequences 47–65 in Tables A1 and A2 were collected with the tower moving at 2.5 cm/s, which is half its normal speed, with the ping repetition rate adjusted to 1 Hz. By reducing the speed, the cable tension and any induced electrical intermittence should be reduced. SAS images generated showed clear "ghost images," so it was concluded the speed of the tower moving along the rail was not a cause.

The "ghost images" were traced to cross-talk between the APL-UW electronics and the NSWC PCD electronics. When the APL-UW source transmitted the 1–30-kHz LFM chirp, the NSWC PCD source acted as a receiver and detected the APL-UW signal. The NSWC PCD power amplifier then re-transmitted the APL-UW signal through the NSWC PCD source. Thus, two sources were active with a slight time delay, and given the spatial separation of the transducers, the "ghost images" were biased to appear on the same side for all true target images and shifted in cross range. The experimental protocol was modified such that the NSWC PCD electronics were turned off during APL-UW transmission and the NSWC PCD source was disconnected from its power amplifier. Data were collected from target configurations 5 and 6 under these conditions.

The tower–rail system also acted as an artificial reef and attracted fish schools. With a sufficient density of fish, the transmitted and/or scattered signal was blocked. This caused dropouts in the received SAS data, appearing as horizontal stripes in the pulse-compressed, baseband signals (Fig. 2, left column). Additionally, a dense fish school contributed to the reverberation via volume scattering. Although the dropouts and increased reverberation do not appreciably effect the ability to form SAS images, the data processing to produce acoustic color templates is affected. An acoustic color template depicts the target strength as a function of frequency and target-centered aspect angle. Each ping in a sequence corresponds to a specific aspect angle, and hence, a dropout or reverberation causes holes in or washed out portions of an acoustic color template. To counter the effects of fish schools on the data and given the limited time for the TREX13 experiments, two runs down the rail to collect two sequences for a given target configuration and target rotation were executed. For GULFEX12, the transit of the tower along the rail, including the initialization of data collection hardware, took ~10 minutes. Data collection for a given source was always taken in the same direction, so the first pings in each

sequence were recorded at least 20 minutes apart. For TREX13, the rail was twice as long, so a ~40-minute delay occurred between the first pings in consecutive sequences. Although the temporal and spatial dynamics of fish schools near the tower–rail system was unpredictable, data collected during GULFEX12 suggested that a 40-minute delay between data runs was sufficient. With two sequences the "best pings" from each were combined into a single new sequence. This method replaced a region of dropouts in one data set with good pings from the other.

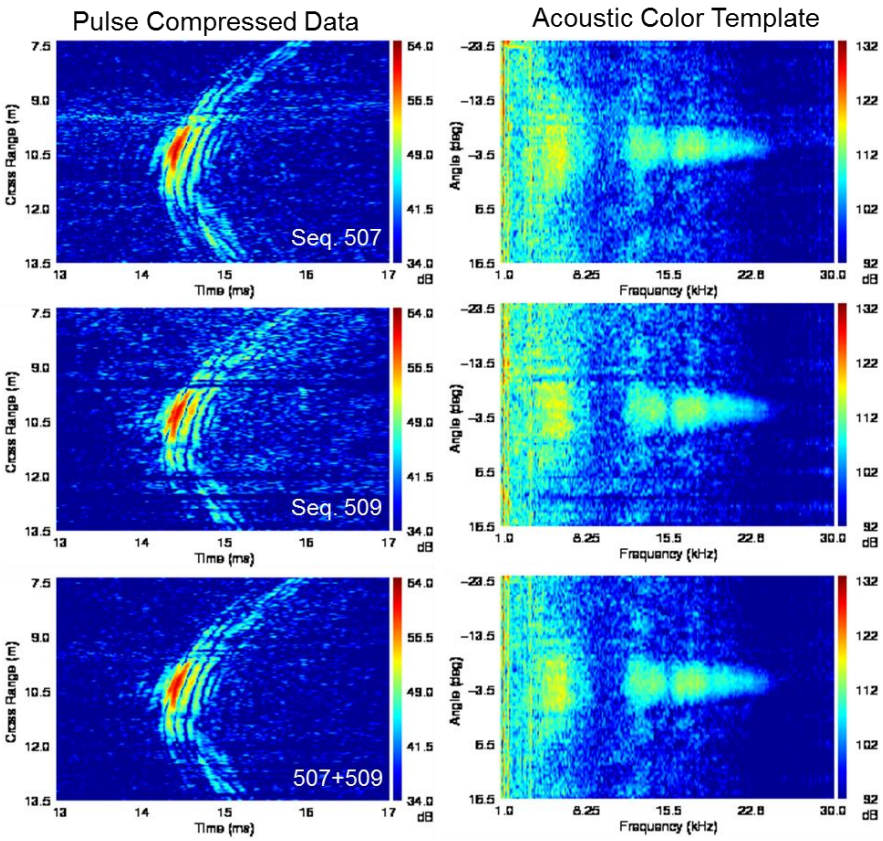


Figure 2. *Fish schools near the APL-UW rail cause artifacts in acoustic color templates during GULFEX12. Sequences 507 and 509 are consecutive data sequences. Drops and reverberation are seen in the pulse-compressed signals in the top left and middle left panels. A simple average of these sequences reduced the problems with dropouts and reverberation. The corresponding acoustic color templates are on the right. Note, the signal processing techniques to isolate the scattering associated with a single target were not used here.*

## B. Target and Reverberation Experiment 2013

The experimental plan for TREX13 followed the GULFEX12 plan. Minor modifications were confined to changes in dates and times for logistics support from NSWC PCD, scheduling the R/V *Sharp*, and routine maintenance and build-up of equipment. The plan was also modified to avoid conflicts between different experiments. For example, SAS data are largely unaffected by a nearby reverberation experiment with an active source, but the converse is not true. The transmission of a SAS signal would corrupt reverberation data. The modifications required to the experimental plan to schedule the various experiments is not reviewed nor are the details

associated with the reverberation and environmental measurements. TREX13 can be broken down into a series of stages. Each is briefly outlined in the following time line.

The mobilization stage for TREX13 occurred 5–20 April 2013. The following tasks were included in this stage:

- Three shipping containers were transported from APL-UW to NSWC PCD. They were packed with the parts to construct three new rail sections, equipment sent back to APL-UW at the completion of GULFEX12, dive gear, etc.
- Equipment stored at NSWC PCD at the completion of GULFEX12 was retrieved from storage, inspected, and routine maintenance performed.
- Structures were constructed. Dock-side testing of electronics and cables was performed.
- Multibeam surveys of the bathymetry at and near the experiment site were conducted. The surveys used 180–420-kHz side-scan sonar to image the sea floor. This allowed the identification and selection of an area of sandy sediment.
- R/V *Sharp* deployed the anchors used for the four-point moor. The GPS coordinates for the anchors were SE anchor 30º 3.517' N and 85º 40.777' W, SW anchor 30º 3.518' N and 85º 40.952' W, NE anchor 30º 3.669' N and 85º 40.776' W, and NW anchor 30º 3.668' N and 85º 40.952' W. The six rail sections were deployed within the box defined by the anchors. Large targets and a wire basket containing small targets were placed on the sea floor east of the rail sections. Gear for other researchers was placed east of the box.

The final task during mobilization was the build-up of laboratories on R/V *Sharp* (e.g., moving equipment and routing cabling).

On the morning of 20 April 2013, the R/V *Sharp* traveled to the experiment site and went into a four-point moor (initial location of 30º 3.593' N and 85º 40.864' W) providing a stable platform for dive operations and deployment of equipment. An initial survey dive was conducted during the late afternoon, and the divers located the six rail sections and the targets. The underwater construction of the rail and deployment of the sonar tower occurred on 21–22 April 2013. Divers positioned the "starter rail" with the aid of air-filled lift bags, and then joined the remaining sections to it. Once the sections were connected into a single 42-m long rail, the divers leveled the rail and tightened the bolts. The rail had a nominally east–west orientation with the target field to the north and the R/V *Sharp* to the south. The tower with the STMS-2 electronics was then lowered into the Gulf of Mexico and divers moved and placed the tower onto the rail. A series of dive operations to observe the tower–rail system followed and included:

- Mast of the tower was lifted into its upright position and the transducer faceplate was lowered to a 10º depression angle
- Initial movement of the tower was observed to confirm drive motors were operational
- Magnetic limit switches for normal and emergency stop of the tower were tested
- Smooth operation of cables trailing the tower over the sea floor was observed

With the tower–rail deployment completed, the divers moved to the task of establishing the target grid.

On 21 April 2012 with the rail's position set, the divers surveyed and laid a grid of light-weight cord to mark lines parallel to the rail (Appendix B, Fig. B1). To accomplish this task, the ends of a 98-m long cord were attached to each end of the 42-m long rail. The endpoints for a line parallel to the rail at a horizontal range of 40 m were found by forming a right triangle. With the endpoints established, cords were then placed at 5–40-m horizontal ranges at 5-m intervals.

Initial acoustics tests were conducted on 21–22 April 2013, where the solid 2:1 aluminum cylinder was placed into the target field at the rail's midpoint and at a 20-m horizontal range (D3 in Fig. B1). The cylinder axis of symmetry was aligned parallel to the rail such that this orientation coincided with a 0º target rotation and was designated as a broadside orientation. Several tests were performed to ensure proper operation of the two on-board computers within STMS-2. Each computer had independent communication to the ship. The motor control system (MCS) operates and monitors the motion of the tower as well as monitors three leak detectors and the internal temperatures of STMS-2 and motor housings. During normal operations, the internal temperature was 28–32°C. The acoustics data acquisition system (ADAS) controls almost all aspects of signal transmission, reception, and data transfer over gigabit (GigE) ethernet.

The original test plan included the transmission of two frequency bands. The APL-UW source transmitted 1–30 kHz, while a 10–50-kHz band was transmitted by the NSWC PCD source. Due to scheduling conflicts, the NSWC PCD source was unavailable. In previous efforts, APL-UW used a 30–50-kHz source, and it was decide that this source could be used to extend the upper frequency limit. This modification to the test plan simplified data transmission. As discussed in Sec. II.A, the NSWC PCD source needed to be powered off and/or disconnected during transmissions from the APL-UW source. In addition, the NSWC PCD source was to be driven by electronics that received an external trigger from STMS-2. Using the APL-UW 30–50-kHz source removed time delays and possible synchronization issues between STMS-2 and the NSWC PCD electronics.

Initial in-water tests of STMS-2 were conducted. With the tower stationary, the APL-UW 1–30 and 30–50-kHz sources transmitted LFM chirps with 6-ms duration, and data were recorded for 70 ms. With satisfactory results of the initial testing, the tower was placed at its home position, which was the west end of the rail and the origin of our coordinate system. Travel from west-to-east is the $+x$ direction; conversely, travel east-to-west is the $-x$ direction. The 1–30-kHz source transmitted for $+x$ travel and the 30–50-kHz source transmitted for $-x$ travel. To mitigate problems contributed by fish schools, the tower traveled along the rail four times; acquiring two sequences for each frequency band. For testing purposes and given that only a single target had been deployed, SAS data were recorded only for a single pass in both the $+x$ and $-x$ directions. Sequences 26 (27) in Table B2 corresponds to transmissions from the 1–30 (30–50) kHz source. These sequences were processed to check that SAS images and acoustic color template processing would produce the expected results for the solid 2:1 aluminum cylinder. In addition, the peak amplitudes of the received signals were checked to ensure that the amplification of the received signals would not clip.

***Target Configuration #1***

Divers deployed target configuration 1 on 21–22 April 2013 by distributing 26 targets (Fig. 3) to their designated locations in the grid (Fig. B1), and then during subsequent dives, divers rotated the tails of the targets towards the rail. This initial target orientation was the –80º position.

On the morning of 24 April 2013, ADAS suffered a system failure. Initially, it was thought that the internal temperature of STMS-2 may have reached a point where ADAS spontaneously rebooted. STMS-2 was powered off and left to cool for about one hour, then STMS-2 was re-activated. During the initial phases of booting, ADAS signaled that an unrecoverable system failure occurred. As ADAS controls the recording of data on the 6-channel receiving array and transmitting from the 30–50 kHz source, it became apparent that the use of STMS-2 to collect SAS data was no longer possible. The system failure was confined to ADAS, and MCS was unaffected. In addition, the signal transmitted from the 1–30 kHz source was not routed through ADAS, and came directly from shipboard electronics. Thus, it was possible to transmit the 1–30 kHz signal, but it was not possible to record the scattered signal. Two options were available: (1) pull the tower up to the deck of the R/V Sharp, remove the faulty hardware, and replace it with new hardware (if possible); or, (2) bypass STMS-2 for data acquisition.

STMS-2 is custom hardware that was built in 2003 and has had only minor modifications since. This equipment has been deployed in the Sediment Acoustic Experiment 2004 (SAX04), PondEx07, PondEx08, PondEx09, PondEx10, and GULFEX12. During PondEx08, concern was raised over a possible STMS-2 system failure due to the harsh operating environment. One of the contingency plans included the acquisition of a 100-m cable that would allow topside operation and recording of the 6-channel array in the event of a failure. On the night of 23 April 2013, the spare cable was transported from shore to the R/V Sharp along with additional equipment to record data. The equipment included a power supply for pre-amps on the low-frequency receiving array, Dash 32HF recorder (Astro-Med, Inc.), and a 90IP pre-amp (Frequency Devices, Inc.). Within a 24-hour period, APL-UW field engineers devised a workable solution to the ADAS failure, which included:

1. testing the spare cable
2. rigging the required ±15V external power supply for the low-frequency receiving array
3. synchronizing the trigger of the Dash 32HF recorder with the trigger of the signal generator used to generated the 1–30-kHz signal
4. testing a 20-dB amplifier for three channels of the receiving array
5. writing software to convert the Dash 32HF recorder internal data format to the NetCDF format used by the analysis software

The combination of 4 and 5 changed the historic channel numbering scheme. Previously, channels 1–6 were data recorded from the 6 array elements from lowest (i.e., closest to sediment) to highest (closest to sea surface) with 20 dB of gain provided by STMS-2. Channels 7–12 were data recorded from the same 6 array elements without 20 dB of gain. In the new scheme, channels 1–6 correspond to the 6 array elements with channel 1 being the element closest to the sea surface and channel 6 being the element closest to the sediment. Channels 1–3 have no gain (other than the gain from pre-amps within the low-frequency receiving array). Channels 4–6 have 20 dB of external gain. Note, the internal pre-amps of the low-frequency receiving array are driving 100-m cables, so there may be some additional cable loss not accounted for in the system calibration.


Figure 3. *Selection of targets deployed during TREX13 and BAYEX14. (left) The top four targets are a 105-mm bullet-shaped UXO, the 152-mm TP-T round, 100-mm UXO, and 105-mm UXO with fins. The last two targets are an aluminum cylinder and pipe with a notch on the left end. (middle) Clutter items: 2:1 section of telephone pole, scuba tank without stem, and 55-gallon drum opened at one end. (right) Burial and local state of the mud layer during BAYEX14.*

On the morning of 24 April 2013, a dive team detached the low-frequency receiving array from STMS-2 and attached the spare cable. The spare cable was routed to the topside 90IP pre-amp and Dash 32HF recorder. A second dive team then inspected and ensured that the spare cable was properly seated and secured to the tower and the cables leading from the tower to the subsea conjunction box. The divers also observed the cable as the tower traversed the length of the rail in both the $+x$ and $-x$ directions.

Data collection began again on 25 April 2013. In collecting SAS data, the Dash 32HF recorder required a manual step to arm it in preparation of a trigger. The signal generator sent the 1–30-kHz LFM pulse to the source at a 2-Hz repetition rate, and data were received by the Dash 32HF recorder. After initiating signal transmission, the tower was engaged to travel. This manual step means that several of the initial pings in a sequence were recorded at the starting location of the tower and the first ping coinciding with the motion of the tower is not ping 0. As it was not possible to transmit a 30–50-kHz pulse due to the STMS-2 failure, 1–30-kHz data were collected

in both the $+x$ and $-x$ directions. Sequences 30 ($+x$) and 31 ($-x$) in Table B2 represent the first data suitable for SAS processing under the new data collection protocol.

The first data sets in the target rotation series for target configuration 1 were collected on the afternoon of 25 Apr 2013 (Table B2). Sequences 32 and 33 have the targets rotated to a –80º orientation, which corresponds to the tail of the targets pointing towards the rail. Rotations were done in a clockwise manner. The intended series of rotations was to start at –80º and then increment the angle by 20º. Due to the symmetry of most targets, rotation from –80º to 80º is sufficient for a full acoustic color template. A few non-symmetric targets (e.g., DEU and rock) require a full 360º rotation to span an entire acoustic color template. The range of target sizes suggests a large variation in the expected target strengths, especially in a near broadside orientation. After the data for the –80º rotation were collected, the targets were rotated to 0º (broadside) and data were collected. Inspection of channel 3 (low gain) and channel 4 (high gain) suggested that usable data could be obtained with the modified experimental protocol. That is, if a portion of a high gain channel saturated, the low gain channel was expected to be usable. Data collection continued for target configuration 1 with target rotations –60º through 40º. SAS images were generated to inspect the quality of the data. The images were 30×40 $m^2$ in "cross-range × range" with a cell resolution of 6.67×6.67 $cm^2$. Pulse-compressed, baseband, (PCB) time signals for sequence 40 are shown in Fig. 4. The SAS image, created from the coherent processing of the data in Fig. 4, is shown in Fig. 5. The PCB time signals and SAS images for several other TREX13 sequences are shown in Figs. B2–B20 (Appendix B).

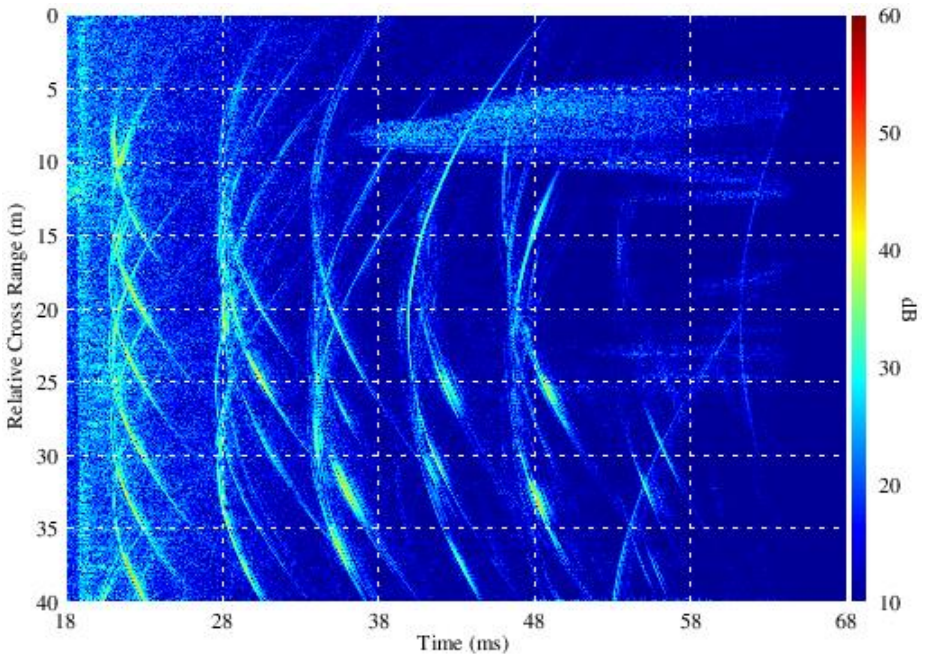


Figure 4. *Pulse-compressed, baseband time signals are displayed for TREX13 sequence 40 from target configuration 1. Targets are rotated to the –20º orientation with respect to the APL-UW rail. The broad feature between 5 to 10 m in cross range and 38 to 58 ms in time is attributed to reverberation associated with a school of fish.*

Divers measured the height of the mast's pivot point to be 3.3 m above the seafloor. From this measure, it is possible to estimate the source and receive array element heights. Data collection was started prior to the start of the tower motion. This was a manual process. The first valid ping for SAS processing was unlikely to occur at the same location along the rail for successive sequences. After removing the first 30 pings prior to SAS processing, a small offset may still persist. Thus, direct comparison of SAS images from different data sets may require small shifts in the cross-range direction to align the targets. The solid 2:1 aluminum cylinder near (20, 15) m was not manipulated during TREX13. Hence, it provides a convenient fiducial mark for alignment of SAS images. It is, however, noted that the current SAS processing uses an estimate of the source and receive array element positions, so only a relative position is possible.

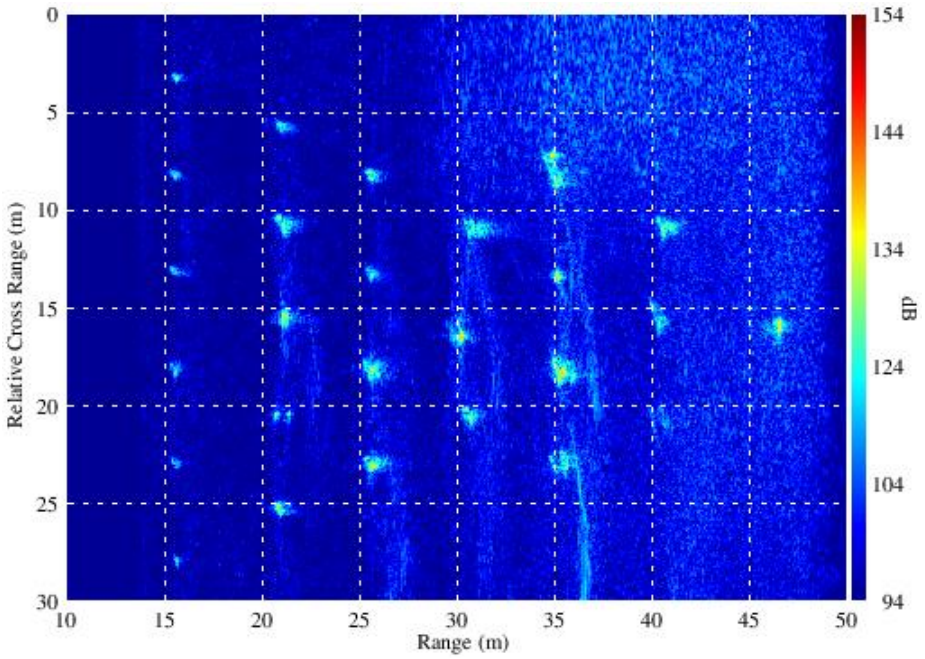


Figure 5. *SAS image created from the data shown in Fig. 4. All 26 targets placed in this target configuration are visible.*

Prior to the ADAS failure, the transmit and receiving system was calibrated, which permitted estimates of the absolute target strength. With the modified data collection protocol, the previous calibration no longer applied. While an *in-situ* calibration may have been preferred, it was proposed that a new calibration (Fig. 6) can be determined by comparisons of the broadside target strength for the solid 2:1 aluminum cylinder from sequence 26 (collected with ADAS in STMS-2), sequence 42 (captured by the Dash 32HF recorder), and the fast ray model described in Sec. III.C. By reducing the pre-amplifier gain by 10 dB, nominal agreement has been attained between the fast ray model, STMS-2 data, and Dash 32HF recorder data. Note, assuming that the fast ray model is correct, the model result is an absolute target strength. The STMS-2 data, using its calibration, also provided an estimate of absolute target strength, but includes some uncertainty due to its experimental nature.

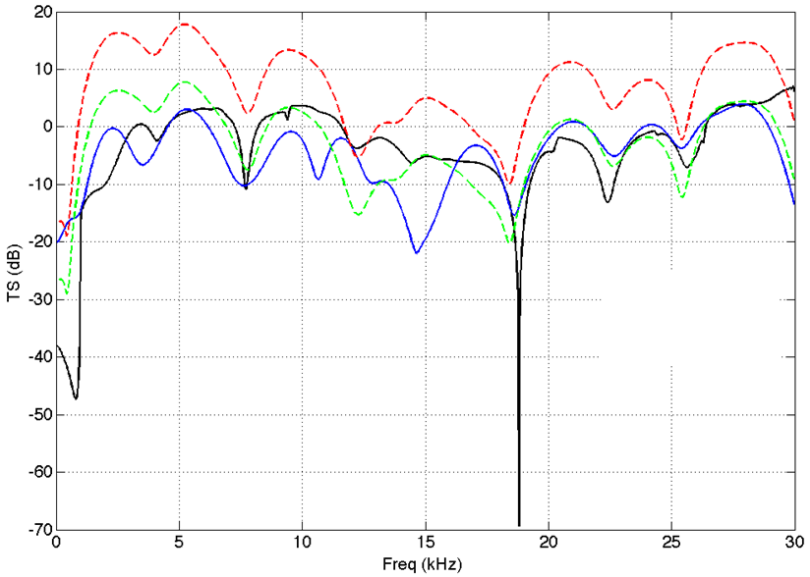


Figure 6. *Recalibration of the signal digitized by the Dash 32HF recorder under the modified protocol. The black line is the target strength that is obtained from the fast ray model (Sec. III.C) for a solid 2:1 aluminum cylinder. The blue line corresponds to sequence 26 and was recorded by ADAS within STMS-2. ADAS was a calibrated system. Sequence 42 was collected on the Dash 32HF recorder. The red line is the Dash 32HF data without any adjustments. The green line represents a simple frequency-independent reduction in gain by 10 dB.*

A look at sequences 38–49 revealed that fish schools near the tower were going to be problematic in the acoustic color template processing. In particular, for the near ranges of 5–15 m, the schools degraded the data in the morning and early afternoon. Although summing channels appeared to help the 20-m and longer ranges, the closer ranges have dropouts and poor SNR. Note that SAS processing can pull out the targets. In the late afternoon the schools started to disperse and fairly clean sequences were collected. Unfortunately, shifting the dive schedule to complete the target manipulations and maximize data collection in the afternoon was impractical; conflicts with other experiments conducted during TREX13, diver safety, and the ship-to-shore shuttling of personnel were factors.

### *Target Configuration 2*

Data collection from target configuration 1 was completed on the morning of 27 April 2013. Sequences 32–49 correspond to target configuration 1 and are listed in Table B2. Divers then moved targets to new locations, which gave target configuration 2. The new locations are enumerated in Table B1. Data acquisition commenced in the afternoon and the sequences associated with target configuration 2 are listed in Table B3. Note that sequence 51 is empty because the manual steps of the modified protocol required that the Dash 32HF recorder be armed to record data, and the arming step was overlooked.

With a mast pivot height of 3.3 m above the seafloor, the known dimensions of the transducer faceplate, and a depression angle of 10º, the coordinates at the home positions for the source and receiving array elements were $r_s$ = (0.38,0.31,3.72), $r_{r1}$ = (0.41,0.00,4.08), $r_{r2}$ = (0.37,0.00,3.88),

$r_{r3}$ = (0.35,0.00,3.78), $r_{r4}$ = (0.34,0.00,3.69), $r_{r5}$ = (0.32,0.00,3.59), $r_{r6}$ = (0.28,0.00,3.39), and $r_r$ = (0.38,0.00,3.74) m. The locations $r_{r1}$–$r_{r6}$ are for the individual channels in the low-frequency receiving array and $r_r$ locates its center. The coordinate for the 1–30-kHz source is $r_s$. As noted elsewhere, the manual synchronization of the tower motion and data acquisition caused a sequence dependent offset in the *y* coordinate.

The replica used in the pulse compression stage of the time-domain SAS processing was found to be somewhat insensitive to the choice of replica; while the acoustic color template processing appeared quite sensitive to the selected replica. The cause was not immediately apparent, but it was suggested that the issue was most prevalent at lower frequencies. Figure 7 displays the magnitude of the spectra of the replica used by the SAS processing. The available replicas include:

- original replica collected during calibration at Leesburg, VA, circa 2003
- replica recorded on a TC-4013 hydrophone during GULFEX12 without a 100-m cable
- replica recorded on a TC-4013 hydrophone during GULFEX12 with a 100-m cable

Because of the ADAS failure, capturing a through-the-system replica was infeasible, as the APL-UW source and low-frequency receiving array were mounted on the transducer faceplate.

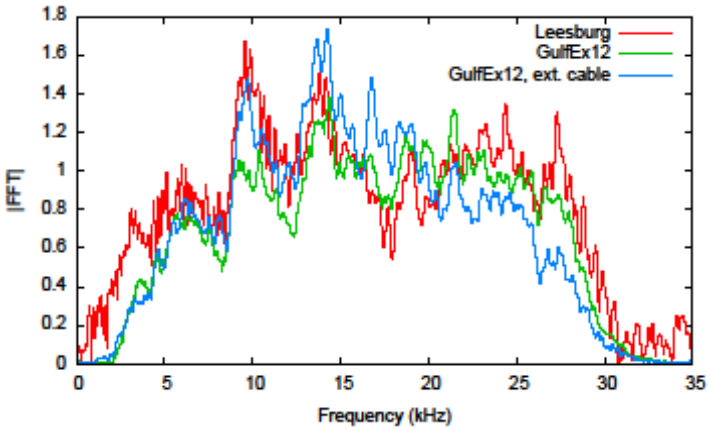


Figure 7. The measured *spectra for the 1–30-kHz LFM pulse transmitted by the APL-UW source. The original calibration (red line) was performed at Leesburg, VA. In-situ replicas recorded during GULFEX12 with a TC-4013 hydrophone without (green) and with 100-m extension cables (blue). The spectra are normalized such that the 16-kHz component has unit amplitude.*

After sequence 57 was acquired the divers noticed that the cables, which drag over the seafloor, had become tangled and pulled taut. The motion sensors on the tower and recorded by MCS suggested that sequence 57 experienced a jerking motion near the end of the run. Thus, sequence 57 was deemed unusable. The dive protocol was modified to include diver inspection of the cables after each target rotation.

### *Target Configuration 3*

The final two rotations for target configuration 2 were collected on the afternoon of 28 April 2013, and then the divers redistributed the targets into target configuration 3. The tire (target 19 in Table B1) was removed from the set of targets and the 81-mm mortar (target 12) was added. With the modified data acquisition protocol and the target field reconfiguration, a total of four data runs were collected. Inspection of sequences 66 and 67 suggested that the digitization may have been inadequate because the full dynamic range of the Dash 32HF recorder was not being exploited. Divers also reported that large amberjack fish arrived at the tower. For the morning

runs, the amberjacks were higher in the water column than the smaller fish. Sequences 68 and 69 were significantly compromised by the reverberation, attenuation, and/or scattering from fish. Data collection continued on 29–30 April 2013 and settled into a routine pattern with data collected from four or five target rotations per day. Divers worked out a method to perform the target rotations for all targets in two dives (about 2 hours). However, the weather forecast for 2–4 May 2013 called for 20-knot winds from the east with 4–6 foot seas expected. It was planned that the R/V *Sharp* would leave the four-point mooring on 1 May 2013. A final run was obtained to complete the set of rotations for target configuration 3. The plan included recovery of equipment used in reverberations experiments and disconnecting the cables to the APL-UW source and low-frequency receiving array. Divers then moved all small targets to the wire basket. The cable to the source was removed and recovered, and other cables tossed overboard.

By 6 May 2013, weather had improved to the point that the R/V *Sharp* returned to the four-point mooring. The initial set of experiments on site were bistatic acoustic scattering experiments and measurements of sediment acoustic properties. The bistatic experiment utilized the rail and were performed over the next two days. Once in the water, divers pulled cables up to the R/V *Sharp*. The cables for the APL-UW source and low-frequency receiving array, tower motors, and underwater camera were reconnected, and basic system testing conducted. SAS data collection was restarted on 8 May 2013. A dive survey showed that the targets, which were left in the target field prior to the weather event, had scoured so that a portion of the targets was now below the water–sediment interface. The scoured targets (Table B1) were 15, 17, 5, 7, 3, 1, and XX, where the corresponding grid location (Fig. B1) were C2, D3, E2, F3, H3, H1, and I2, respectively. In addition, the weather event created a new rippled surface. So, instead of moving to a new target configuration 4, divers placed the smaller targets back into their target field configuration 3 locations in a broadside orientation with noses pointing east. Divers were instructed to minimize disturbance of the sediment and to leave the scoured targets alone. Sequences 120 and 121 were recorded against this target field.

### *Target Configuration 4*

Divers then deployed target configuration 4 by placing 10 targets along the 5 and 10-m lines. The transducer faceplate was lowered to a 30º depression angle. The last sets of data for the day were collected to check pre-amplifier settings to ensure that received signals were not clipped. Sequences 122–125 (Table B5) were acquired for this purpose.

Inspection of sequences 122–125 revealed that the no-gain channels 1–3 had a drifting DC offset. This drift is apparent though not pronounced in sequences 76 and 82. Channels 1–3 were re-routed through the 90IP pre-amp with the gain set to 0 dB. As long as the signals did not clip in the old data, the DC offset was removed in the pulse compression algorithm. Sequences 122–125 were also recorded out to 20 ms. It was determined that recording out to 30 ms was desirable as the tails of the target arcs in the pulse-compressed baseband images seem to be truncated. It was also decided that the voltage from the signal generator would be reduced by a factor of two from the previous setting to retain the dynamic range covered by the channels while possibly mitigating clipping the data on the high-gain channels 4–6. Target rotations were completed for –80º through 0º for proud targets in target configuration 4. The final rotations of 20º to 80º were finished on 11 May 2013. The targets on the 10-m line were then buried to nearly 1/2 of their diameters and the targets at the 5-m line were fully buried with about 5 cm of

sand above each target. The paddle targets (targets 23 and 24 in Fig. 3) were set at a rotation angle of 40º to 45º with the paddle pointing towards the beach and rotated so the paddle face was pointing up at ~45º. These targets were not rotated, but went through a set of burial depths: proud, 1/4, 1/2, 3/4, and fully buried. Targets 23 and 24 were then rotated to 135º. These orientations for the paddle targets were selected because model predictions indicated a strong coupling into a torsional mode of vibration.

***Target Configuration 5***

The last three rotations were completed on 12 May 2013 and then the target field was reconfigured one last time to give target configuration 5 (Table B1). The targets at the 10-m line were moved to the 5-m line (except the solid 2:1 solid aluminum cylinder) and the targets at the 5-m line were moved to the 10-m line except the paddle targets. The solid paddle target was moved to the 15-m line and placed at a 40º rotation. The paddle target was then rotated about its axis to see how the orientation of the paddle affected the scattering. In the new target field, targets were also placed along the 15-m line. The solid 3:1 aluminum cylinder at the C6 grid location was slant buried at an ~44º inclination angle and the howitzer shell in the A6 location was at ~54 º. Targets 23 and 24 with the paddles were put at C1 and C1.5. Four passes were conducted as the last runs of the day. For the slant buried targets, the tails were pointing to the east. The four data sets collected the previous day suffered substantial reverberation due to fish. Both $+x$ and $-x$ runs were completed, but data were captured for only the $+x$ direction (sequence 166) because the Dash 32HF recorder was not armed for the $-x$ travel (sequence 167).

Overnight, the slant-buried solid 3:1 aluminum cylinder appeared to settle. It was originally measured to be at ~44º, but a morning check found that the cylinder was at ~29º with a long edge along the top of the cylinder of 73.7 cm and a short edge (nearest the sediment) of 8.89 cm. Divers lowered the angle to ~25º with a long edge still at 73.7 cm and no short edge. The howitzer shell was found now at 65º, where it was measured originally at ~54º. The long edge was 47.6 cm and after lowering the howitzer shell to 25º, it was at 47 cm. The short edge was 35.6 cm, and after diver intervention it was 34.3 cm. This means the morning run of sequence 166 had different slant buried orientations than the previous sequences 162–165. Verification of the target slant angles was not accomplished as the digital inclinometer turned itself off before the measurement was attempted. The inclinometer was housed in a water-tight container, and had to be activated prior to a dive. Divers also raised concerns about the reliability of the digital inclinometer, and then confirmed that the digital inclinometer was not functioning correctly underwater. Divers measured a burial angle, then changed the orientation of the inclinometer to give a different reading.

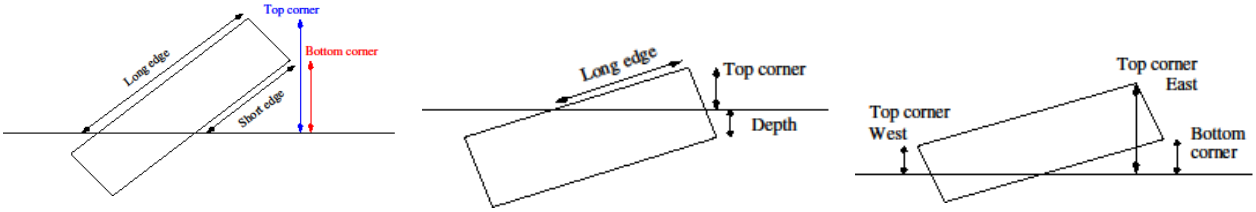


(a) Howitzer shell (b) 3:1 Aluminum Cylinder (c) 3:1 Aluminum Cylinder

Figure 8: *Under slant burial conditions, the length of exposed edges and the height of exposed corners were measured for the 3:1 aluminum cylinder and howitzer. The slant angle was determined from*

*these measurements*.

Upon re-measuring the burial angle, the measurement did not agree with the first measurement and in fact was significantly different. The burial angle was considered to no longer be a reliable measurement. Divers were instructed to measure the long and short edge of the targets as well as other fiducial points (e.g., highest point above the sediment interface). Figure 8 depicts various burial states for the solid 3:1 aluminum cylinder and howitzer shell. The measured values recorded by divers of the various edges and corner elevations are shown in Table 1.

| Angle | Target | Long Edge | Short Edge | Top Corner | Bottom Corner | Comment |
|---|---|---|---|---|---|---|
| –40º | Cylinder | 84.5 | | | | |
| –20º | Cylinder | 91.8 | | 26.7 | | |
| 0º | Cylinder | 92.1 | | 25.4 | –5.08 | |
| 20º | Cylinder | | | 7.3, 34.9 | 3.81 | |
| –40º | Howitzer | 48.3 | 30.5 | | | |
| –20º | Howitzer | 48.3 | 21.6 | | 12.7 | T1 |
| –20º | Howitzer | 50.2 | 25.1 | | 12.7 | T2 |
| 0º | Howitzer | 35.2 | 17.8 | | 7.62 | |
| 20º | Howitzer | 52.4 | 26.0 | | 14.0 | |
| 40º | Howitzer | 53.2 | 25.4 | | 14.0 | |
| 60º | Howitzer | 51.1 | 17.8 | | 9.84 | |
| 80º | Howitzer | 65.4 | 25.4 | | 7.62 | |

Table 1. *Under slant burial conditions, the length of exposed edges and height of exposed corners were measured for the 3:1 aluminum cylinder and howitzer. Dimensions are in centimeters. The T1 and T2 comments note a discrepancy in measurements, where T2 measurements were recorder before the divers performed the 0º target rotation (about 30–40 minutes after T1).*

One pass at the current orientation was collected on 14 May 2013, and then the final three rotations were performed to complete data collection from target configuration 5. Near the end of recording sequence 178, the ship-to-shore shuttle approached the R/V *Sharp*. Sequence 178 may contain boat noise, which is not expected to affect SAS imaging but may compromise the construction of an acoustic color template.

### *Target Configuration 6*

Divers repopulated the large target field with target configuration 6 (Table B1) for post-TREX13 NSWC PCD tests, which were scheduled for later in June. All targets were proud and placed at random orientations with respect to the rail. SAS data were collected, but the transducer faceplate was aimed at a 0º depression angle. That is, the acoustic axes of the APL-UW source and low-frequency receiving array were parallel to the seafloor. The source amplitude into the power amplifiers was 0.5 $V_{rms}$.

On 15 May 2013, a decision was made to capture an *in-situ* pulse replica with either a F41 or TC-4013 hydrophone. With the transducer faceplate in its 0º depression orientation, replicas

were recorded with both hydrophones. These replicas showed a fairly low level in the 10–14-kHz range of the spectrum of the LFM chirp. The APL-UW source contains four staves, and each stave is driven by a power amplifier and a portion of the complete frequency spectrum. To maintain the horizontal beamwidth across the entire 1–30-kHz frequency band, all staves are active at low frequencies while only a single stave is active at the upper end of the spectrum. Upon inspection, it was determined that the signal from one of the power amplifiers was 180º out-of-phase with the other signals, because the wiring was reversed. Thus, the horizontal beamwidth was frequency dependent, which necessitated a measurement of the actual beam pattern. Divers placed the TC-4013 hydrophone on a pole and rigged it to be at about the 10 m line in the target field. The tower was scanned along the rail for about 10 m and the transmitted signal was recorded. Both the in-phase and out-of-phase stave configurations were captured. The out-of-phase data were reduced to a beam pattern correction, so that absolute target strength could be extracted from the SAS data. At the completion of the beam pattern measurement, the target scattering portion of TREX13 was completed. Recovery of the deployed equipment was initiated.

### C. Bay Experiment 2014

The Bay Experiment 2014 was conducted from 29 April 2014 through 1 June 2014. This experiment followed the same stages as TREX13: pre-experiment planning and maintenance, mobilization (7 days), on-site experiment (21 days), and demobilization (4 days). Most of the details for these stages are give in Sec. II.B, so only changes or differences mandated by the conditions in St. Andrew's Bay are reported here.

After TREX13, two critical pre-experiment tasks were initiated. First, the system failure in ADAS was diagnosed as a failure of the mainboard of the computer system. This mainboard utilizes a PowerPC processor and uses a VMEbus to communicate with peripheral devices. It was determined that ADAS could be repaired if a suitable replacement mainboard could be acquired. The APL-UW Ocean Engineering Department located a replacement mainboard, tore down STMS-2 to insert the new board, reconstructed STMS-2, and then tested and certified its performance. This repair had significant impact on data throughput for BAYEX14, because the emergency data acquisition method used in TREX13 required a lengthy translation from the data format of the Dash 32HF recorder to the format used by our analysis software. The second task re-introduced a high-frequency (HF) source and receivers onto the APL-UW tower, which were used during SAX04. Although SERDP MR-2231 was primarily concerned with low-frequency SAS data, these transducers allow the collection of SAS data in the 100–200-kHz band and allowed us to perform on-site assessments of the orientations for proud targets.

After a week of build-up and dock-side testing of the equipment, the at-sea deployment commenced on 7 May 2014, when the R/V *Sharp* traveled to the experiment site and went into a four-point mooring at 30º 3.593' N and 85º 40.864' W. An initial survey dive was conducted during the late afternoon and the divers located the six rail sections. In addition, the targets were lowered to the seafloor for later deployment. The first sonar transmissions occurred on 10 May 2014. SAS data were then collected over the next 16 days from three primary target configurations (Tables C1–C4) with an additional seven target configurations (See Tables C5–C8) for specific targets and target orientations to fill gaps in the measurements from the primary target configurations. In all, 98 sets of SAS data were collected. Environmental measurements

also were collected under SERDP MR-2229 and provided environmental properties needed for numerical simulations. Recovery of the deployed equipment and demobilization occurred from 26 May 2014 through 1 Jun 2014.

A number of targets (Table C1) were distributed in eleven different target configurations. The number of targets distributed into a primary target field ranged from 11 to 26. A few measurements were repeated with only a few targets in the field, because the original data were deemed unusable due to misalignment whether in range or target orientation. Four classes of targets were used (Fig. 3). The munitions class included a Diver Evaluation Unit (DEU, a mine-like simulator), 155-mm howitzer shell without end-cap, 152-mm TP-T round, 81-mm mortar, 100-mm UXO, 105-mm UXO #1, 155-mm howitzer with end-cap, 105-mm UXO #2, and 105-mm shell with fins. The UXO-like class contained solid aluminum replicas #1 and #2 of the 100-mm UXO and a steel replica of the 100-mm UXO. The scientific class contained a solid 5:1 aluminum cylinder (38.1 cm length by 7.62 cm diameter), solid 3:1 aluminum cylinder (91.4 cm by 30.5 cm), 2:1 aluminum pipe (61 cm by 30.5 cm with 0.95 cm wall thickness), solid 2:1 aluminum cylinder (61 cm by 30.5 cm), a 30-cm radius stainless steel spherical shell, a small solid aluminum cylinder with a notch, and a small aluminum pipe with a notch. The fourth and final class contained clutter items: a rock, cement block, water-filled 55-gallon drum with an external fixture, water-filled 55-gallon drum, a car tire, water-filled scuba tank without stem, and water-filled scuba tank with stem. Both drums had one open end and one closed end.

Diver surveys of the selected site in St. Andrew's Bay revealed a mud layer over a hard sand bottom. The thickness of the layer varied from approximately 15 cm to more than 30 cm. All targets, when placed by divers on the water–mud interface, sank to some extent into the mud. The right-hand column in Fig. 3 shows photographs of four targets taken during a time of high visibility. The smaller heavier targets such as the 105-mm UXO and replicas of the 100-mm UXO tended to be completed buried in the mud layer while larger targets were observed in various states of burial. During BAYEX14, two- and three-man dive teams conducted 200 dives to deploy and maintain equipment, survey in the target field grid lines, and distribute and manipulate targets. The brackish water in St. Andrew's Bay offered 0.25–2 m of visibility. The nearly 450 individual dives represent about 338 hours of bottom time for the divers.

The water depth was ~8 m. The sound speed, temperature, and salinity measurements of the water column revealed a low-salinity (almost freshwater) layer of water over a colder seawater layer. The sonar was located in the colder layer where the sound speed was about 1524 m/s. While the environmental measurements for the mud properties are being analyzed, the initial model–data comparison used a density of 1300 kg/m$^3$ and 1550 m/s, which are taken from measurements in mud near the TREX13 site.

Example SAS images, generated from BAYEX14 data with a frequency-domain imaging algorithm [9], are shown in Fig. 9. Figure 9(a) is a HF SAS image produced after match filtering with a replica of the transmitted 110–190-kHz LFM pulse. Figure 9(b) is a low-frequency (LF) SAS image that corresponds to the 1–30-kHz LFM pulse transmission. It is important to note that data were collected simultaneously in both frequency bands. Thus, the LF and HF SAS images are automatically spatially registered. Inspection of Fig. 9(a) shows seven horizontal lines across the image at 10, 15, …, 40 m ranges. These lines are caused by the light-weight cord, which the divers used to establish the target field grid. To achieve high-quality images, the

ω-*k* imaging algorithm implemented a second order phase correction to de-jitter the data; otherwise, the HF SAS processing is sensitive to small deviations from the assumed straight line SAS path over the 42-m rail. This phase correction is then applied to the LF data, which also helps sharpen its focus.

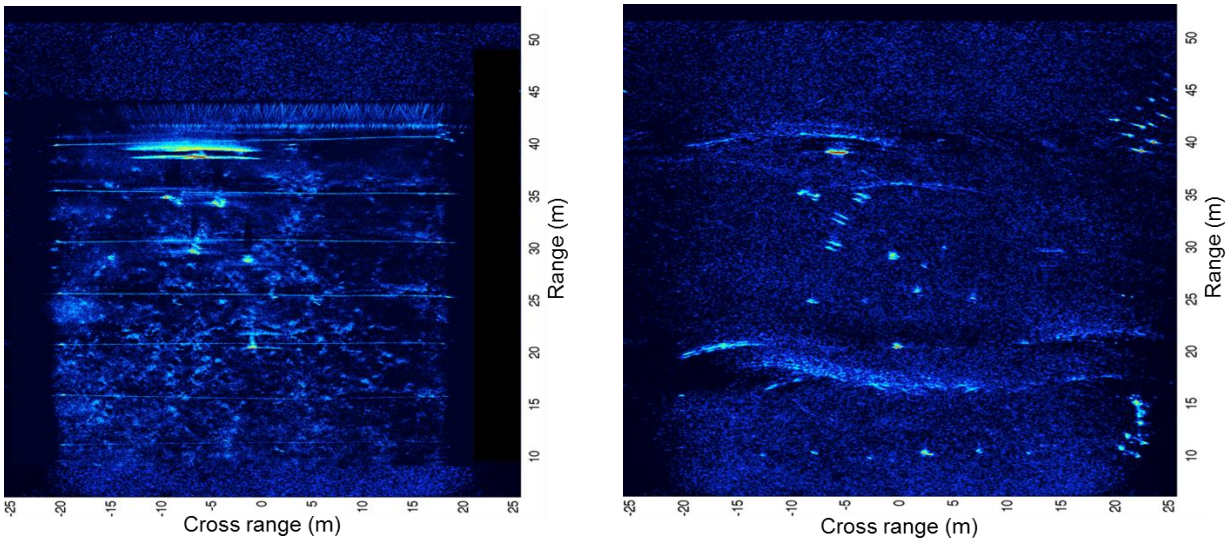


*(a) High-frequency SAS image* *(b) Low-frequency SAS image*

Figure 9: *High and low-frequency SAS images generated from BAYEX14 data.*

A broad feature between 15 and 20 m in range and spanning –10 to 20 in cross range (Fig. 9b) is due to the geometry of the experiment and the depth of water. The APL-UW rail was deployed parallel and nominally 10 m from the R/V *Sharp* in water with a depth of 8 m. Sound transmitted from the back of the source scattered from the R/V *Sharp* and contaminated the data for targets placed along the 15 m line. Thus, the experimental protocol was altered to eliminate the use of the 15-m line. The feature with four bright corners near (22, 10) in Fig. 9(b) is the wire basket, which was lowered to the sea floor with the smaller targets. The group of features centered at (22, 42) in Fig. 9(b) are due to objects in a staging area. Finally, a comparison of the LF and HF SAS images demonstrates the utility of low frequency for the detection of (partially) buried targets. Almost all targets along the 10-m line are not observed in the HF SAS image, and the targets at 25, 30, and 35-m ranges appear to be better resolved than in the HF SAS image.

## III. Data Processing and Discussion

### A. Processing of Experimental Data

The data were processed using time-domain and frequency-domain SAS algorithms [9–11]. The initial step is pulse compression by match filtering the pings with a replica of the transmitted LFM chirp. For GULFEX12 and TREX13 only a 1–30-kHz LFM pulse was transmitted. For BAYEX14, 1–30 and 110–190-kHz LFM pulses were transmitted simultaneously from two independent sources. When considering BAYEX14 data, the appropriate pulse replica is used during pulse compression. During the match filtering, a Hilbert transform converts real-valued

recorded pings to complex-valued signals. Pulse-compressed baseband (PCB) data are then obtained by removing the angular carrier frequency $\omega_0$ via multiplication by $\exp(i\omega_0 t)$, where our processing scheme assumes a negative time convention. Figure 4 shows the magnitude of the PCB pings for TREX13 sequence 40. The corresponding SAS image is displayed in Fig. 5. In addition, PCB and SAS images for several other TREX13 sequences are shown in Figs. B2–B20.

The scattered acoustic field from an individual target interferes with its neighbors (Fig. 4). For SAS processing the coherent addition of complex time signals is unaffected by this overlap. To produce a SAS image using a time-domain algorithm, the data are processed with a simple delay-and-sum beamformer. For each pixel in a SAS image, the signals are time-shifted to account for propagation delays from the source to the pixel and then from the pixel to the receiver. Once the time shift is performed, the signals are added coherently to determine a complex reflectivity for the pixel. This time shifting is done for each pixel in a SAS image. The color bar in Fig. 4 is an absolute target strength. Images for individual channels of the receiving array as well as the superposition of the six channels have been constructed.

The overlap of the scattered acoustic fields from adjacent targets has an important consequence for the acoustic color template processing. The PCB data were further processed to generate acoustic color templates, where pictorially an acoustic color template is a colored representation of the target strength as a function of frequency and a target-centered aspect angle. Due to the relatively small separation distances of ~5 m between adjacent targets, the scattered acoustic fields overlap (Fig. 4). To generate an acoustic color template, a synthetic aperture deconvolution (SAD) algorithm was used to isolate the acoustic response of individual targets and to suppress reverberation noise. A detailed description of SAD is given by Marston et al. [11], where they implemented a frequency-domain SAS imaging algorithm. A pictorial description of this technique is shown in Figure 10 and a brief summary is as follows. The raw SAS data set is deconvolved with a target arc for a single selected location in an image plane, and a SAS image is formed. As an observation point in the SAS image moves away from the selected location, the image becomes defocused because the target arc is not appropriate for these locations. The SAS image is then windowed in the spatial domain about the selected location. This windowed SAS image contains the information to reconstruct the portions of the time signals associated with a given target via a convolution with the same target arc. It is noteworthy that the deconvolution and convolution processes are linear operations, and hence in the absence of multiple scattering the recovered signal isolates the acoustic response of the selected target.

Inspection of the PCB data in Fig. 5 suggests that, at most, an aspect angle range for a given target at a 10-m range in a given sequence spans approximately ±15°. This motivated the choice of target rotations from −80° to 80° in 20° increments for the axisymmetric targets. Adjacent rotation angles provide an overlap in the aspect angle ranges (e.g., 20°±15° and 40°±15°), which permits the nine sequences to be stitched together to form an acoustic template. The overlapping regions can be determined by a cross-correlation of the aspect angle ranges for adjacent rotation angles or aligned by eye (given sufficient structure in the color plots). Once the overlap is established, the two angular ranges are merged by a smoothing operation over the overlap region.

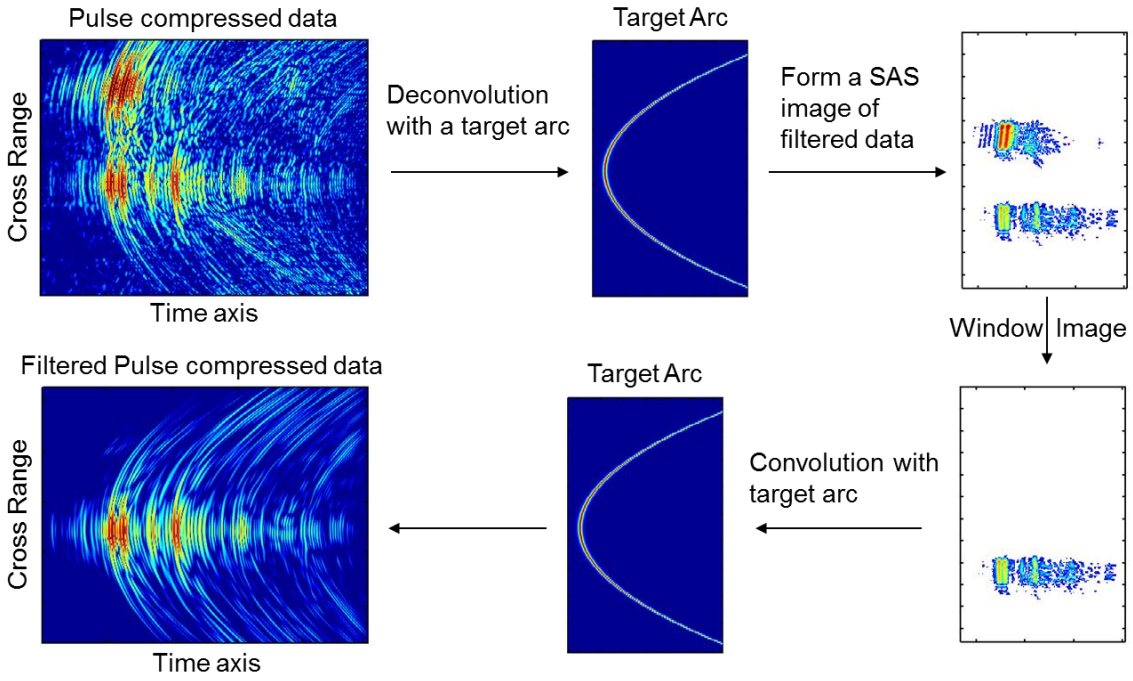


Figure 10. *The synthetic aperture deconvolution (SAD) algorithm is applied to the acoustic scattering from a solid 2:1 aluminum cylinder (upper target) and a 2:1 aluminum pipe (lower target). The top row depicts the deconvolution of a target arc located at the pipe. The right column depicts the spatial windowing and the bottom row is the convolution with the same target arc to recover the scattering from the pipe. The final PCB data contain only the pipe response and noise associated with surface reverberation has been suppressed.*

The SAD algorithm was applied to data collected during PondEx10 and to a small portion of the data collected during TREX13. This algorithm relies on setting the magnitude of a Weiner noise suppression parameter, which is an independent parameter. Recently, Zartman et al. [12] proposed and demonstrated a quasi-holographic imaging method that can be used to isolate the scattering from individual targets. One advantage of this method is the elimination of the Weiner noise suppression parameter. The quasi-holographic method is now the preferred technique to isolate the scattered signals. The left panel in Fig. 11 displays the scattered signal from the 2:1 aluminum cylinder (target 17 in TREX13), which was extracted with the quasi-holographic method. The central panel is the acoustic color template associated with the signal in the left panel. The right panel in Fig. 11 is a complete 360° acoustic color template for target 17 at a distance of 30 m from the APL-UW rail. Full acoustic color templates for all targets deployed in TREX13 are shown in Figs. B21–B33.

Figure 11 is a screen shot of a MatLab™ GUI-based application that collects all of the isolated target scattering signals into an extensible database. The upper legend in Fig. 11 gives the target type, horizontal range of the target from the APL-UW rail, sediment type, burial condition, and the orientation of the target within its target-centered coordinate geometry, where we have imposed the condition that 0° aligns the axis of symmetry of cylindrical targets parallel with the rail. To date, the database contains scattered signals from the eleven targets deployed in

PondEx10 and the scattered signals from all targets deployed during TREX13. Table 2 enumerates the TREX13 targets and indicates the targets for which data were analyzed fully to yield acoustic color templates used in our initial binary classification effort.

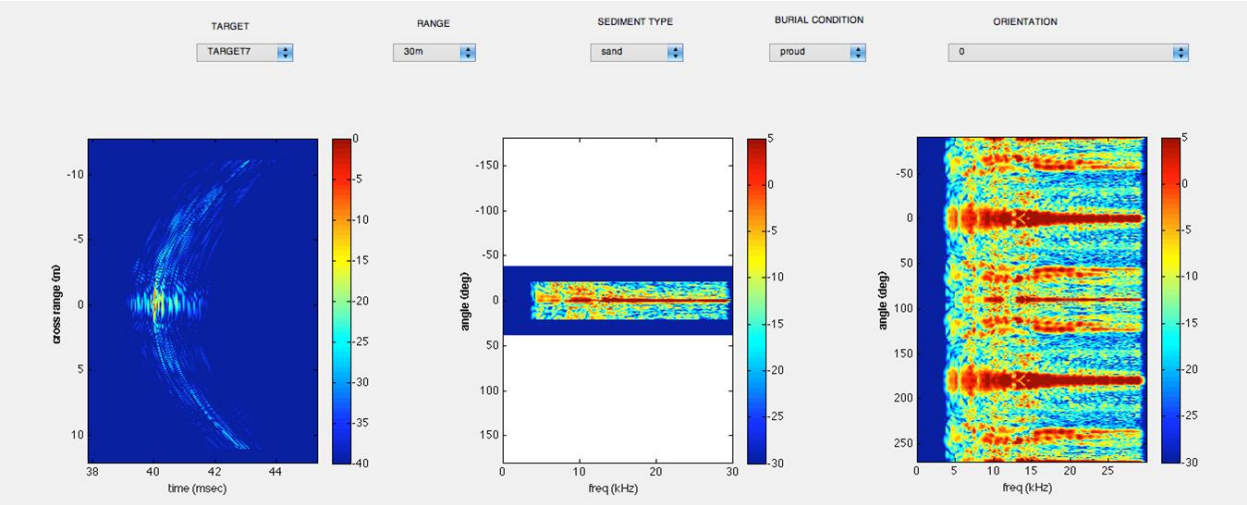


Figure 11: *Scattered signal from target 17 isolated from TREX13 data. MatLab™ GUI-based application displays the isolated scattered signal (left), its representation as an acoustic color template (center), and the complete acoustic color template for the target (right).*

Inspection of the acoustic color template (Fig. 11 and those that follow) suggests that a portion of a complete acoustic color template may be used as a fingerprint to identify a given target. It is, however, noteworthy that PondEx10 data were collected in a single freshwater location under fairly well-controlled and well-measured environmental conditions while TREX13 data were collected at a single location in the Gulf of Mexico. Whether observable structure in an acoustic template is robust under variations in the environment or geometry remains to be established.

## B. Finite-element Models and Comparisons to Data

The experimental acoustic color templates serve as ground truth for acoustic color templates generated from predictions of target responses from a hybrid model. The hybrid model combines $N$×2D FE models, which solve the 3D problem of the interaction of an acoustic field with a target in terms of a superposition of $N$ azimuthal Fourier modes, with a 3D Helmholtz–Kirchoff propagation integral. The targets are axisymmetric, but the incident field is generally not axisymmetric. The $N$×2D FE method allows us to solve problems over the entire frequency bandwidth without resorting to supercomputers. Details of the underlying assumptions and implementation are given in several studies by Zampolli et al. [13–15].

Table 2. *Targets were deployed at various ranges from the APL-UW rail during TREX13. The top row shows the horizontal ranges in meters and the first column contains the assigned target number. The numbers under each range corresponds to a target configuration in Appendix B. The red typeface denotes data that were isolated by the quasi-holographic method and reduced to acoustic color templates. These templates were available for our initial efforts towards binary classification of target versus non-target. The black typeface represents data that had not been isolated and reduced to acoustic color templates at the time of the classification work. Target numbers 4, 26, and 27 with "XXXXXX" were assigned to targets, but these targets were not deployed.*

| TARGET | RANGE (Mark with the field config number) | | | | | | | |
|---|---|---|---|---|---|---|---|---|
| | 5 | 10 | 15 | 20 | 25 | 30 | 35 | 40 |
| 1 | | | | | | | 1,2 | 3 |
| 2 | | | | | | | 1,2 | 3 |
| 3 | | | | | | | 1,2 | 3 |
| 4 | XXXXXX | XXXXXX | XXXXXX | XXXXXX | XXXXXX | XXXXXX | XXXXXX | XXXXXX |
| 5 | | | | | 3 | 2 | | 1 |
| 6 | | | | | 3 | | 2 | 1 |
| 7 | | | 5 | | | 3 | 1 | 2 |
| 8 | 4 | 5 | | | 3 | 2 | | 1 |
| 9 | 5 | 4 | 2 | 1 | | | 3 | |
| 10 | | | | 3 | 2 | 1 | | |
| 11 | 5 | 4 | | 2 | 1 | | 3 | |
| 12 | | | 3,5 | | | | | |
| 13 | | | 2 | | 1 | | 3 | |
| 14 | | | 3,5 | 2 | 1 | | | |
| 15 | | | 3 | 2 | 1 | | | |
| 16 | | | 3 | | 2 | 1 | | |
| 17 | | 4,5 | | 1,2,3 | | | | |
| 18 | | | 5 | | | | | |
| 19 | | | | 1 | | | | |
| 20 | 5 | 4 | 1 | | | 3 | | 2 |
| 21 | 5 | 4 | 1 | | 3 | 2 | | |
| 22 | 4 | 5 | | 1 | | 3 | | 2 |
| 23 | 4 | | 1,2,5 | 3 | | | | |
| 24 | 4 | | 1,2,5 | 3 | | | | |
| 25 | 4 | 5 | 1 | 3 | 2 | | | |
| 26 | XXXXXX | XXXXXX | XXXXXX | XXXXXX | XXXXXX | XXXXXX | XXXXXX | XXXXXX |
| 27 | XXXXXX | XXXXXX | XXXXXX | XXXXXX | XXXXXX | XXXXXX | XXXXXX | XXXXXX |
| 28 | 5 | | 3 | | 2 | 1 | | |
| 29 | | | 1 | 2 | | | 3 | |
| 30 | 4 | 5 | 2,3 | 1 | | | | |

What level of detail is needed in a FE model to reproduce the observed structure in an experimental acoustic template? FE meshes for the 100-mm bullet-shaped artillery shell were constructed with and without the grooves and ridges on its surface. The material properties of the actual artillery shell are unknown, so the FE model was executed with the properties of aluminum to compare with the acoustic color template created from PondEx10 data. The density, compressional sound speed, and shear sound speed for aluminum are $\rho = 2700$ kg/m$^3$, $c_l = 6568$ m/s, and $c_s = 3149$ m/s, respectively. The smoothed mesh contains 3533 elements and 24526 degrees of freedom (DOF); the mesh with grooves and ridges contains 9608 elements and 77233 DOF (Fig. 12). The sand sediment was treated as a viscous fluid with density $\rho_1 = 2000$ kg /m$^3$ and complex sound speed of $c_1 = 1694 + i13.55$.

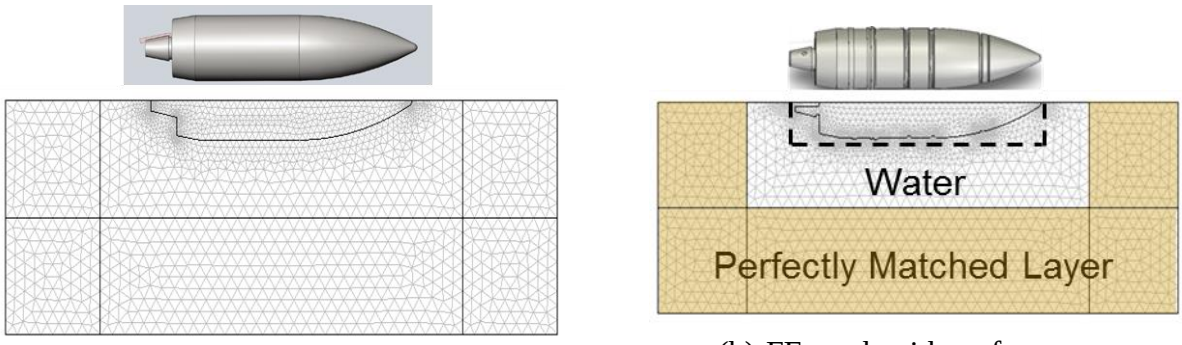


(a) Smooth FE mesh for 100-mm UXO.

(b) FE mesh with surface structure

Figure 12. *Meshes used in FE simulations for a 100-mm UXO. The fine structure on the UXO surface requires an increase in the number of elements and DOFs. The additional elements are concentrated near this fine structure. This then leads to an increase in computational complexity. The dashed line in (b) denotes a locus of points where the pressure and normal derivatives are recorded in the near field of the target.*

The predicted acoustic color templates and the templates generated from PondEx10 data (Fig. 13) for an aluminum replica of the 100-mm UXO on a water–sand sediment interface show that at low frequencies, both FE meshes capture the elastic response of the target. As the frequency increases, the grooves and ridges must be included in the FE model to recover the observed structure. The highest frequency in the experiments and simulations is 30 kHz and with a nominal sound speed in water of 1464 m/s, the wavelength is ~4.9 cm. The depth, height, and width of the grooves and ridges are on the order of a few millimeters. The separation distances between adjacent surface features are on the order of a wavelength. Hence, it seems that the propagation of acoustic energy along the surface is affected by the spacing of the surface features, and this gives rise to some of the observed differences in the acoustic color templates (Fig. 13).

With the required FE mesh fidelity established, the material properties of the steel replica were used to compute an acoustic color template. The material properties for mild steel are $\rho$ = 7710 kg/m$^3$, $c_l$ = 5890 m/s, and $c_s$ = 3240 m/s. The hybrid model was exercised with the FE mesh containing grooves and ridges, and the results are in good agreement with PondEx10 data for the steel replica. Comparison of the hybrid model results with the PondEx10 data for the actual 100-mm UXO (Fig. 14) show that the steel replica result is in much better agreement than an aluminum replica result. Given that the targets are geometrically identical, it is the elastic response of the targets (i.e., the material properties) that gives rise to the observed agreement. It is, however, noteworthy that the steel replica result and PondEx10 data do show some distinct disagreement. This can be attributed to a mismatch in the unknown material properties of the steel of the actual UXO and mild steel. In addition, the hybrid model simulation does not include noise contributions for surface reverberation whereas the PondEx10 data contain some reverberation even though the divers had artificially smoothed the water–sediment interface.

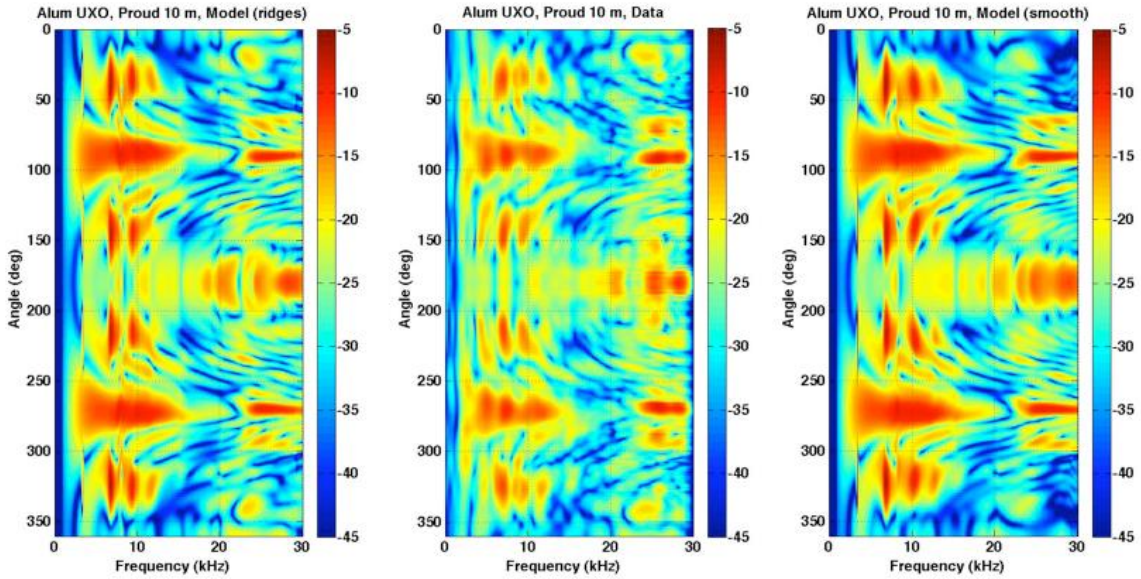


Figure 13. *Acoustic color templates for the target with the smoothed FE mesh (right), the target with the FE mesh that contains grooves and ridges (left), and PondEx10 data (center) for an aluminum replica of the 100-mm bullet-shaped UXO. Agreement is satisfactory at low frequency, but as the frequency increases above ~15 kHz, the simulation with the grooves and ridges captures structure observed in the data (compare the 0°–50°, 160°–200°, and 300°–360° ranges).*

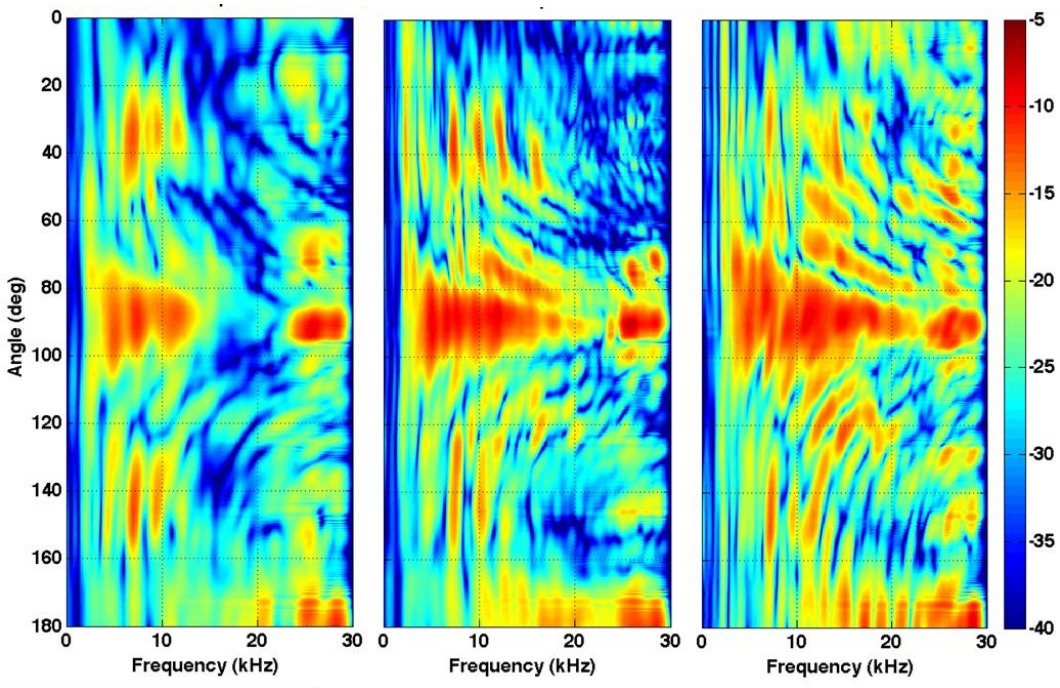


Figure 14. *Acoustic color templates for aluminum (left) and steel (center) replicas of the 100-mm UXO produced by the FE model where the mesh with grooves and ridges was used. The acoustic color template for the actual 100-mm UXO is constructed from PondEx10 data (right).*

With the good agreement between the FE simulations for aluminum and steel replicas of the 100-mm bullet-shaped artillery shell and the excellent agreement for the 2:1 aluminum cylinder reported by Williams et al. [16], FE meshes for several other targets were constructed. These include 3:1 solid aluminum cylinders, 2:1 aluminum pipe with a 0.94-cm wall thickness, a 105-mm bullet-shaped artillery shell, a 155-mm howitzer shell with and without its end cap. Figure 15 displays the FE meshes for a 105-mm artillery shell and a 155-mm howitzer. For these two targets, FE simulations were completed for both air-filled and water-filled targets.

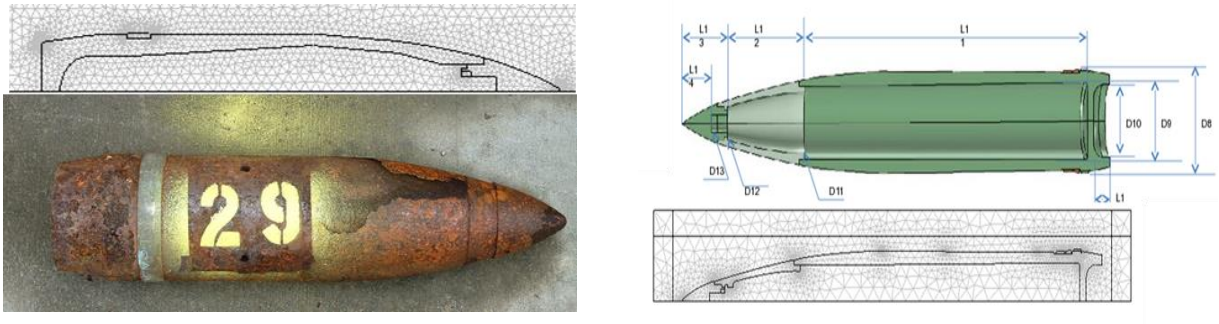


(a) 105-mm artillery shell (b) 155-mm howitzer shell

Figure 15. *FE meshes for two inert UXO targets deployed during TREX13 and BAYEX14. A concentration of elements is observed at junctions between segments of the shells' body.*

## C. Fast Ray Model

When the wavelength of sound is much smaller than the depth of a waveguide, the scattering of sound from a target within the waveguide may be approximated by an acoustic ray model [8, 17]. For our applications, the waveguide is a homogeneous layer of water bounded above by air and below by a homogeneous sediment. Figure 16(a) depicts the scattering problem, and displays the direct path arrival as well as the ray paths that interact once with the upper and/or lower boundaries. In this figure, the source, receiver, and target are denoted by $S_0$, $R_0$, and T. By considering image sources and receivers reflected about the boundaries, one can associate acoustic ray paths with these images. Figure 16(b) shows the image sources and receivers and associated acoustic rays, and demonstrates the reduction of the waveguide scattering problem to an equivalent superposition of many free-field scattering problems. The sediment is assumed to be homogeneous, and has been modeled as either an attenuating fluid with a frequency-independent loss parameter [18] or as a fluid described by an effective density fluid model [19].

Figure 16. *(a) Diagram of paths that interact at most once with the upper and/or lower boundaries of a waveguide. (b) Equivalent superposition of freefield scattering involving image sources and receivers. The first two image sources are $S_1$ and $S_2$ while $R_1$ and $R_2$ correspond to image receivers.*

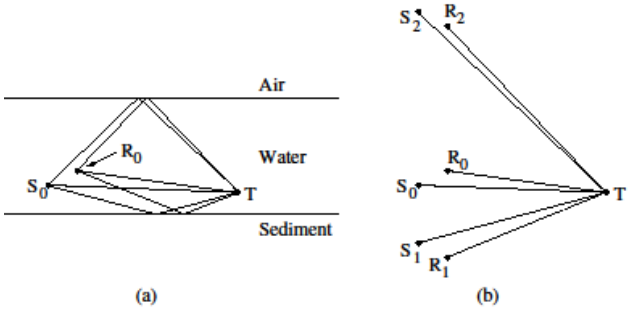

The scattering of an incident plane-wave pressure leads to a scattered pressure of the form $p_t \approx p_0 f(\theta,\phi,\omega)\exp(ik_1 r)/r$ in the far field of a finite target in the free field. The constant $p_0$ carries units of pressure and $r$ is the distance to a field point in the far field of the target. The wavenumber, $k_1 = \omega/c_1$, is defined by the angular frequency $\omega$ and speed of sound in the water $c_1$. The scattering amplitude $f(\theta,\phi,\omega)$ has units of distance [18, Eq. (23)], where $\theta$ and $\phi$ are polar and azimuthal angles for the field point in a target-centered spherical coordinate system. Inspection of $p_t$ shows that the target is point-like with the directionality of the scattered field contained within $f(\theta,\phi,\omega)$ along with information about the material properties of the target. When the source and field point are located at arbitrary finite distances in the far field of the free-field target, the scattering amplitude has the general form $f(\theta_s,\phi_s,\theta_r,\phi_r)$ where the subscript $s$ denotes polar and azimuthal angles associated with the source location. For co-located source and field point and by exploiting the symmetry of a target to define the target-centered coordinate system, the angular dependency can be reduced to fewer angles. For example, the data–model and model–model comparisons assume monostatic scattering and an axis of symmetry for the target parallel to the waveguide boundaries, which reduces the number of angles from four to two. Finally, the scattering amplitude can be determined from analytic solutions to scattering problems (e.g., scattering from a spherical target), direct measurements from actual targets, or numerical simulations (e.g., a FE model for a given target).

The approximation of the waveguide scattering problem by a superposition of many free-field scattering problems contains two underlying assumptions. The first is that the surface of contact between the target and the water–sediment boundary has no effect on the scattered pressure. The second neglects the possibility of multiple scattering (e.g., a portion of the incident field scatters from the target to the sediment surface and then back to the target). Williams et al. [16] consider the scattering from an aluminum cylinder on a water–sand sediment boundary. They show comparisons of a full 3D FE simulation with experimental data, an early version of the hybrid model, and a physical acoustics model (similar to the model presented here). The full 3D FE simulation does not use these assumptions and includes all relevant physics. The hybrid model and the physical acoustics model include the assumptions. The excellent agreement in their comparisons and our results here suggest that the contributions from these effects are negligible.

With $\boldsymbol{r}_i$, $\boldsymbol{r}_j$, and $\boldsymbol{r}_t$ representing source, receiver, and target locations, respectively, we define the distances $d_{ti} = |\boldsymbol{r}_t - \boldsymbol{r}_i|$ and $d_{jt} = |\boldsymbol{r}_j - \boldsymbol{r}_t|$. Here, the actual source (receiver) corresponds to $i = 0$ ( $j = 0$) and its images have $i > 0$ ( $j > 0$). The propagation time along the ray joining the $i^{\text{th}}$ source and target is then $t_{ti} = d_{ti} / c_1$; and likewise, the propagation time from the target to the $j^{\text{th}}$ receiver is $t_{jt} = d_{jt} / c_1$. The contribution of the $i^{\text{th}}$ source and the $j^{\text{th}}$ receiver to the spectrum of the total scattered signal is then

$$P_{ij}(\omega) = \left[\frac{U^{n(j)}L^{m(j)}\exp(i\omega t_{jt})}{d_{jt}}\right]\left[\frac{U^{n(i)}L^{m(i)}\exp(i\omega t_{ti})}{d_{ti}}\right] f(\theta,\varphi,\omega) r_0 P_{src}(\omega) \qquad (1)$$

The reflection coefficients at the upper and lower boundaries are $U(\theta_g)$ and $L(\theta_g)$, where $\theta_g$ is a local grazing angle and is given by either $\cos(\theta_i) = R_{ti} / d_{ti}$ or $\cos(\theta_j) = R_{jt} / d_{jt}$. Here, we define the horizontal distances $R_{ti} = |\boldsymbol{R}_t - \boldsymbol{R}_i|$ and $R_{jt} = |\boldsymbol{R}_j - \boldsymbol{R}_t|$ with $\boldsymbol{R} = x\,\boldsymbol{e}_x + y\,\boldsymbol{e}_y$ such that $\boldsymbol{e}_x$ and $\boldsymbol{e}_y$ are Cartesian unit vectors. The $m(i)$, $n(i)$, $m(j)$, and $n(j)$ exponents enumerate the number of interactions a ray has with a given boundary. In Eq. (1), the scattering process is seen to be a multiplication of a free-field scattering amplitude $f(\theta_{ij},\phi_{ij},\omega)$ with the frequency spectrum of the

transmitted wave packet, $P_{src}(\omega)$. The target-centered angles $\theta_{ij}$, and $\phi_{ij}$ are related to $\theta_i$ and/or $\theta_j$ and may also depend on the orientation of the target within the waveguide. Finally, $r_0$ is a reference distance associated with the calibration of the source.

Under typical operational conditions for a short-range SAS platform, the air–water interface can be ignored, because paths that interact with this interface are either removed by time-gating the received signals or suppressed by the directivity patterns of the source and receiver. In addition, the separation distance between the actual source and actual receiver is much smaller than $d_{ti}$ and $d_{jt}$, so the source and receiver can be considered to be co-located. Under these conditions, only the four ray paths associated with the actual source and receiver and their first images in the sediment contribute to the scattered pressure (i.e., $i = 0,1$ and $j = 0,1$). For simplicity, we set $d_0 = d_{t0} = d_{0t}$ and $d_1 = d_{t1} = d_{1t}$, which gives the spectrum for the scattered pressure as

$$P(\omega) = \left[\frac{f_1 \exp(i\omega t_0)}{d_0^2} + \frac{2L(\theta_2) f_2 \exp(i\omega t_2)}{d_0 d_1} + \frac{L^2(\theta_4) f_4 \exp(i\omega t_4)}{d_1^2}\right] r_0 P_{src}(\omega) \qquad (2)$$

with $t_0 = 2d_0/c_1$, $t_2 = (d_0 + d_1)/c_1$, $t_4 = 2d_1/c_1$, and the local grazing angles $\theta_2$ and $\theta_4$. The reflection coefficient for a fluid-like sediment is

$$L(\theta) = \frac{\rho \sin(\theta) - \sqrt{K^2 - \cos^2(\theta)}}{\rho \sin(\theta) + \sqrt{K^2 - \cos^2(\theta)}} \qquad (3)$$

where $\rho = \rho_2 / \rho_1$, $K = k_2 / k_1 = (1 + i\,\delta)/\nu$, and $\nu = c_2/c_1$ is a real index of refraction. Here, $c_2$, $\rho_2$, and $\delta$ are the sound speed, density, and loss parameter for the sediment, respectively. The scattering amplitudes, $f_q = f_q(\theta_{ij},\phi_{ij},\omega)$, depend on the locations of the source, receiver, and target, and target orientation (in the Fraunhoffer region, an equivalent expression with some useful angle definitions are found in Williams et al. [16, Eq. (3)]). An inverse Fourier transform of Eq. (2) then gives a generated sonar signal that includes the four primary acoustic paths for a target near an interface. The first term within the brackets of Eq. (2) is the direct path. The second term includes the two paths that interact once with the bottom. These paths are reciprocal and are associated with a bistatic scattering direction. The last term is a backscattering path with two bottom interactions.

Many of the targets deployed during PondEx10, TREX13, and BAYEX14 have cylindrical symmetry. To understand the interaction of an acoustic field with an axisymmetric target and its environment, we employed the hybrid model described in Sec. III.B. This model generates the scattering amplitude required by Eq. (2) and aids in the validation of the ray model.

The hybrid model uses a FE model to predict the scattered pressure and derivatives in the near field of a target, and then a Helmholtz integral is used to propagate the pressure to the far field. It takes advantage of the symmetry of the target by decomposing the full 3D problem into a series of independent 2D Fourier modal sub-problems. The target is embedded in water, and the entire domain is surrounded by a perfectly matched layer that serves to truncate the problem to a finite, manageable size. For the target shown in Fig. 12(b), the mesh consists of 9608 elements and 77233 degrees of freedom. Near sharp features (e.g., at corners and at the small grooves and ridges that circumscribe the target), a high number of mesh elements are required to ensure numerical convergence. During PondEx10, the speed of sound in water was estimated to be $c_1$ = 1464 m/s; it was 1530 m/s in TREX13 and GULFEX14. The density is taken to be $\rho_1$ = 1000 kg/m$^3$. To arrive at an appropriate $f(\theta,\phi,\omega)$ needed for the ray model, the target is subjected to

plane waves with angular frequency $\omega$ and an incident angle with respect to the surface normal denoted by $\phi_{cyl}$. The grazing angle of the incoming plane waves is $\theta_g = 0°$. The resulting scattered pressure and derivatives are recorded on a discrete set of points closely surrounding the target (see dashed line in Fig. 12(b)). The pressure, derivatives, and free-field Green's function are then used in a discrete form of the Helmholtz integral to propagate the scattered pressure to a receiver in the far field. The angle between the incoming wave vector and a vector connecting the target center and the receiver location is $\theta_{cyl}$. The scattered pressure was tabulated in a look-up table for the frequency range 1–30 kHz in 200-Hz increments, incident angles $\phi_{cyl}$ from –90° (tail) to 90° (nose) in 1° increments, and receiver locations defined by $\theta_{cyl}$ from 0° (backscattering) to 180° in 1° increments.

The angles $\phi_{cyl}$ and $\theta_{cyl}$ in the hybrid model need to be transformed into target-centered angles $\theta$ and $\phi$, which are needed for the ray model. The scattering amplitudes in Eqs. (1) and (2) assume a target-centered coordinate system. The translated unit vectors for the $i^{th}$ source and $j^{th}$ receiver are

$$e_i = \frac{\boldsymbol{r}_t - \boldsymbol{r}_i}{|\boldsymbol{r}_t - \boldsymbol{r}_i|}, \quad e_j = \frac{\boldsymbol{r}_j - \boldsymbol{r}_t}{|\boldsymbol{r}_j - \boldsymbol{r}_t|} \tag{4}$$

with $\boldsymbol{e}_i \bullet \boldsymbol{e}_j = -1$ corresponding to monostatic scattering. The $i^{th}$ source then has the horizontal vector $\boldsymbol{S}_i = (x_t - x_i)\boldsymbol{e}_x + (y_t - y_i)\boldsymbol{e}_y$, and an angular location $\alpha$ in the $xy$-plane given by

$$\alpha = \beta, \quad \text{if } y_i \geq y_t \text{ and } x_i \geq x_r, \tag{5a}$$
$$\alpha = \pi - \beta, \quad \text{if } y_i \geq y_t \text{ and } x_i < x_t, \tag{5b}$$
$$\alpha = -\beta, \quad \text{if } y_i < y_t \text{ and } x_i \geq x_r, \tag{5c}$$
$$\alpha = -(\pi - \beta), \quad \text{if } y_i < y_t \text{ and } x_i < x_t, \tag{5d}$$

where $\cos(\beta) = |x_t - x_i| / S_i$ and $|\beta| \leq \pi/2$. The angles $\phi_{cyl}$ and $\theta_{cyl}$ are given by Williams et al. [14] as

$$\phi_{cyl} = \sin^{-1}(\cos\theta_g \sin\psi), \quad \theta_{cyl} = \cos^{-1}[(\cos\theta_g \cos\psi) / (1 - \cos^2\theta_g \sin^2\psi)^{1/2}], \tag{6}$$

where the axis of symmetry of an axisymmetric target is parallel to the water–sediment boundary. The grazing angle is $\theta_g$ and $\psi$ is a target rotation angle defined by $\boldsymbol{e}_{z,cyl} = \sin\psi \boldsymbol{e}_x + \cos\psi \boldsymbol{e}_y$. For a rotation of the target within its coordinate system by an angle $\alpha_t$, we then have $\psi = \alpha \pm \alpha_t$, where the choice of sign allows clockwise or counter-clockwise rotation. The construction of the look-up table has imposed the condition that $\alpha_t = 0°$ gives a broadside orientation of the target (i.e., $z_{cyl}$ is aligned with the rail).

Validation of the ray model considered two measurements from PondEx10, which involved the solid aluminum replica of the 100-mm inert UXO. In these measurements, the replica was at horizontal ranges of 5 m and 10 m from the rail. In both cases, the target was proud on the water–sediment interface. The acoustic color templates constructed from nine PondEx10 SAS data sets are shown in Figs. 17(a) and (b) and correspond to the target at horizontal ranges of 10 m and 5 m, respectively. In these figures, the replica had a broadside orientation for a rotation of 0°, 180°, and 360°. The tail (nose) of the replica is directed at the rail in the 90° (270°) orientation. The data–model comparisons in Figs. 17(a) and (b) re-affirm the validation of the

hybrid model that was demonstrated in Williams et al. [16] with a 2:1 solid aluminum cylinder. The structure centered around 90° and 270° results from the coupling of acoustic energy into elastic resonant modes of the target. Although the hybrid model is in general agreement with the data, the PondEx10 data contains noise due to reverberation from the sediment bottom. In addition, the data contains experimental error due to the manipulation of the target by the divers to collect the nine data sets. That is, divers must lift the target off the water–sediment interface, rotate it by 20°, and place it again on the sediment while maintaining buoyancy to minimize disturbance of the sediment. These experimental sources of error, which have an impact on the signal-to-noise, are not captured by the hybrid model.

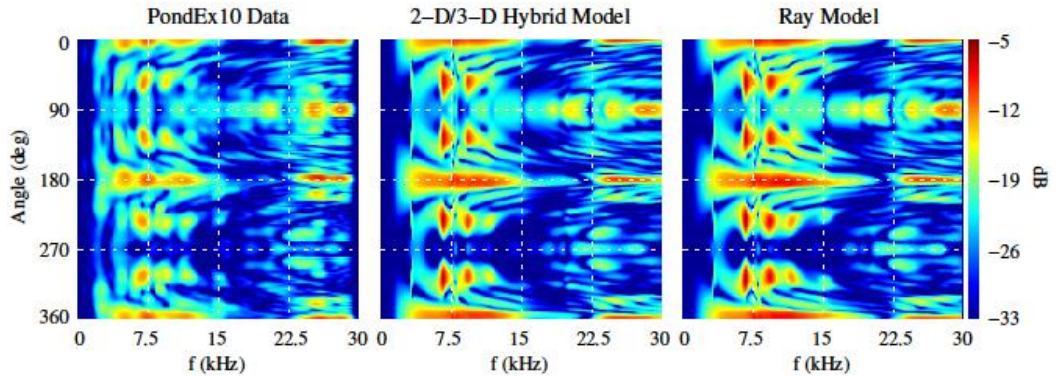


*(a) Horizontal range of 10 m*

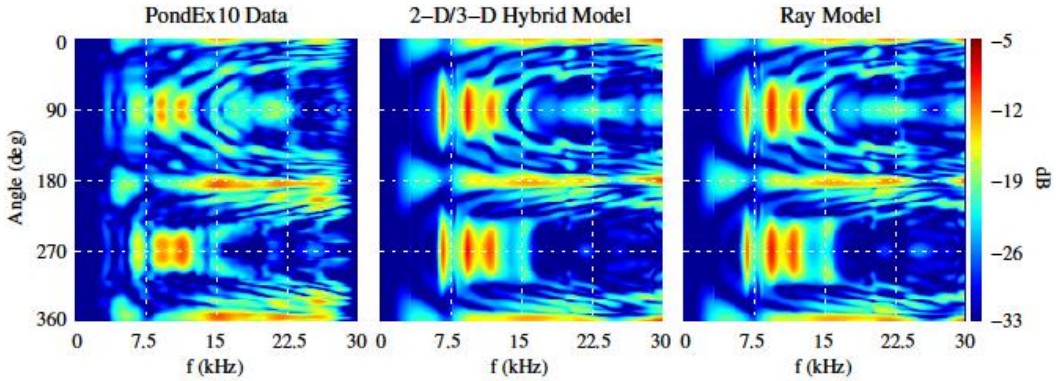


*(b) Horizontal range of 5 m*

Figure 17. *Model–model and data–model comparisons for the aluminum replica of a 100-mm bullet-shaped UXO.*

In lieu of nine simulations to model the PondEx10 data sets and the construction of acoustic color templates, the ray model simulations considered circular SAS (CSAS) with the target at the center of the path. The source and receiver were co-located, 3.8 m above a sand sediment, and the radii of the circular path was 5 m or 10 m. The angular spacing between adjacent signals in the CSAS data was 1° and 360 signals were computed. The transmitted signal was a LFM chirp with a 16-kHz carrier frequency, 30-kHz bandwidth, and 6-ms duration. Each received signal has a 30-ms duration and it was sampled at 200 kHz. To compute the scattered signals, based on Eq. (2), the scattering amplitudes $f_1$, $f_2$, and $f_4$ were obtained from a look-up table derived from the free-field hybrid model results and interpolation. The scattering amplitude is independent of range, and a single look-up table was generated with the hybrid model.

The model–model comparison in Fig. 17(a) shows good agreement, which may be anticipated as $f(\theta,\phi,\omega)$ is derived from a hybrid simulation for the target in the free field with a receiver at a 10-m range. For the target at a 5-m range, Fig. 17(b) provides the salient model–model comparison. The ray model uses the same $f(\theta,\phi,\omega)$ as the model–model comparison (Fig. 17a). Close visual inspection of the model–model comparisons shows minor differences, which can be attributed partially to the inherent smoothing from the required interpolations in both frequency and angles. It is also noted that Eqs. (1) and (2) rely on a far field assumption. The Rayleigh distance of an acoustic radiator is $d_R = k_1 D^2/2$, where $D$ is a characteristic dimension of the radiator. This distance denotes a transition from the near field to the far field. A carrier frequency of 16 kHz, speed of sound in water of 1464 m/s, and $D$ = 0.4 m (i.e., length of the target), yields $d_R$ = 5.49 m. At a 5-m range, it is anticipated that this assumption may break down.

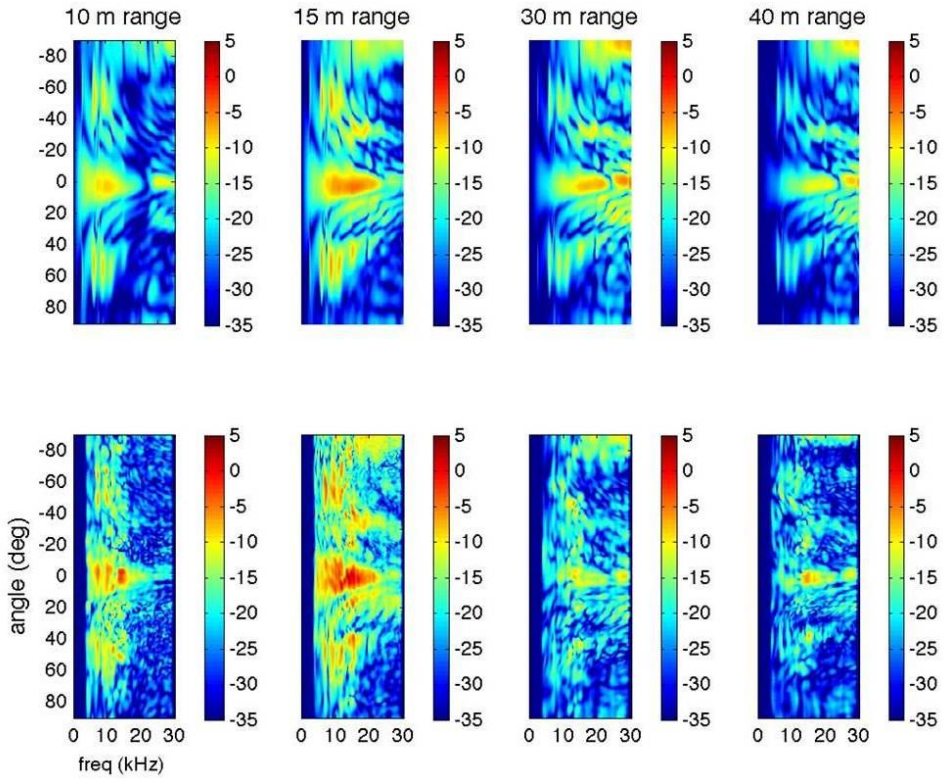


Figure 18: *Model–data comparison for scattering from a 100-mm aluminum UXO replica. (top) Ray model predictions at the horizontal range indicated above each acoustic color template. (bottom) Acoustic color templates constructed from TREX13 data.*

The acoustic ray model was exercised to predict the scattering from several targets deployed during TREX13 at various horizontal ranges. Figure 18 shows model–data comparisons for the acoustic color templates for the aluminum replica of the 100-mm UXO. The comparison suggests that the model adequately captures the TIER for this target. It is important to note that the acoustic ray model does not include sources of noise, which are present in the measurements collected in the Gulf of Mexico. Although the signal-to-noise in the data is not very high, inspection of the acoustic color templates from the model and data in Fig. 18 reveals several features visually correlated in the data and model.

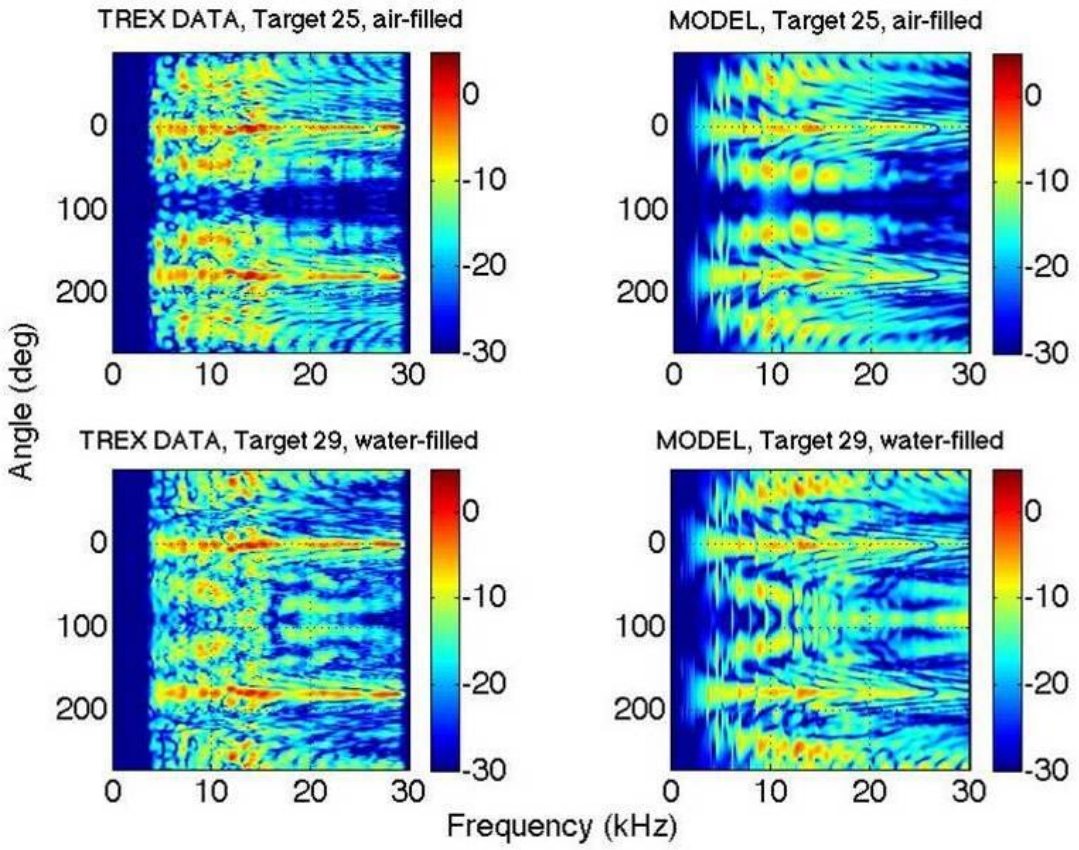


Figure 19: *Model–data comparison for scattering from targets 25 and 29. Target noses are pointing at the APL-UW rail at 90°; 0° and 180° are broadside orientations.*

Figure 19 shows the model–data comparison for targets 25 and 29, listed in Table B1, deployed at 10-m range during TREX13. These targets are geometrically identical 105-mm artillery shells. An important difference is that target 25 is known to have contained air while target 29 contained water. A striking feature that is present in both the model and TREX13 data is the low target strength for the air-filled artillery shell in comparison to the water-filled artillery shell at a 90° orientation. The internal fluid loading of the shell affects the observed TIER. This suggests that internal loading of a shell may yield observable structure in an acoustic color template, which may allow one to differentiate between an inert ordnance and an intact ordnance. Finally, the model results appear to capture the structure associated with coupling into the elastic resonant modes of the 100-mm UXO observed in the TREX13 data.

It is important to note that the two hybrid model results required separate FE runs with the associated computation time. The ray model requires only a single FE run, where afterwards calculations for different geometries and/or sediment types can be determined at high speed and high fidelity with no further FE requirement. Although the models outlined above provide a high level of fidelity in the predicted acoustic color templates for a target near an interface, the utility of the models is found in its computational efficiency. Hybrid model results, similar to those displayed in Figs. 13, 14, and 17 required 24 to 72 hours of CPU time on currently available computer systems. The computational complexity of an FE simulation is directly related to the

number of elements and DOFs in the FE mesh. As the complexity of a target increases, so must the complexity of the FE mesh. The acoustic ray model requires access to a free-field scattering amplitude, so there is an associated one-time up-front cost in its tabulation. However, once it is available, a ray model simulation requires a few CPU seconds. The salient point is that a change in the scattering geometry or environment necessarily requires a new hybrid model simulation while the ray model can re-use a previously obtained scattering amplitude.

### D. Binary Classification: Relevance Vector Machine and the Carin Kernel

In our initial investigation of target classification, we considered binary classification (i.e., target versus non-target) primarily with a Relevance Vector Machine (RVM), using a kernel presented by Carin [20, 21]. Figure 20 is a simplified diagram of the processing chain for this work. The end product of applying the processing chain to either experimental data or model-generated data is a receiver operating characteristic (ROC). Much of SERDP MR-2231 concentrated on the first two stages of the data processing chain, where the raw data are the scattered signals and the data products are the acoustic color templates. Our raw data are the isolated scattered signals from PondEx10 and TREX13 and/or simulated scattered signals from our models. Here, our feature set extraction stage computed the peak value in the magnitude of 2D cross-correlations for portions of complete acoustic color templates. Here, acoustic color templates are data products.

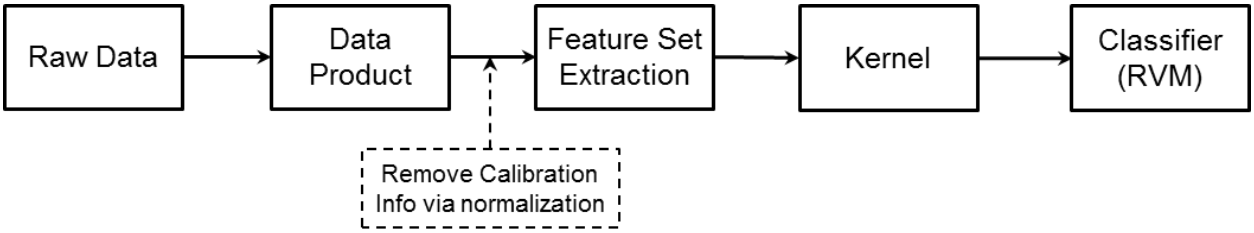


Figure 20. *Processing chain for binary classification. "Raw Data" represents either experimental or model-generated scattered acoustic signals. "Data Product" is the reduction of the raw data into some intermediate result (e.g., acoustic color template or SAS image). "Feature Set Extraction" manipulates the "Data Product" into a representation amenable to the computational "Kernel". The kernel applies mathematical transformations on the feature set to aid the separation or grouping of features by the "Classifier". The processing chain used here imposed a normalization step, which actually removed the calibration from the data.*

Recall that a ROC graph shows the probability of correctly identifying an object as a target versus identifying a non-target as a target (i.e., a false alarm). The upper left corner of a ROC graph corresponds to correctly classifying all targets as targets with no false alarms. The goal within our preliminary investigation is not developing new classifiers (the last block in Fig. 20), but to have a classifier-based metric to test how well data products derived from models compare to those derived from experimental data. One measure often applied to comparisons of ROC graphs is the area-under-the-curve (AUC), where an AUC approaching 1 is considered an excellent result.

The initial classification work used PondEx10 data. "Virtual experiments" were conducted to generate both training data and test data for nine targets and two rocks. A data set was derived

from the original data in such a way that clutter (i.e., the rock data) could be added to target data, thereby creating additional data to test the effects of nearby clutter on the binary classifier. A pass of the APL-UW tower down the rail gave data over a ~40° by 30 kHz region. Full acoustic color templates for the targets and rocks at a 10-m range were divided into 99 matrices [i.e., 11 objects with 9 (40° by 30 kHz) matrices per object]. The feature set extraction then computed the 2D cross-correlations for these 99 matrices and extracted the peak values in magnitude. The RVM classifier is typically told the number of features it should identify during training. For 19 features, the RVM identified the matrices in Fig. 21 (magenta boxes) as the most relevant for classification.

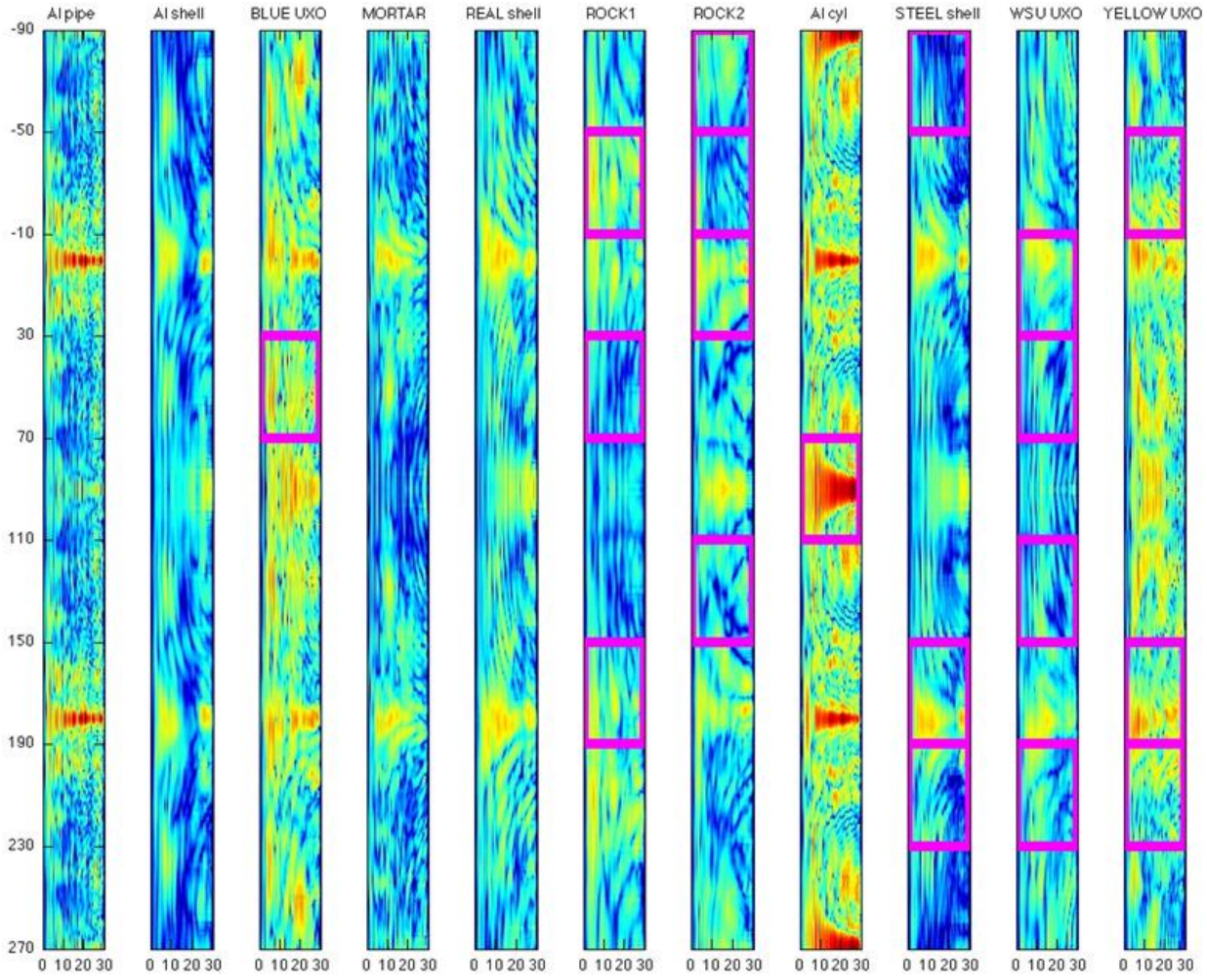


*Figure 21. Acoustic color templates for nine targets and two rocks deployed in PondEx10. The magenta boxes identify 19 matrices used by a RVM classifier to produce ROC graphs.*

In the first success in applying the processing chain (Fig. 20) to PondEx10 data, the ROC graphs (Fig. 22) indicate the performance in separating an aluminum replica of the 100-mm UXO from non-targets. The non-targets were the two rocks, a 2:1 aluminum pipe, and a solid 2:1 aluminum cylinder. Here (Fig. 22), only 72 matrices from 8 full acoustic color templates were used. The peak values in the magnitude of the 2D cross-correlations between these matrices formed the

feature set. The RVM training, using Carin's nonlinear kernel, resulted in seven matrices chosen as the most relevant for the testing phase. These seven were then cross correlated with the testing data. For one test run, testing data consisted of random draws of 500 matrices that were cross-correlated with the seven most relevant matrices. Fifty test runs were performed so that AUC statistics could be determined. Full acoustic color templates for the aluminum replica of the 100-mm UXO came from one of three sources: experimental data, model predictions from the hybrid model, or model predictions from the fast ray model. The salient point is that, using the AUC as a metric, the models gave only slightly lower performance (within the error bounds).

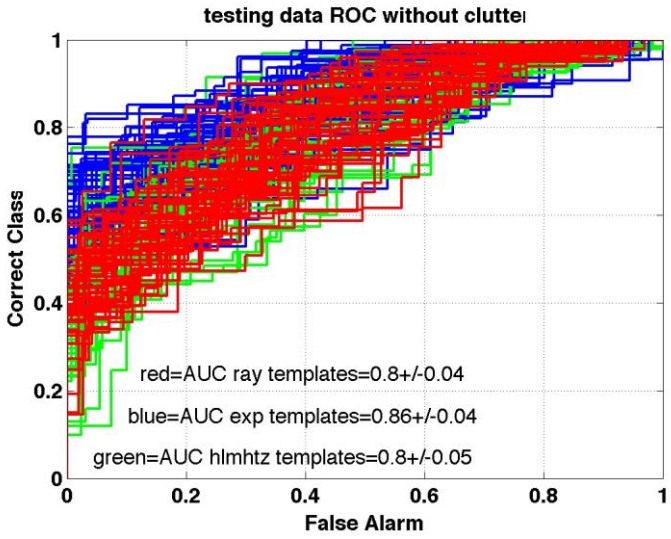


Figure 22. *ROC graphs for the classification of the solid aluminum replica of the 100-mm UXO from non-targets. The collection of non-targets included two rocks, solid 2:1 aluminum cylinder, and 2:1 aluminum pipe. The blue, red, and green curves correspond to features extracted from experimental data, fast ray model predictions, and hybrid model predictions, respectively.*

Prior to completing the investigation of the amount of data required for training, we also carried out binary classification with two additional classifiers: kernel matching pursuit (KMP) and support vector machine (SVM). These schemes again are based on the computational methods of Carin and Rabenold [20]. Training was carried out using 99 matrices derived directly from the full acoustic color templates and then testing was performed using 500 virtual experiments with no clutter and 500 virtual experiments including clutter. A testing feature derived from the data is one exemplar made via a random selection from all available PondEx10 data, where target and rock data can be superimposed. For testing feature sets with clutter, the acoustic scattering from a rock was superimposed such that the rock was approximately 1 m in cross-range from the target. Figure 23 indicates that clutter causes a significant reduction in performance. The classifiers tested with our data are classifiers used within the mine countermeasure community [21] and we treated these as "black boxes." No attempts were made to specifically tune these classifiers to the problem of UXO classification. While some tuning may be possible (e.g., removing the normalization step in Fig. 20), it is noteworthy that the isolation of target scattering via either the SAD algorithm or holographic back-projection may be an important preconditioning tool, because these methods can help mitigate the effects of nearby clutter via the spatial filtering.

(a) (b) (c)

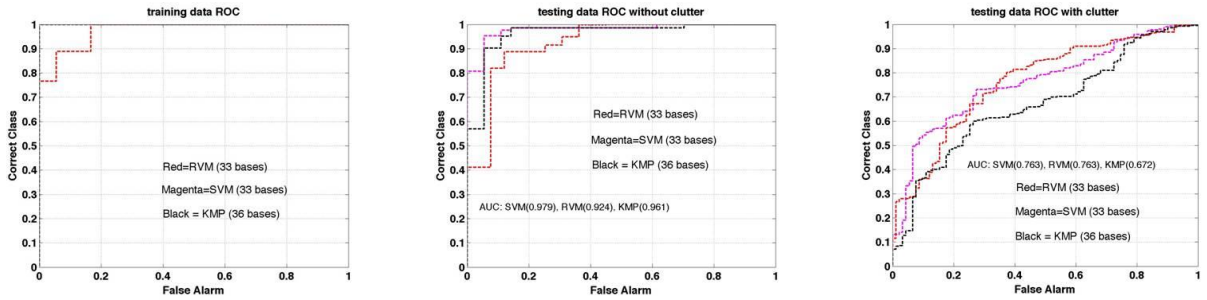


Figure 23. *ROC graphs for PondEx10 data and different classifiers. (a) Training data. (b) Test data without clutter. (c) Test data with clutter. The AUC is one metric for the quality of a classifier. While both RVM and SVM classifiers have an AUC of 0.763 when targets are in the presences of clutter, SVM may have a slight advantage if an acceptable false alarm rate cannot exceed ~30%.*

A much more extensive classification effort, using the same scheme, was recently carried out using a much larger data set generated from the TREX13 experiment. Although only 26 targets were deployed during TREX13, 49 full acoustic color templates are available because some targets were deployed at multiple ranges. Splitting a full acoustic color template into nine matrices yields 441 matrices that can be used to train and test. As this effort proceeded we examined blocks 4 and 5 from Fig. 20 in more detail. Figure 24 is a composite showing the definition of the TREX13 targets on the right and the Carin Kernel (block 4) matrix values derived using the cross correlations. The vertical axis included acoustic color templates for target 20 derived from the fast ray model predictions, while the horizontal axis used experimental acoustic color templates for target 20. The acoustic color templates listed on the axes of Fig. 24 can be cross-referenced to those displayed in Figs. B21–B33. Close examination shows that the cross correlation between the same target at different ranges can be low, again indicating the need to understand the Target-In-the-Environment-Response (TIER).

The bold red box in Fig. 24 indicates targets whose large-valued (close to one) matrix elements indicate there is significant ambiguity between them from a classification standpoint. It is important to note that all these targets have similar shape (including physical size). One might expect, and indeed we found, that the non-target/target classification within this group is difficult for the scheme being used. This difficulty translates to the ROC curves. The large red rectangular regions in Fig. 24 also show cross correlations with significant values. For example, the line denoted target 2 at a 35-m horizontal range has a high correlation with targets 20–24 at horizontal ranges 10–40 m. These significant correlations are then likely to appear as false alarms in the ROC graphs produced by the RVM.

The classification effort undertaken was to separate target 20 from all other targets, i.e., there is one target and everything else is clutter. From the 441 matrices, 44 are chosen via the RVM as

most relevant. The ROC curves and AUC obtained during the testing phase are given in Fig. 25. Use of models for target 20 results in slightly lower performance.

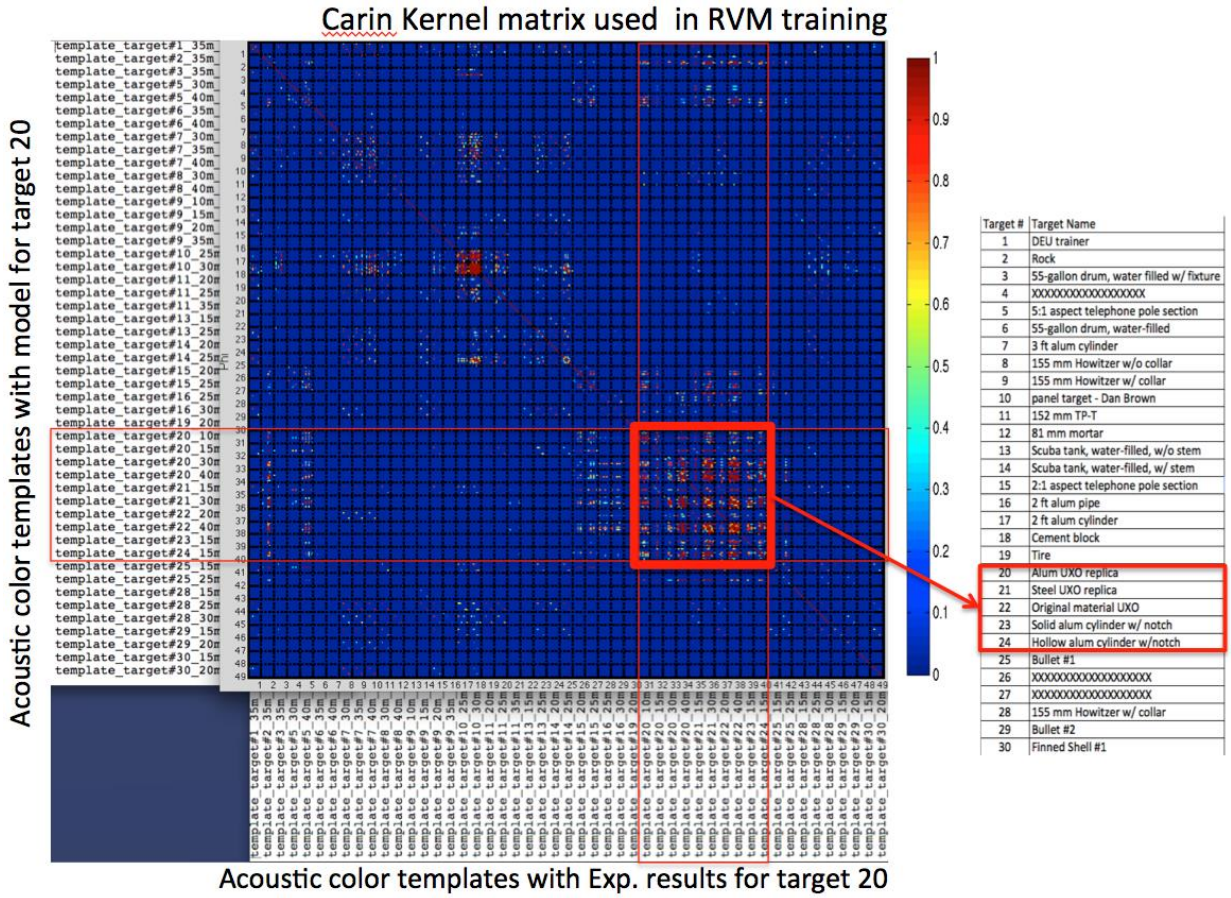


Figure 24. *Carin kernel matrix used in RVM training. The composite image shows the definition of the TREX13 targets on the right and the Carin Kernel (block 4) matrix values derived using the cross correlations of the 441 matrices. The axes correspond to the various targets deployed during TREX13 where some targets had been deployed at multiple ranges. Each small square visible in the Carin Kernel matrix is a 9×9 matrix of the cross correlation of a full acoustic color template with another full acoustic color template.*

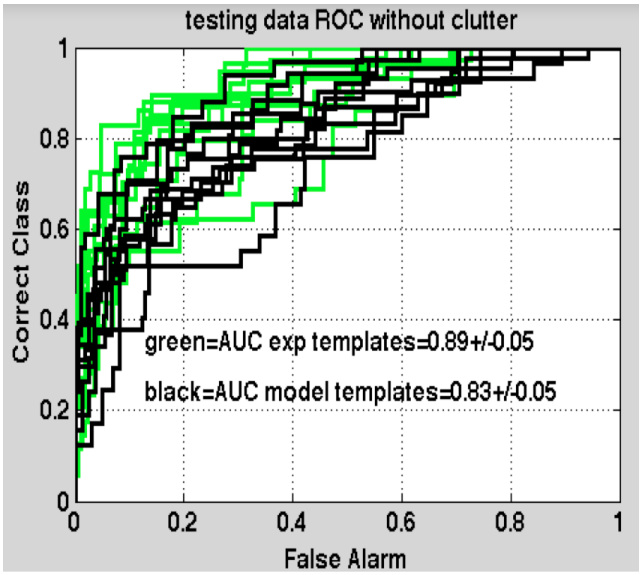


Figure 25. *ROC graphs for separating target 20 from all other targets identified along the axes of Fig. 24. Green curves are obtained from TREX13 acoustic color templates and the black curves are obtained from acoustic color templates derived from fast ray model simulations.*

## IV. Conclusion

The central hypothesis throughout our research is that the environment within which a UXO must be detected and classified alters the acoustic response of the UXO; the environment must be taken into account to develop robust detection and classification strategies. The research conducted under SERDP MR-2231 took a two-prong approach towards resolving issues identified in our previous effort (SERDP MR-1665) that affect sonar detection and classification algorithms of underwater UXO using sonar. The objectives of the reported research were to acquire sonar data on proud, partially buried, and buried targets over a broad frequency range and aspect angle range in natural environments. The targets included inert UXO, scientific targets, and clutter items. These data were reduced to an inventory of TIER signatures and were used in the validation of our acoustic scattering models. With the TIER inventory and validated models, a study of binary classification (target versus non-target) was undertaken.

The first prong of our approach involved acoustic scattering measurements from a large set of targets in natural environments. GULFEX12 was conducted in the Gulf of Mexico as an engineering field test of major modifications to the APL-UW tower-rail system and to establish an experimental protocol for TREX13 and BAYEX14. TREX13 also was performed in the Gulf of Mexico and expanded our TIER inventory of target signatures acquired during PondEx10. These data were used to validate new FE models for the 105-mm bullet-shaped targets (i.e., targets 25 and 29), the 155-mm howitzer with and without its endcap (target 8, 9, and 28), and a stemless scuba tank. The TIER inventory was then analyzed by a RVM classifier for binary target classification. The sediment in GULFEX12 and TREX13 was composed of medium-fine sand with minor amounts of shell fragments. This sediment type is consistent with the sediment in PondEx10. To investigate variations in the environment of TIER, BAYEX14 was conducted in St. Andrew's Bay, FL, which was a shallow water environment (~8 m depth) with brackish water and a sediment consisting of a mud layer over a sand basement. The mud layer was estimated to be 15–30 cm thick. Upon placing targets on the water–mud interface, all targets

buried to some extent. Smaller, heavy targets (100-mm UXO replicas, 105-mm bullet-shaped shells) were completely buried while larger targets would be partially buried.

The TIER inventory of target signatures is currently composed of the scattered signals recorded during PondEx10 and TREX13. The SAD algorithm was used with PondEx10 data to isolate the scattered signal for individual targets. The isolation of the scattered signals for targets deployed in TREX13 originally used the SAD algorithm. Recently, our spatial filtering step has been updated to use an algorithm based on holographic back-projection. One reason for switching from the SAD algorithm to holographic back-projection is that the SAD algorithm requires a Weiner noise parameter. This parameter is a free parameter and its value is simply set by trial and error. The database that underlies the TIER inventory is extensible. Work is on-going to isolate the scattered signal from the BAYEX14 data. As new signals are added to the TIER inventory, the training and testing of classification schemes can be improved.

Finite element models have been developed for several targets under SERDP MR-2231 and an ONR-funded MCM program at APL-UW. These models included aluminum and steel replicas of a 100-mm UXO, 105-mm bullet-shaped artillery shell, 155-mm howitzer with and without an endcap, solid 2:1 and 3:1 aluminum cylinders, an aluminum pipe, and a stemless scuba tank. For the 105-mm shell and the 155-mm howitzer with an endcap, the internal material was modeled as either air or water. In all, 11 FE models were exercised to produce the free-field scattered pressure on a hemisphere centered on the target, where the source and receiver are co-located. (The radius of the hemisphere was 10 m.) The simulated scattered pressure for each target was converted to a scattering amplitude and tabulated for use with the fast ray model. The FE+ray model allows us to simulate additional data for these targets at various ranges and different sediment types. The simulated data then can augment the experimental data in our classification studies. It is important to recall that the scattering amplitude contains all the information about the target, the directionality of the scatter field, and is independent of range.

Acoustic color templates derived from experimental and simulated data were used to test three classifiers available to us from the mine countermeasure community (i.e., RVM, SVM, and KMP). These classifiers are all binary classifiers, where the outcome determines whether an object is target-like or non-target-like. The results presented in this report (and elsewhere) have focused primarily on the RVM classifier. With limited experimental data, "virtual experiments" were conducted where portions of the TIER data were superposed to produce new data or augmented by simulated data. This allowed sufficient data to train and test the classifiers. While the ROC graphs in Figs 22, 23, and 25 demonstrate that these classifiers can separate targets from non-targets, the ROC graphs suggest additional work needs to be performed to understand and reduce the high false alarm rate. It is noted that the classifiers were designed with underwater mine and mine-like objects (i.e., the targets are typically larger than those used in TREX13 and BAYEX14) in mind, and we made no attempts at this time to tune the classifiers to UXO other than the standard training procedure.

Figure 20 is a basic block diagram of the processing chain used by the RVM classifier. Much of the work performed under SERDP MR-2231 and reported here focused on the first two blocks, namely, "raw data" and "data product." For our classification studies, "data product" is acoustic color templates. Improvements to the ROC graphs and the separation of targets from non-targets may be affected by supplementing the acoustic color templates with other "data products" such

as SAS images or wavelet decomposition of the data. In addition, it may be profitable to remove the normalization stage shown in Fig. 20 because the absolute target strengths for the targets deployed in TREX13 and BAYEX14 can differ by more than 10 dB. The "feature set extraction" stage used the peak values in 2D cross-correlations of 40° by 30-kHz sections of full acoustic color templates. This choice was motivated by the "kernel" block where the Carin Kernel was implemented in the RVM classifier that was available to us. Research has recently been proposed to specifically address the last three blocks in Fig. 20.

**Acknowledgment**

The experiments were conducted with additional support from the Office of Naval Research. Dr. Joseph Lopes, Dr. Jermaine Kennedy, and Dr. Raymond Lim from NSWC PCD, and Prof. Philip Marston and Dr. Timothy Marston from Washington State University contributed to various aspects of data analysis, and insights into the structures observed in the SAS images and acoustic color templates. The hybrid model predictions were provided by Dr. Aubrey España from APL-UW, who leveraged her research with Dr. Martin Nijhof from TNO (ONR Global Grant N62909-10-1-7153).

## References

[1] TP Long, "A global prospective on underwater munitions," *Mar. Technol. Soc. J.*, **43**, 5-10 (2009).

[2] ML Overfield, LC Symons, "The use of the RUST database to inventory, monitor, and assess risk from Undersea Threats," *Mar. Technol. Soc. J.*, **43**, 33-40 (2009).

[3] A Schwartz, E Brandeburg, "An overview of underwater technologies for operations involving underwater munitions," *Mar. Technol. Soc. J.*, **43**, 62–75 (2009).

[4] JA Bucaro, BH Houston, M Saniga, LR Dragonette, T Yoder, S Dey, L Kraus, L Carin, "Broadband acoustic scattering measurements of underwater unexploded ordnance (UXO)," *J. Acoust. Soc. Am.*, **123**, 738-746 (2008).

[5] JA Bucaro; H Simpson, L Kraus, LR Dragonette, T Yoder, BH Houston, "Bistatic scattering from submerged unexploded ordnance lying on a sediment," *J. Acoust. Soc. Am.*, **126**, 2315-2323 (2009)

[6] ZJ Waters, HJ Simpson, A Sarkissian, S Dey, BH Houston, JA Bucaro, TJ Yoder, "Bistatic, above-critical angle scattering measurements of fully buried unexploded ordnance (UXO) and clutter," *J. Acoust. Soc. Am.*, **132**, 3076-3085 (2012)

[7] SG Kargl, KL Williams, TM Marston, JL Kennedy, JL Lopes, "Acoustic response of unexploded ordnance (UXO) and cylindrical targets," *Proc. OCEANS 2010 MTS/IEEE*, Seattle WA, pp. 6, DOI: 10.1109/OCEANS.2010.5664392.

[8] SG Kargl, AL Espana, KL Williams, JL Kennedy, JL Lopes, "Scattering From Objects at a Water Sediment Interface: Experiment, High-Speed and High-Fidelity Models, and Physical Insight," *IEEE J. Ocean. Eng.*, DOI: 10.1109/JOE.2014.2356934, pp. 11, (2014).

[9] PT Gough, DW Hawkins, "Unified framework for modern synthetic aperture imaging algorithms," *Int. J. Imaging Syst. Technol.*, **8**, 343-358 (1997).

[10] SG Kargl, KL Williams, EI Thorsos, JL Lopes, "Bistatic synthetic aperture sonar measurements and preliminary analysis," in *Boundary Influences in High Frequency, Shallow Water Acoustics*, NG Pace and P Blondel (Eds.), University of Bath, UK, Sept., 2005, pp. 137-143.

[11] TM Marston, KL Williams, PL Marston, "Scattering resonances, filtering with reversible SAS processing, and applications of quantitative ray theory," *Proc. OCEANS 2010 MTS/IEEE*, Seattle WA, 2010.

[12] DJ Zartman, DS Plotnick, TM Marston, PL Marston, "Quasi-holographic processing as an alternative to synthetic aperture sonar," *Proc. Meet. Acoust*., Acoust. Soc. Am., **19**, pp. 5, DOI: 10.1121/1.4800881, (2013).

[13] M Zampolli, A Tesei, FB Jensen, N Malm, JB Blottman, "A computationally efficient finite element model with perfectly matched layers applied to scattering from axially symmetric objects," *J. Acoust. Soc. Am.*, **122**, 1472 (2007).

[14] M Zampolli, A Tesei, G Canepa, OA Godin, "Computing the far field scattered or radiated by objects inside layered fluid media using approximate Green's functions," *J. Acoust. Soc. Am.*, **123**, 4051 (2008).

[15] M Zampolli, AL Espana, KL Williams, SG Kargl, EI Thorsos, JL Lopes, JL Kennedy, PL Marston "Low- to mid-frequency scattering from elastic objects on a sand sea floor: Simulation of frequency and aspect dependent structural echoes", *J. Comp. Acoust*., vol. 20, p. 1240007 (14 pp.), 2012, DOI: 10.1142/S0218396X12400073.

[16] KL Williams, SG Kargl, EI Thorsos, DS Burnett, JL Lopes, M Zampolli, PL Marston, "Acoustic scattering from a solid aluminum cylinder in contact with a sand sediment: Measurements, modeling, and interpretation," *J. Acoust. Soc. Am*., **127**, 3356-3371 (2010).

[17] LM Brekhovskikh and YP Lysanov, *Fundamentals of Ocean Acoustics*, 2nd ed. New York, NY: Springer-Verlag, 1991.

[18] SG Kargl, KL Williams, and EI Thorsos, "Synthetic aperture sonar imaging of simple finite targets," *IEEE J. Ocean. Eng.*, **37**, 516–532, (2012).

[19] KL Williams, "An effective density fluid model for acoustic propagation in sediments derived from biot theory," *J. Acoust. Soc. Am*., **110**, 2276–2281, (2001).

[20] L Carin, P Rabenold, Classifier Design for Multi-aspect Low-Frequency Broadband Target Signatures, Technical Report TR-2008/01, ONR contract N00014-06-C-0026.

[21] J Stack, "Automation for underwater mine recognition: current trends and future strategy," *Proc. SPIE - Int. Soc. Opt. Eng*., **8017**, 80170K-1 – 80170K-21, (2011).

## Appendix A: GULFEX12 Target Configurations

Illustrations for the six target configurations deployed during GULFEX12 (Fig. A1) are labeled to identify the following targets: 155-mm howitzer shell (**HS**), aluminum replica of a 100-mm artillery shell (**AL UXO**), solid 2:1 aluminum cylinder (**AL CYL**), 105-mm artillery shells with a bullet shape (**Bullet**), Mark 82 destructor (**MK82**), Diver Evaluation Unit (**DEU**), water-filled vinyl bladder (**bladder**), and 105-mm UXO with fins (**FS**).

Target configuration 1 is depicted in Fig. A1(a). Several of the recorded data sequences were collected during diagnostic testing of the APL-UW source, NSWC PCD source, and low-frequency receiving array. For some tests, the tower remained stationary. In particular, a TC-4013 hydrophone was placed 2 m from the APL-UW or NSWC PCD source and the projected signal recorded. The APL-UW source projected a 1–30-kHz LFM chirp with a 6-ms duration, and the NSWC PCD source projected a 10–50-kHz chirp with a 6-ms duration. The TC-4013 hydrophone was recorded on a spare channel of the STMS-2 electronics package. The pulse replica for the APL-UW source was compared to a historic waveform, and the new waveform was found to be in good agreement. The signature for the NSWC PCD source provided the pulse replica needed for pulse compression. After recording the projected signals, the TC-4013 hydrophone was replaced by a F41 omni-directional hydrophone. The F41 hydrophone was mounted securely to the faceplate of the APL-UW tower near the 6-channel low-frequency receiving array. This provided a means to record the scattered signal on an additional independent receiver, and permitted a comparison of SAS images created with data from the 6-channel receiving array and the F41 hydrophone. As discussed in Sec. II.A, "ghost images" were observed in SAS images created from data collected with the F41 hydrophone. This gave additional support that the 6-channel low-frequency receiving array was functioning properly.

Target configuration 2 is an extension of target configuration 1, where an additional aluminum replica of the real 100-mm UXO has been inserted at a 10-m range. This target configuration (Fig. A1b) was used primarily in experiments involving time reversal techniques. These experiments were performed by other organizations participating in GULFEX12. SAS data for each source were recorded to aid those researchers in localizing the targets within the target field and to aid the alignment of the sources and receiving array.

Target configuration 3 (Fig. A1c) was again used in time reversal experiments. The significance of this target configuration is that the aluminum replicas of the 100-mm real UXO were moved to 5-m and 7-m horizontal ranges. As with target configuration 2, SAS data were collected principally to aid time reversal experiments. It is noted that the left target at the 5-m location is flush buried and oriented with its nose pointing towards the APL-UW rail, while the right target is at a –50º rotation and proud on the surface. In Table A3, the annotation "Haari array is firing" recorded that a LF source used in a reverberation experiment was transmitting and could possibly corrupt data in the 3–6-kHz frequency band.

Target configuration 4 (Fig. A1d) extended target configuration 3 by the insertion of a water-filled vinyl bladder. The material properties of vinyl are close to those of water, and hence the bladder should be transparent to the SAS transmissions. Images generated from the collected SAS data confirmed that the scattering from the bladder was too weak to be detectable with our system. Thus, a vinyl bladder may be used in the design of targets with specified target strengths

(e.g., the bladder could contain a gel with a known void fraction of stabilized microbubbles to tailor the target strength).

Target configuration 5 (Fig. A1e) extended target configuration 4 by placing two howitzer shells at a 40-m horizontal range. These shells were embedded into the sediment at oblique angles with the nose buried in the sand and the tail in the water column. Nearly half of the howitzer shell was below the sediment interface. This target configuration was used primarily to test changes to the experimental protocol to remove "ghost images" in the data.

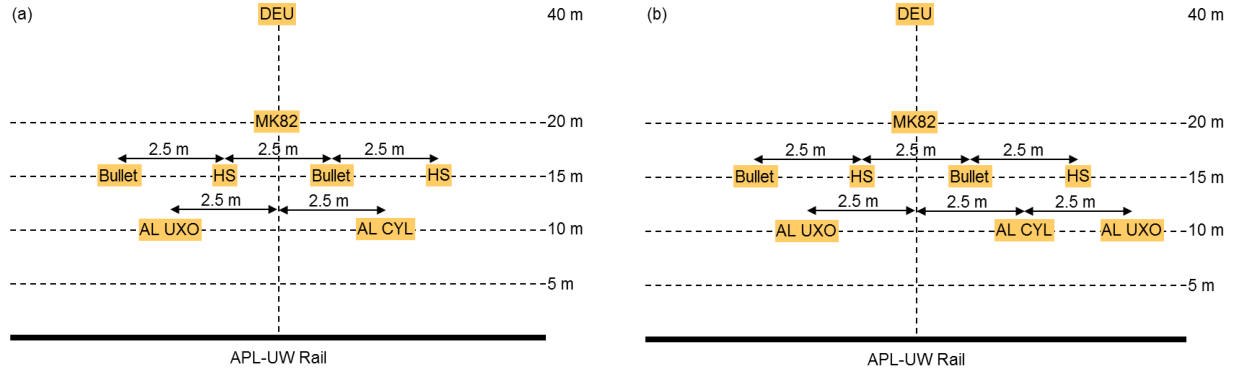


*(a) Target configuration 1*




*(b) Target configuration 2*

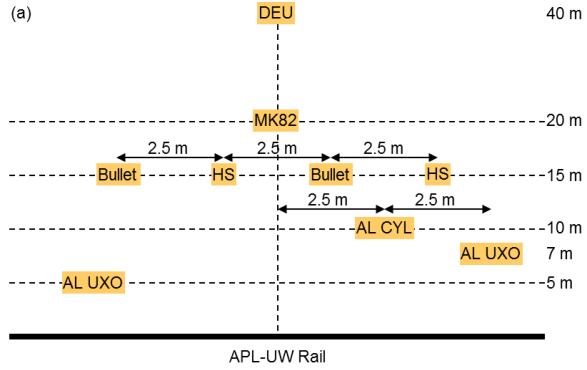


*(c) Target configuration 3*

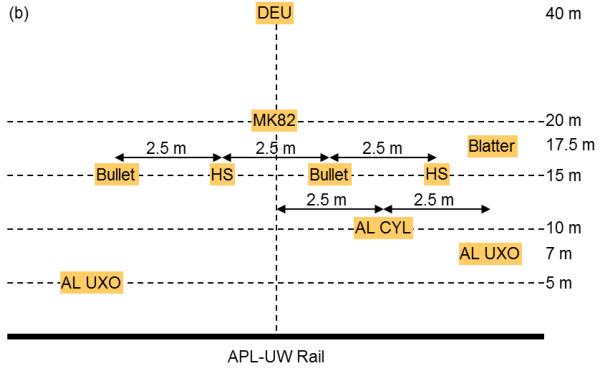


*(d) Target configuration 4*

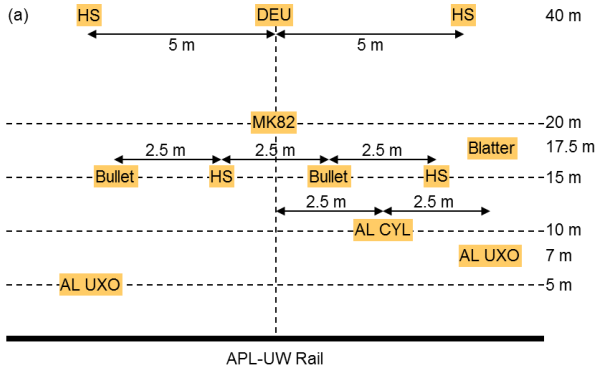


*(e) Target configuration 5*

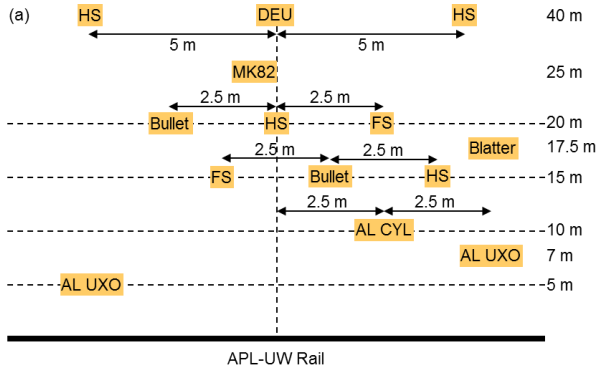


*(f) Target configuration 6*

Figure A1. *Target configurations deployed during GULFEX12. Not drawn to scale.*

Target configuration 6 was the final deployment (Fig. A1f). The recorded data demonstrate that the modified experimental protocol, where the NSWC PCD source is disconnected from its electronics, suppresses the "ghost images" in SAS images. For this data, the APL-UW source projected a 6-ms, 1–30-kHz LFM chirp with a 0.5 $V_{rms}$ input to the power amplifier. The array was tilted at a 15º depression angle. The targets at 5 m and 7 m horizontal ranges were used in an earlier experiment. These targets are not sufficiently ensonified at this depression angle, so imaging these targets is not possible.

Tables A1–A7 contain information for each data sequence. The + and – directions denote a west-to-east and east-to-west movement of the APL-UW tower, respectively. If a direction is not indicated, the tower is stationary. The third column lists the depression angle for the sources and receivers. This angle is then the incident grazing angle for the acoustic axes of the sources and receivers. The columns labeled by 5, 7, 10, 15, and 20 m are the horizontal ranges to the deployed targets, and the listed angle is a rotation angle. Rotation angles are in a clockwise manner.

| Seq. # | Dir. | Angle (deg) | Amp. ($V_{rms}$) | 10 m (deg) | 15 m (deg) | 20 m (deg) | Comment |
|---|---|---|---|---|---|---|---|
| 2 | + | 15 | 0.500 | –80, 0 | –80 | 0 | Tower stuck at east end. No data. L6 amplifier channel flipped – bad. |
| 4 | + | 15 | 0.500 | –80, 0 | –80 | 0 | L6 amplifier channel flipped – bad. |
| 6 | + | 15 | 0.500 | –80, 0 | –80 | 0 | L6 amplifier channel flipped – bad. |
| 8 | + | 15 | 0.125 | –80, 0 | –80 | 0 | L6 amplifier off for first ~5 pings. L6 amplifier channel flipped – bad. |
| 10 | + | 15 | 0.500 | –80, 0 | –60 | 0 | Intentionally flipped L6 output. Phase issue correction. |
| 11 | | 20 | 0.500 | –80, 0 | –40 | 10 | No motion, Stave 1 only (white). |
| 12 | | 20 | 0.500 | –80, 0 | –40 | 10 | No motion, Stave 2 only (blue). |
| 13 | | 20 | 0.500 | –80, 0 | –40 | 10 | No motion, Stave 3 only (violet). |
| 14 | | 20 | 0.500 | –80, 0 | –40 | 10 | No motion, Stave 4 only (green). |
| 15 | + | 20 | 0.500 | –80, 0 | –40 | 10 | |
| 16 | + | 20 | 0.500 | –80, 0 | –40 | 10 | 100 m extension cables removed. |
| 17 | | 20 | 0.025 | –80, 0 | –40 | 10 | Calibration. Ext. cables removed. |
| 18 | | 20 | 0.050 | –80, 0 | –40 | 10 | Calibration. Ext. cables removed. |
| 19 | | 20 | 0.100 | –80, 0 | –40 | 10 | Calibration. Ext. cables removed. |
| 20 | | 20 | 0.200 | –80, 0 | –40 | 10 | Calibration. Ext. cables removed. |
| 21 | | 20 | 0.025 | –80, 0 | –40 | 10 | Calibration. Ext. cables removed. |
| 22 | | 20 | 0.050 | –80, 0 | –40 | 10 | Calibration. Ext. cables removed. |
| 23 | | 20 | 0.100 | –80, 0 | –40 | 10 | Calibration. Ext. cables installed. |
| 24 | | 20 | 0.200 | –80, 0 | –40 | 10 | Calibration. Ext. cables installed. |
| 37 | + | 15 | 0.500 | –50, 0 | –80 | 10 | 100 m extension cables installed. Something wrong? Signal dropout. |
| 39 | + | 15 | 0.500 | –50, 0 | –60 | 10 | Bad signal level. |
| 41 | + | 15 | 0.500 | –50, 0 | –60 | 10 | Error Checking. |
| 42 | + | 15 | 0.500 | –50, 0 | –60 | 10 | 30 ms window. |
| 43 | – | 15 | 0.500 | –50, 0 | –60 | 10 | Reconnected Cables (dive ops). Tower did not move. |
| 44 | – | 15 | 0.500 | –50, 0 | –60 | 10 | |
| 45 | | 15 | 0.500 | –50, 0 | –60 | 10 | Tower at 11.5 m to test dropout. |
| 46 | – | 15 | 0.500 | –50, 0 | –60 | 10 | |
| 47 | + | 15 | 0.500 | –50, 0 | –60 | 10 | Half speed test. Tower speed 2.5 cm/s. 1 Hz ping rate (1 ping per second). |
| 48 | – | 15 | 0.500 | –50, 0 | –60 | 10 | Half speed. 70 ms window. |
| 49 | + | 15 | 0.500 | –50, 0 | –80 | 10 | Half speed. Dolphin noises? |
| 51 | + | 15 | 0.500 | –50, 0 | –60 | –90 | Half speed. Dolphin noises? |
| 53 | + | 15 | 0.500 | –50, 0 | –40 | –70 | Half speed. Listen on F41. |
| 55 | + | 15 | 0.500 | –50, 0 | –20 | –50 | Half speed. Listen on F41 from now on. |
| 57 | + | 15 | 0.500 | –50, 0 | 0 | –30 | Half speed. |
| 59 | + | 15 | 0.500 | –50, 0 | 20 | 0 | Half speed. |
| 61 | + | 15 | 0.500 | –50, 0 | 40 | 20 | Half speed. Divers in water. |
| 63 | + | 15 | 0.500 | –50, 0 | 60 | 50 | Half speed. |
| 65 | + | 15 | 0.500 | –50, 0 | 80 | 80 | Half speed. |

Table A1. *Notes for GULFEX12 target configuration 1 with APL-UW source. Nose of targets pointed at the rail for –90º. For the 10-m range, angles are for the targets from the left to right. All targets were proud. DEU at 40 m is not rotated and is in a broadside orientation.*

| Seq. # | Angle (deg) | Amp. ($V_{rms}$) | 10 m (deg) | 15 m (deg) | 20 m (deg) | Comment |
|---|---|---|---|---|---|---|
| 3 | 15 | 1.000 | –80, 0 | –80 | 0 | Intermittent transmission |
| 5 | 15 | 1.000 | –80, 0 | –80 | 0 | |
| 7 | 15 | 1.000 | –80, 0 | –80 | 0 | |
| 9 | 15 | 0.295 | –80, 0 | –60 | 0 | z-switch-220 on L2 amplifier. Heavy rain (broadband noise) |
| 25 | 20 | 1, –19 dB | –80, 0 | –40 | 10 | Calibration, ~15º off beam center (0.5 m offset, 2 m out.) |
| 26 | 20 | 1, –9 dB | –80, 0 | –40 | 10 | Calibration, ~15º off beam center (0.5 m offset, 2 m out.) |
| 27 | 20 | 1, –12 dB | –80, 0 | –40 | 10 | Calibration, ~15º off beam center (0.5 m offset, 2 m out.) |
| 28 | 20 | 1, –15 dB | –80, 0 | –40 | 10 | Calibration. Center of attenuation. (untrusted) |
| 29 | 20 | 1, –9 dB | –80, 0 | –40 | 10 | Calibration. Center of attenuation. (untrusted) |
| 30 | 20 | 1, –12 dB | –80, 0 | –40 | 10 | Calibration. Center of attenuation. (untrusted) |
| 31 | 20 | 1, –15 dB | –80, 0 | –40 | 10 | Calibration. Center of attenuation. (untrusted) |
| 32 | 20 | 1, –13 dB | –80, 0 | –40 | 10 | Calibration. Center of attenuation. (untrusted) |
| 33 | 20 | 1, –10 dB | –80, 0 | –40 | 10 | Calibration. Center of attenuation. (untrusted) |
| 34 | 20 | 1, –12 dB | –80, 0 | –40 | 10 | Calibration. New Attenuator. |
| 35 | 20 | 1, –15 dB | –80, 0 | –40 | 10 | Calibration. New Attenuator (close). |
| 36 | 20 | 1, –21 dB | –80, 0 | –40 | 10 | Calibration. New Attenuator (good). |
| 38 | 15 | 1, –9 dB | –50, 0 | –80 | 10 | |
| 40 | 15 | 1, –9 dB | –50, 0 | –60 | 10 | |
| 50 | 15 | 1, –9 dB | –50, 0 | –80 | 10 | Half speed. Possible dolphin noises. |
| 52 | 15 | 1, –9 dB | –50, 0 | –60 | –90 | Half speed. |
| 54 | 15 | 1, –9 dB | –50, 0 | –40 | –70 | Half speed. Listening on F41. |
| 56 | 15 | 1, –9 dB | –50, 0 | –20 | –50 | Half speed. |
| 58 | 15 | 1, –9 dB | –50, 0 | 0 | –30 | Half speed. |
| 60 | 15 | 1, –9 dB | –50, 0 | 20 | 0 | Half speed. |
| 62 | 15 | 1, –9 dB | –50, 0 | 40 | 20 | Half speed. Divers in water for 1st minute. |
| 64 | 15 | 1, –9 dB | –50, 0 | 60 | 50 | Half speed. |
| 66 | 15 | 1, –9 dB | –50, 0 | 80 | 80 | Half speed. |

Table A2. *Notes for GULFEX12 target configuration 1 with NSWC PCD source. Nose of targets pointed at the rail for –90º. For the 10-m range, angles are for the targets from left to right. All targets were proud. Tower was moving in the – direction for all measurements except sequences 25–36 where it remained stationary. DEU at 40 m is not rotated and is in a broadside orientation.*

| Seq. # | Dir. | Source | 10 m (deg) | 15 m (deg) | 20 m (deg) |
|---|---|---|---|---|---|
| 67 | + | APL-UW | –50, 0, 0 | –20 | 80 |
| 68 | – | NSWC PCD | –50, 0, 0 | –20 | 80 |

Table A3. *Notes for GULFEX12 target configuration 2. Target rotations with respect to the APL-UW rail are given in degrees. The nose of a target pointed at the rail for –90º. For the 10-m range, the angles are for targets from the left to right. Sources were tilted at a 15º depression angle. The input to the power amplifiers for the APL-UW source had a 0.5 $V_{rms}$ amplitude, while the drive amplitude for the NSWC PCD was 1 V (–9 dB). All targets were proud. DEU at 40 m is not rotated and is in a broadside orientation.*

| Seq. # | Dir. | 5 m (deg) | 7 m (deg) | 10 m (deg) | 15 m (deg) | 20 m (deg) | Comment |
|---|---|---|---|---|---|---|---|
| 467 | + | –90 | –50 | 0 | –20 | 80 | Haari array is firing and a small boat arrived. |
| 468 | – | –90 | –50 | 0 | –20 | 80 | Haari array is firing and a small boat arrived. |
| 469 | + | –90 | –50 | 0 | –20 | 80 | Haari array is firing. |
| 470 | – | –90 | –50 | 0 | –20 | 80 | |
| 471 | + | –90 | –50 | 0 | –20 | 80 | |

Table A4. *Notes for GULFEX12 target configuration 3. The nose of a target pointed at the rail for –90º. The target at the 5-m line was buried flush with the sediment interface and all other targets are proud. Only the APL-UW source was used as a transmitter.*

| Seq. # | Dir. | 5 m (deg) | 7 m (deg) | 10 m (deg) | 15 m (deg) | 20 m (deg) |
|---|---|---|---|---|---|---|
| 472 | – | –90 | –50 | 0 | –40 | 80 |
| 472 | + | –90 | –50 | 0 | 70 | 80 |

Table A5. *Notes for GULFEX12 target configuration 4. The nose of a target pointed at the rail for –90º. The input to the power amplifiers for the APL-UW source had a 0.5 $V_{rms}$ amplitude. It was tilted at a 15º depression angle. The target at the 5-m line was buried flush with the sediment interface. All other targets were proud. The alignment string was not symmetric across the frame, which resulted in a nominal rotation angle of ~70º for sequence 472. DEU at 40 m is not rotated and is in a broadside orientation.*

| Seq. # | Dir. | Source | 5 m (deg) | 7 m (deg) | 10 m (deg) | 15 m (deg) | 20 m (deg) | Comment |
|---|---|---|---|---|---|---|---|---|
| 488 | – | NSWC | –90 | –50 | 0 | 40 | 0 | |
| 489 | + | APL | –90 | –50 | 0 | 40 | 0 | |
| 490 | – | NSWC | –90 | –50 | 0 | 60 | 20 | |
| 491 | + | APL | –90 | –50 | 0 | 60 | 20 | |
| 492 | – | NSWC | –90 | –50 | 0 | 80 | 40 | |
| 493 | + | APL | –90 | –50 | 0 | 80 | 40 | |
| 494 | – | NSWC | –90 | –50 | 0 | 20 | 60 | |
| 495 | + | APL | –90 | –50 | 0 | 20 | 60 | |
| 496 | – | NSWC | –90 | –50 | 0 | –80 | 60 | |
| 497 | + | APL | –90 | –50 | 0 | –80 | 60 | |
| 498 | – | APL | –90 | –50 | 0 | –80 | 60 | NSWC equipment ON. |
| 499 | + | APL | –90 | –50 | 0 | –80 | 60 | NSWC equipment OFF. |
| 500 | – | APL | –90 | –50 | 0 | –60 | 40 | Cable disconnected. Shorted. |
| 501 | + | APL | –90 | –50 | 0 | –40 | 20 | Cable disconnected. Shorted. |
| 502 | – | APL | –90 | –50 | 0 | –20 | 0 | Cable disconnected. Shorted. |
| 503 | + | APL | –90 | –50 | 0 | 0 | –20 | Cable disconnected. Shorted. |
| 504 | – | APL | –90 | –50 | 0 | 20 | –40 | Cable disconnected. Shorted. |
| 505 | + | APL | –90 | –50 | 0 | 40 | –60 | Cable disconnected. Shorted. |
| 506 | – | APL | –90 | –50 | 0 | 60 | –80 | Cable disconnected. Shorted. |
| 507 | + | APL | –90 | –50 | 0 | 80 | –100 | Cable disconnected. Shorted. |
| 508 | – | APL | –90 | –50 | 0 | 80 | –100 | Cable disconnected. Shorted. |
| 509 | + | APL | –90 | –50 | 0 | 60 | –100 | Cable disconnected. Shorted. |
| 510 | – | APL | –90 | –50 | 0 | 40 | –100 | Cable disconnected. Shorted. |
| 511 | + | APL | –90 | –50 | 0 | 20 | –100 | Cable disconnected. Shorted. |
| 512 | – | APL | –90 | –50 | 0 | 0 | –100 | Cable disconnected. Shorted. |
| 513 | + | APL | –90 | –50 | 0 | –20 | –100 | Cable disconnected. Shorted. Program error. First ~100 pings corrupted. |
| 514 | – | APL | –90 | –50 | 0 | –20 | –100 | Cable disconnected. Shorted. |
| 515 | + | APL | –90 | –50 | 0 | –40 | –100 | Cable disconnected. Shorted. |
| 516 | – | APL | –90 | –50 | 0 | –60 | –100 | Cable disconnected. Shorted. Program error. First ~100 pings corrupted. |
| 517 | + | APL | –90 | –50 | 0 | –80 | –100 | Cable disconnected. Shorted. Program error. First ~100 pings corrupted. |

Table A6. *Notes for GULFEX12 target configuration 5. The nose of a target pointed at the rail for 0º. The target at the 5-m line was buried flush with the sediment interface. All other targets were proud. Sources were tilted at a 15º depression angle. DEU at 40 m is not rotated and is in a broadside orientation.*

| Seq. # | Dir. | 5 m (deg) | 7 m (deg) | 10 m (deg) | 15 m (deg) | 20 m (deg) | 25 m (deg) |
|---|---|---|---|---|---|---|---|
| 518 | – | –90 | –50 | 0 | –80 | –80 | –80 |
| 519 | + | –90 | –50 | 0 | –60 | –60 | –50 |
| 520 | – | –90 | –50 | 0 | –40 | –40 | –50 |
| 521 | + | –90 | –50 | 0 | –20 | –20 | –50 |
| 522 | – | –90 | –50 | 0 | 0 | 0 | 0 |
| 523 | + | –90 | –50 | 0 | 20 | 20 | 20 |
| 524 | – | –90 | –50 | 0 | 40 | 40 | 40 |
| 525 | + | –90 | –50 | 0 | 60 | 60 | 60 |
| 526 | – | –90 | –50 | 0 | 80 | 80 | 80 |

Table A7. *Notes for GULFEX12 target configuration 6. The nose of a target pointed at the rail for 0º. The target at the 5-m line was buried flush with the interface. All other targets were proud. Targets at 40 m are not rotated. DEU is in a broadside orientation.*

## Appendix B: TREX13 Target Configurations

The targets were distributed into six different target configurations during TREX13. These configurations are determined by inserting targets at grid locations as shown in Fig. B1 and enumerated in Table B1. All locations were marked with tags affixed to the lightweight cords that comprised the grid except for a1.5, c1.5, i1, and i2. The latter locations, denoted with lowercase letters, were estimated by divers when targets were inserted into the target field. The grid lines are separated by 5 m in horizontal range and each line is 40 m in length, where the APL-UW rail is 42 m long. When the area shaded in light tan contained targets, the source and receiving array were aimed at the sediment with a 30º grazing angle. For the unshaded area, the grazing angle for the source and low-frequency receiving array was set to 10º. In Table B1, target field configuration 1 is abbreviated by TF1 and likewise for the others. A selection of PCB signals and SAS images, produced from the PCB signals, for each target configuration is given after Tables B2–B8.

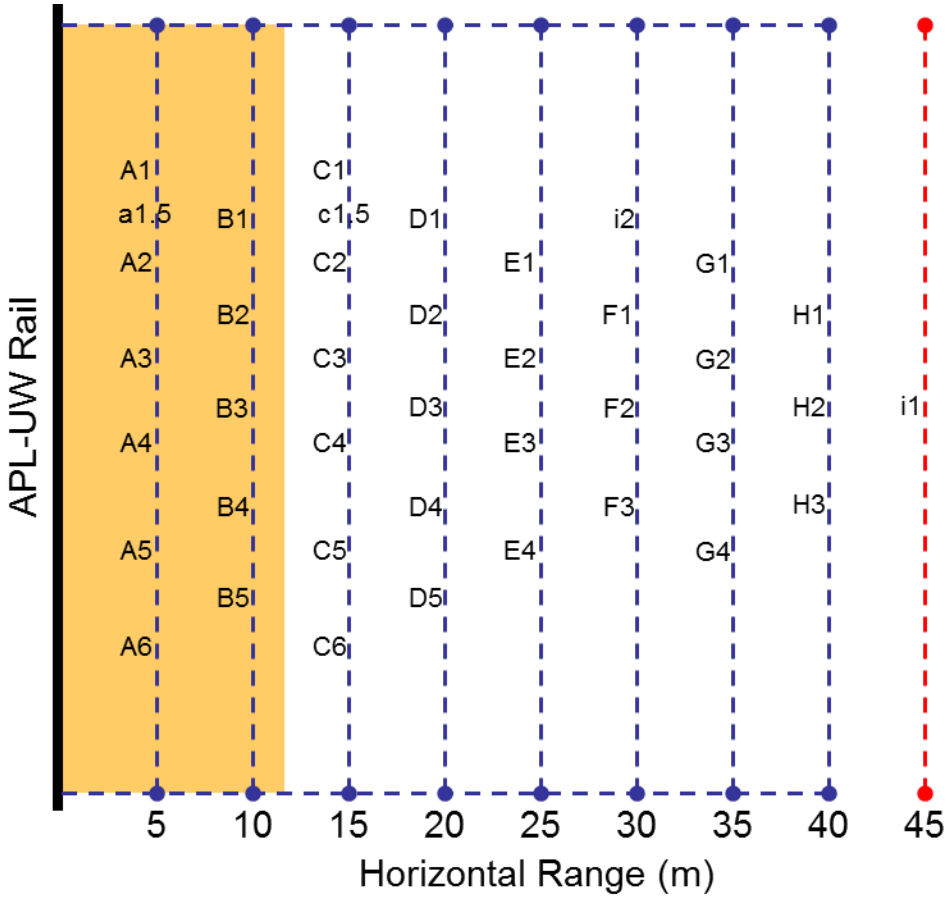


Figure B1. *Target grid installed in TREX13. The blue dotted lines represent lightweight cord that was used to establish a grid for locating targets within the target field. The red dotted line does not represent a cord in the grid. It is included as an aid to guide the eye for the alignment of location i1. The small blue dots along the upper and lower edges of the grid are the location of screw anchors that the divers inserted into the sediment to hold the lines in place. The numbered locations along a line represent a location where a target may be placed.*

| Target # | Target | TF1 | TF2 | TF3 | TF4 | TF5 | TF6 | Notes |
|---|---|---|---|---|---|---|---|---|
| 1 | Diver Evaluation Unit | G1 | G1 | H1 | | | H1 | 1 |
| 2 | Rock | G2 | G2 | H2 | | | H2 | 2 |
| 3 | 55-gallon drum | G4 | G4 | H3 | | | H3 | 3 |
| 5 | 5:1 telephone pole | H2 | F2 | E2 | | | E2 | 4 |
| 6 | 55-gallon drum | H3 | G3 | E3 | | | | 5 |
| 7 | 3:1 aluminum cylinder | G3 | H3 | F3 | | C6 | C6 | |
| 8 | 155-mm howitzer without collar | H1 | F1 | E1 | A6 | B4 | G4 | |
| 9 | 155-mm howitzer with collar | D2 | C2 | G2 | B4 | A5 | E3 | |
| 10 | Panel target from ARL-PSU | F2 | E2 | D2 | | D2 | D2 | 6 |
| 11 | 152-mm TP-T round | E1 | D1 | G1 | B3 | A4 | D4 | |
| 12 | 81-mm mortar | | | C5 | | C5 | C5 | |
| 13 | Water-filled scuba tank | E3 | C3 | G3 | | | G3 | 7 |
| 14 | Water-filled scuba tank | E4 | D4 | C4 | | C4 | C4 | 8 |
| 15 | 2:1 telephone pole | E2 | D2 | C2 | | | E1 | 4 |
| 16 | 2:1 aluminum pipe | F1 | E1 | C1 | | | | |
| 17 | 2:1 aluminum cylinder | D3 | D3 | D3 | B5 | B5 | D3 | |
| 18 | Cement block | | | | | C3 | C3 | |
| 19 | Tire | D4 | C4 | | | | E4 | |
| 20 | Aluminum replica of target 22 | C2 | H2 | F2 | B2 | A3 | F3 | |
| 21 | Steel replica of target 22 | C3 | F3 | E4 | B1 | A2 | | |
| 22 | 100-mm inert artillery shell | D1 | H1 | F1 | A3 | B1 | G2 | |
| 23 | Solid Al cylinder with notch | C6 | C6 | D5 | A1.5 | C1 | | 9 |
| 24 | Hollow Al cylinder with notch | C1 | C1 | D1 | A2 | C1.5 | | 9 |
| 25 | 105-mm bullet-shaped UXO #1 | C4 | E4 | D4 | A4 | B2 | D1 | |
| 28 | 155-mm howitzer with collar | F3 | E3 | C3 | | A6 | D5 | |
| 29 | 105-mm bullet-shaped UXO #2 | C5 | D5 | G4 | | C2 | C2 | |
| 30 | 105-mm finned shell #1 | D5 | C5 | C6 | A5 | B3 | F2 | |
| XX | Al panel from Georgia Tech | I1 | I1 | I2 | | | F1 | 10 |

Table B1. *Enumeration of targets and target field locations during TREX13. The first column is the number assigned and painted onto the targets, except for the target XX, which was not painted. The second column is the actual target. Columns TF1–TF6 represent the six target configurations. Location can be determined from Fig. B1. Last column refers to a note given below.*

1. Zinc end is tail.
2. Arrow points to nose of rock.
3. Drum is water filled with an attached fixture. Fixture is the nose of drum.
4. Painted end is the tail for TF1. Painted end is the nose for all other target fields.
5. Drum is water-filled and the opened end is the tail.
6. Panel is perpendicular to sediment and the numbered end is the tail.
7. Stem is the nose of target. Stem is removed.
8. Stem is the nose of target.
9. Notched end is the tail and tape along axis points up.

10. Square panel lies parallel to water-sediment interface.

Measurement from pivot point on the tower's mast down to the water–sediment interface is 3.3 m. Angle convention is –80º corresponds to the tail of the target pointing towards the towards rail (i.e., points south). Rotations are clockwise in 20º increments. In Table B2, the rotation angle for cylindrically symmetric targets are given in black, and targets without cylindrical symmetry, which require a 360º rotation, are in red.

| Date | Time | Seq. | Dir. | 15 m (deg) | 20 m (deg) | 25 m (deg) | 30 m (deg) | 35 m (deg) | 40 m (deg) | 45 m (deg) | Note |
|---|---|---|---|---|---|---|---|---|---|---|---|
| 4/25 | 0937 | 30 | + | –80, –80 | –80 | –80 | –80 | –80, –80 | –80 | 0 | 1,2,3 |
| 4/25 | 0953 | 31 | – | –80, –80 | –80 | –80 | –80 | –80, –80 | –80 | 0 | 2,3 |
| 4/25 | 1416 | 32 | + | –80, –80 | –80 | –80 | –80 | –80, –80 | –80 | 0 | 2,4 |
| 4/25 | 1433 | 33 | – | –80, –80 | –80 | –80 | –80 | –80, –80 | –80 | 0 | 2,4 |
| 4/25 | 1626 | 34 | + | 0, 0 | 0 | 0 | 0 | 0, 0 | 0 | 0 | 2,4,5 |
| 4/25 | 1642 | 35 | – | 0, 0 | 0 | 0 | 0 | 0, 0 | 0 | 0 | 2,4,5 |
| 4/26 | 0902 | 36 | + | –60, –60 | –60 | –60 | –60 | –60, –60 | –60 | 0 | |
| 4/26 | 0917 | 37 | – | –60, –60 | –60 | –60 | –60 | –60, –60 | –60 | 0 | |
| 4/26 | 1058 | 38 | + | –40, –40 | –40 | –40 | –40 | –40, –40 | –40 | 0 | |
| 4/26 | 1113 | 39 | – | –40, –40 | –40 | –40 | –40 | –40, –40 | –40 | 0 | |
| 4/26 | 1302 | 40 | + | –20, –20 | –20 | –20 | –20 | –20, –20 | –20 | 0 | |
| 4/26 | 1317 | 41 | – | –20, –20 | –20 | –20 | –20 | –20, –20 | –20 | 0 | |
| 4/26 | 1457 | 42 | + | 20, 20 | 20 | 20 | 20 | 20, 20 | 20 | 0 | |
| 4/26 | 1512 | 43 | – | 20, 20 | 20 | 20 | 20 | 20, 20 | 20 | 0 | |
| 4/26 | 1637 | 44 | + | 40, 40 | 40 | 40 | 40 | 40, 40 | 40 | 0 | |
| 4/26 | 1652 | 45 | – | 40, 40 | 40 | 40 | 40 | 40, 40 | 40 | 0 | 6 |
| 4/27 | 0836 | 46 | + | 60, 60 | 60 | 60 | 60 | 60, 60 | 60 | 0 | |
| 4/27 | 0851 | 47 | – | 60, 60 | 60 | 60 | 60 | 60, 60 | 60 | 0 | |
| 4/27 | 1058 | 48 | + | 80, 80 | 80 | 80 | 80 | 80, 80 | 80 | 0 | |
| 4/27 | 1113 | 49 | – | 80, 80 | 80 | 80 | 80 | 80, 80 | 80 | 0 | |

Table B2. *Notes for TREX13 target configuration 1. The source was aimed down at a 10º depression angle. The source amplitude into the power amplifiers was 0.5 $V_{rms}$. All targets were proud.*

1. Dash32 HF recorder did not start capturing data until 3 minutes into run.
2. Target 17 at D3 is broadside to the rail (i.e., 0º orientation)
3. Possible noise due to divers in water.
4. Channels 1–3 in the receiving array had 0 dB gain, and channels 4–6 had 20 dB gain.
5. Target 19 at D4 did not rotate and was left at –80º.
6. Dash32 HF recorder may have missed a couple of triggers (on the order of four).

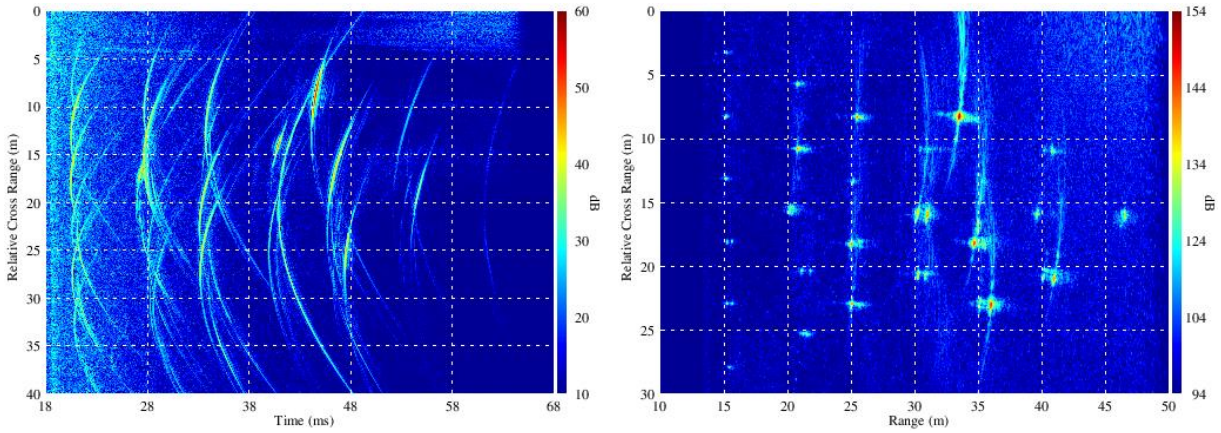


(a) PCB time signals for sequence 32 (b) SAS Image for sequence 32

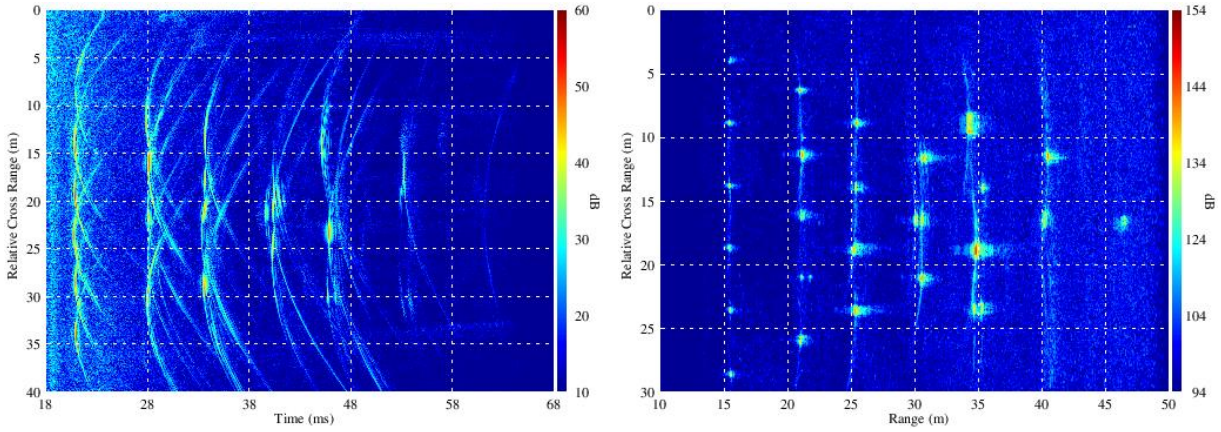


(c) PCB time signals for sequence 34 (d) SAS Image for sequence 34

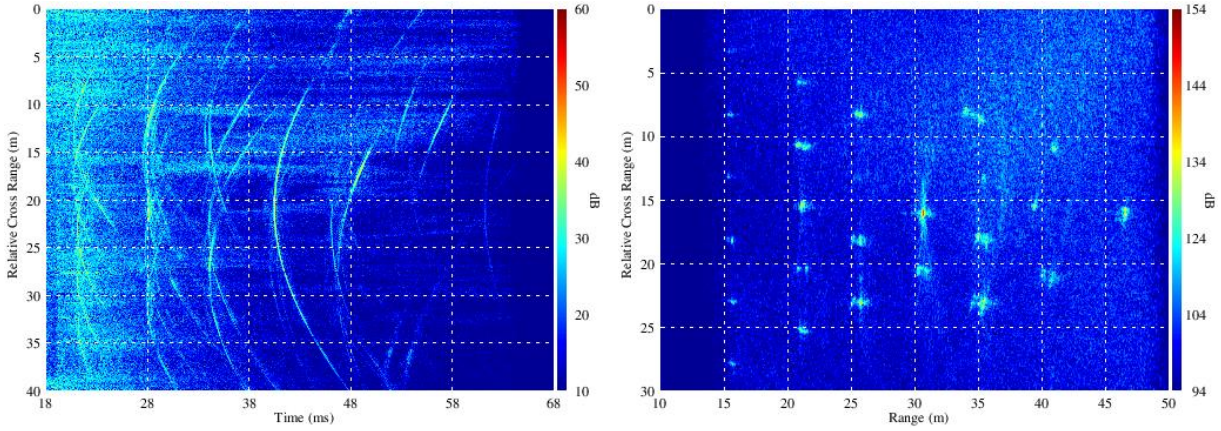


(c) PCB time signals for sequence 36 (d) SAS Image for sequence 36

Figure B2. *Initial processing step produces PCB time signals. Coherent time-domain beamforming of the PCB time signals produces a SAS image.*

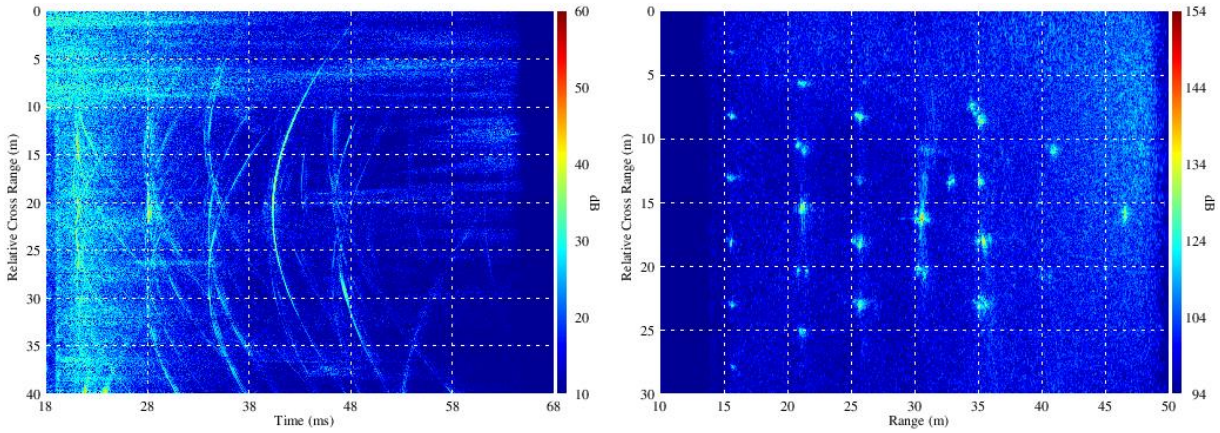


(a) PCB time signals for sequence 38 (b) SAS Image for sequence 38

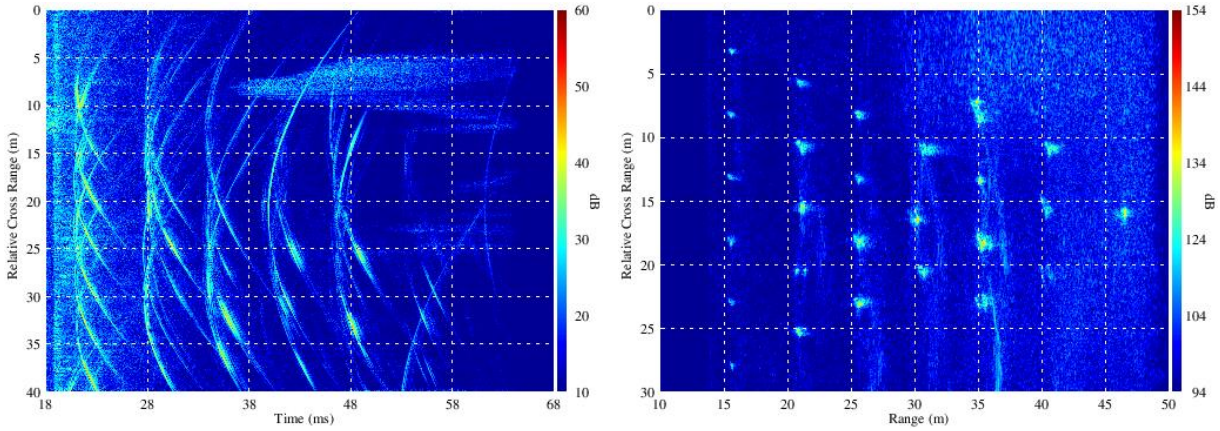


(c) PCB time signals for sequence 40 (d) SAS Image for sequence 40

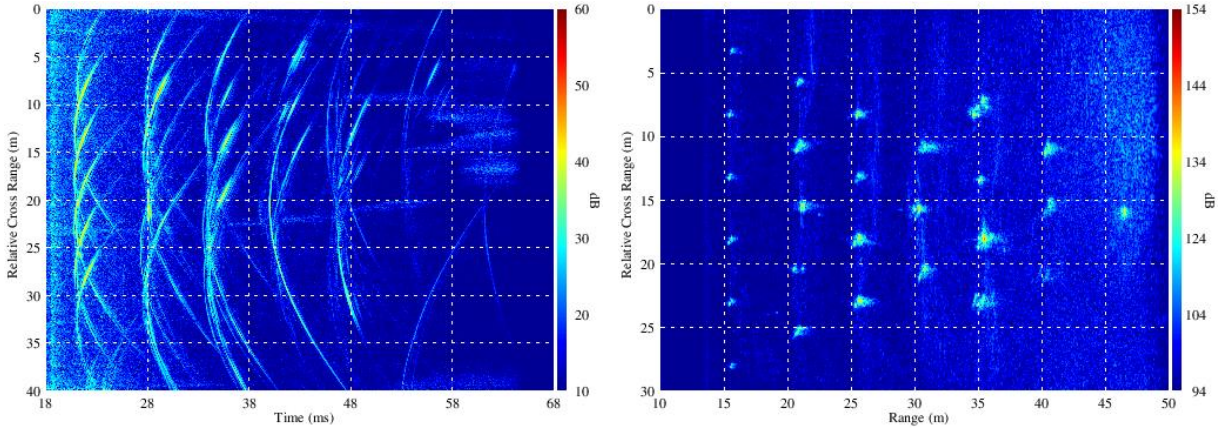


(c) PCB time signals for sequence 42 (d) SAS Image for sequence 42

Figure B3. *Initial processing step produces PCB time signals. Coherent time-domain beamforming of the PCB time signals produces a SAS image.*

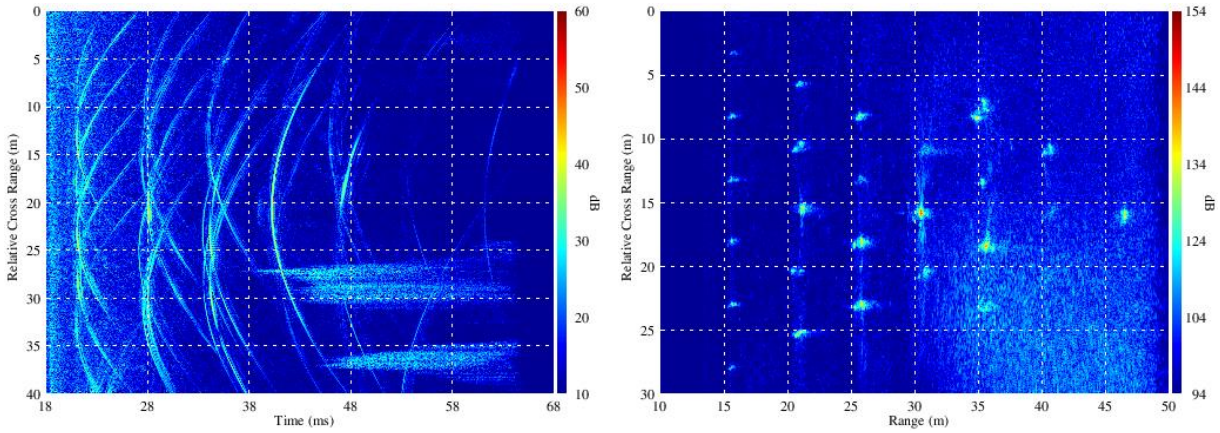


(a) PCB time signals for sequence 44 (b) SAS Image for sequence 44

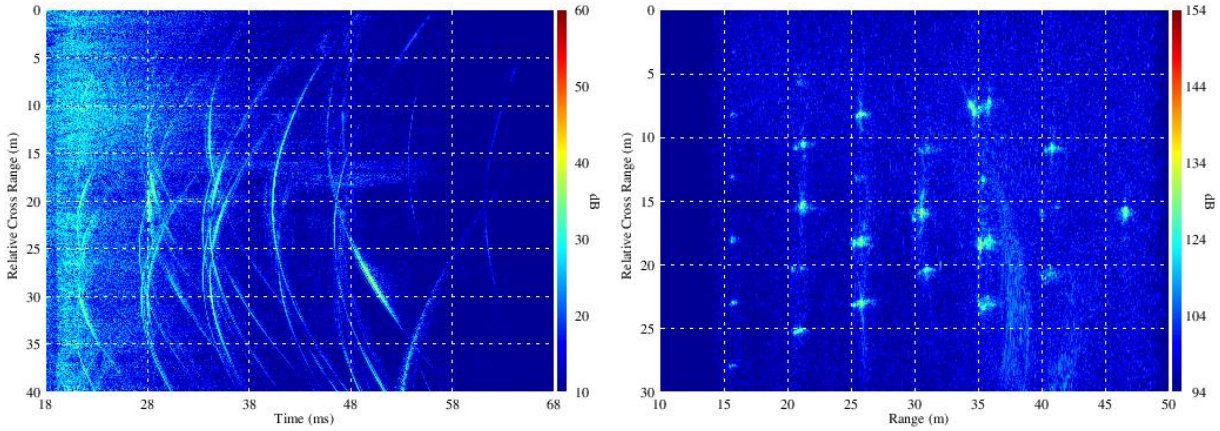


(c) PCB time signals for sequence 46 (d) SAS Image for sequence 46

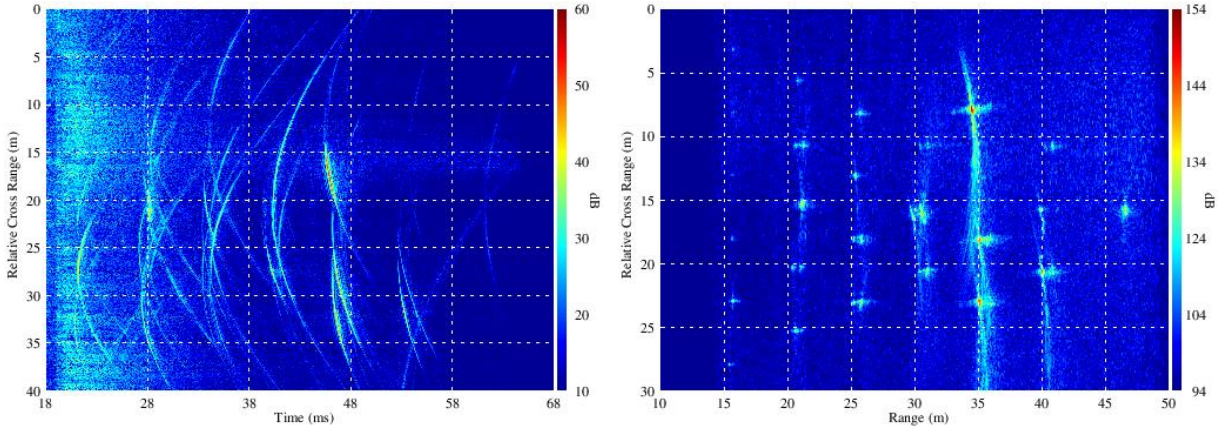


(c) PCB time signals for sequence 48 (d) SAS Image for sequence 48

Figure B4. *Initial processing step produces PCB time signals. Coherent time-domain beamforming of the PCB time signals produces a SAS image.*

| Date | Time | Seq. | Dir. | 15 m (deg) | 20 m (deg) | 25 m (deg) | 30 m (deg) | 35 m (deg) | 40 m (deg) | 45 m (deg) | Notes |
|---|---|---|---|---|---|---|---|---|---|---|---|
| 4/27 | 1535 | 52 | + | –80, 100 | –80 | –80 | –80 | –80, 100 | –80 | 0 | |
| 4/27 | 1550 | 53 | – | –80, 100 | –80 | –80 | –80 | –80, 100 | –80 | 0 | |
| 4/27 | 1724 | 54 | + | –60, 120 | –60 | –60 | –60 | –60, 120 | –60 | 45 | 1 |
| 4/27 | 1739 | 55 | – | –60, 120 | –60 | –60 | –60 | –60, 120 | –60 | 45 | |
| 4/28 | 0908 | 57 | – | –40, 140 | –40 | –40 | –40 | –40, 140 | –40 | 45 | |
| 4/28 | 1042 | 58 | + | –40, 140 | –40 | –40 | –40 | –40, 140 | –40 | 45 | |
| 4/28 | 1218 | 60 | + | –20, 160 | –20 | –20 | –20 | –20, 160 | –20 | 45 | |
| 4/28 | 1233 | 61 | – | –20, 160 | –20 | –20 | –20 | –20, 160 | –20 | 45 | |
| 4/28 | 1409 | 62 | + | 0, 180 | 0 | 0 | 0 | 0, 180 | 0 | 45 | 2 |
| 4/28 | 1423 | 63 | – | 0, 180 | 0 | 0 | 0 | 0, 180 | 0 | 45 | |
| 4/28 | 1588 | 64 | + | 20, 200 | 20 | 20 | 20 | 20, 200 | 20 | 45 | |
| 4/28 | 1603 | 65 | – | 20, 200 | 20 | 20 | 20 | 20, 200 | 20 | 45 | |
| 4/28 | 1845 | 66 | + | 40, 220 | 40 | 40 | 40 | 40, 220 | 40 | 45 | |
| 4/28 | 1859 | 67 | – | 40, 220 | 40 | 40 | 40 | 40, 220 | 40 | 45 | |
| 4/29 | 0834 | 68 | + | 60, 240 | 60 | 60 | 60 | 60, 240 | 60 | 45 | |
| 4/29 | 0848 | 69 | – | 60, 240 | 60 | 60 | 60 | 60, 240 | 60 | 45 | |
| 4/29 | 1057 | 70 | + | 80, 260 | 80 | 80 | 80 | 80, 260 | 80 | 45 | |
| 4/29 | 1112 | 71 | – | 80, 260 | 80 | 80 | 80 | 80, 260 | 80 | 45 | |

Table B3. *Notes for TREX13 target configuration 2. The source was aimed down at a 10º depression angle. The source amplitude into the power amplifiers was 0.5 $V_{rms}$. All targets were proud.*

1. Aluminum panel (target XX) at 45 m rotated by 45º, so that a corner points towards the rail.
2. Divers noted that 55 gallon barrels (targets 3 and 6) have the open end facing west.

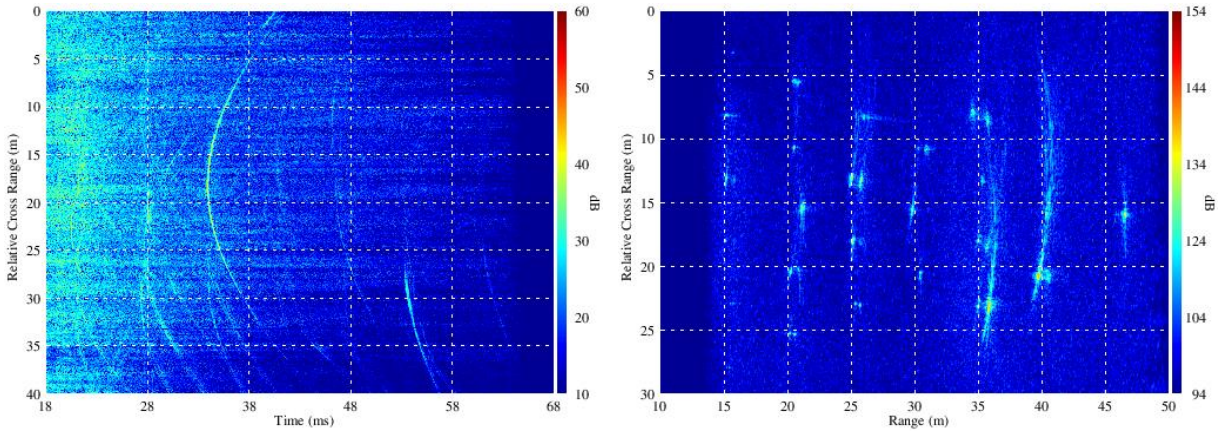


(a) PCB time signals for sequence 52 (b) SAS Image for sequence 52

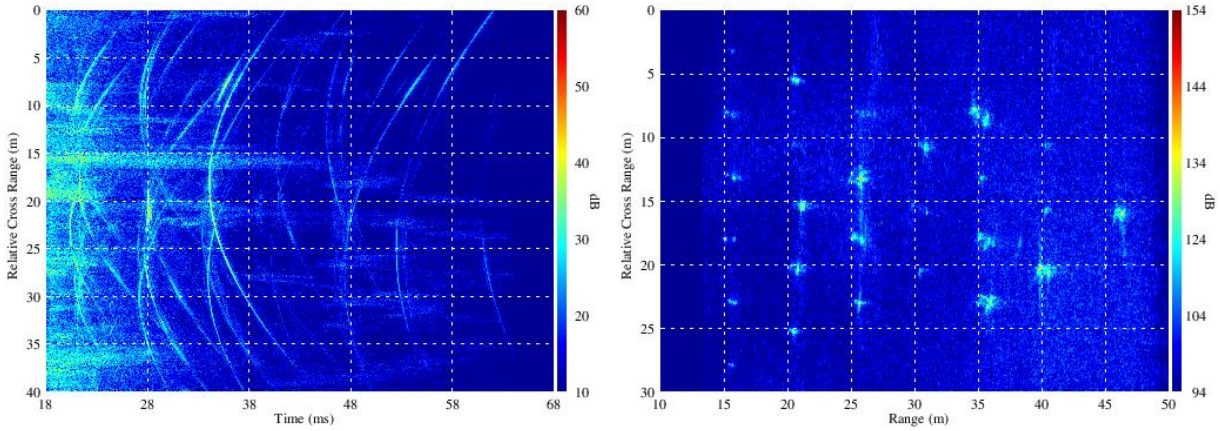


(c) PCB time signals for sequence 54 (d) SAS Image for sequence 54

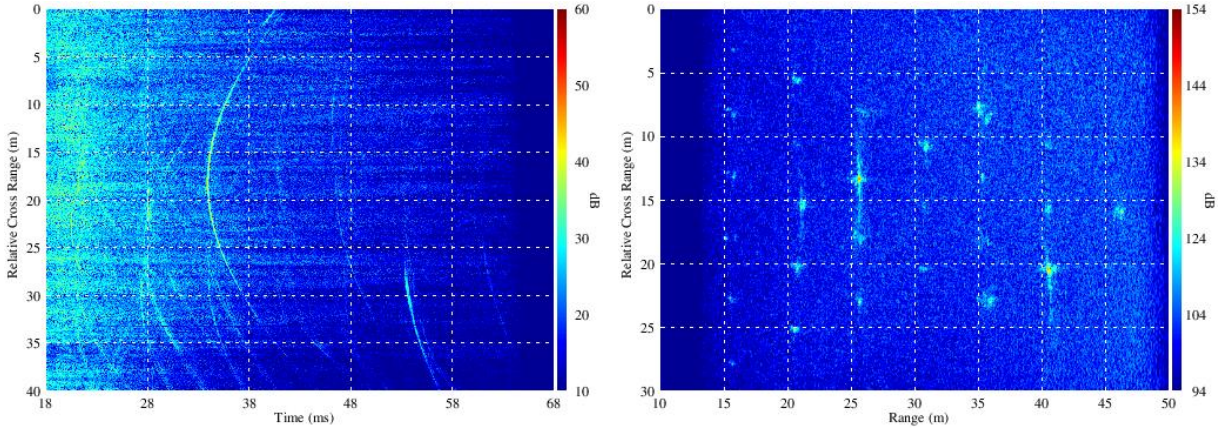


(c) PCB time signals for sequence 58 (d) SAS Image for sequence 58

Figure B5. *Initial processing step produces PCB time signals. Coherent time-domain beamforming of the PCB time signals produces a SAS image.*

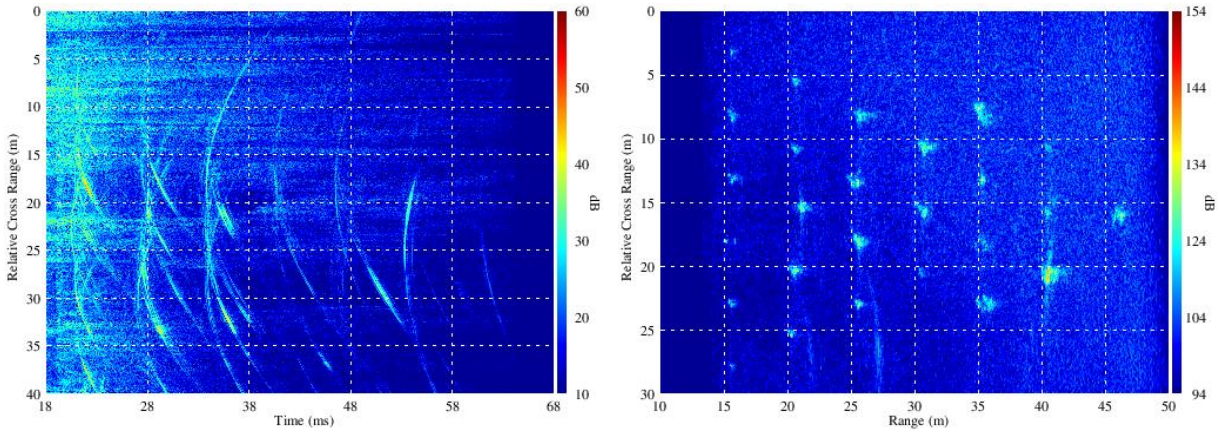


(a) PCB time signals for sequence 60 (b) SAS Image for sequence 60

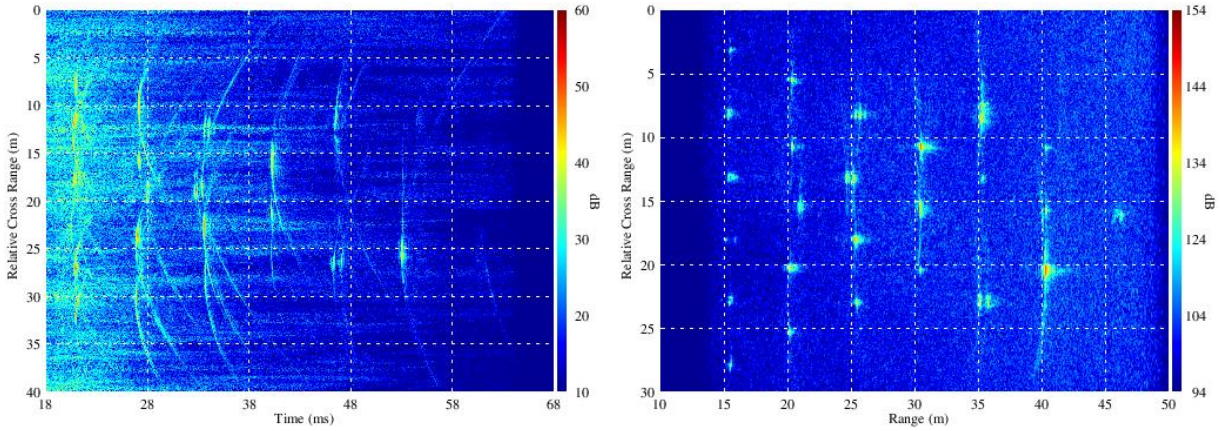


(c) PCB time signals for sequence 62 (d) SAS Image for sequence 62

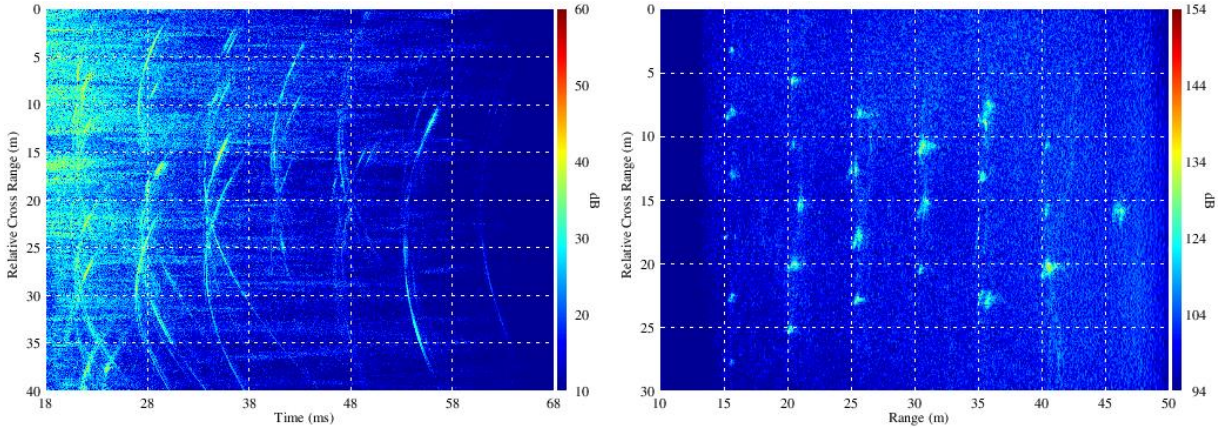


(c) PCB time signals for sequence 64 (d) SAS Image for sequence 64

Figure B6. *Initial processing step produces PCB time signals. Coherent time-domain beamforming of the PCB time signals produces a SAS image.*

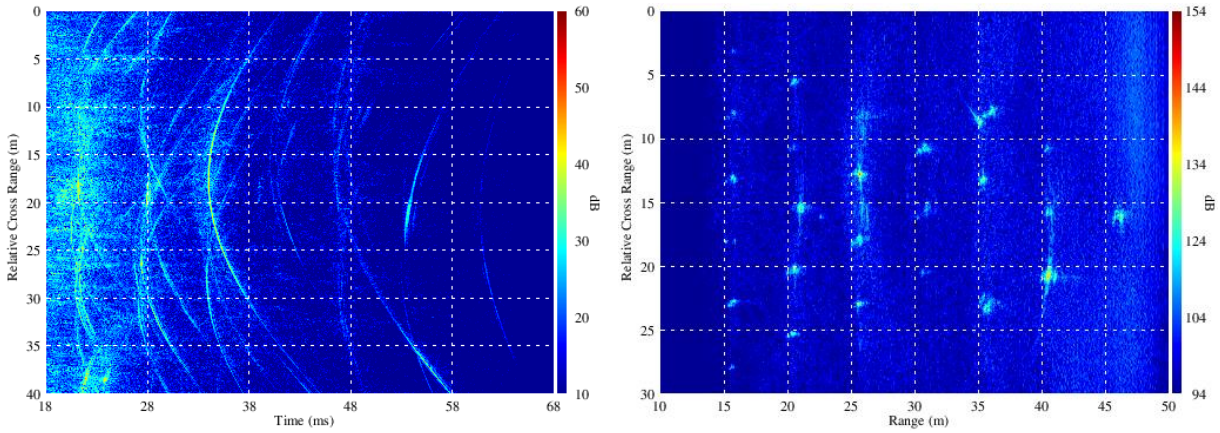


(a) PCB time signals for sequence 66 (b) SAS Image for sequence 66

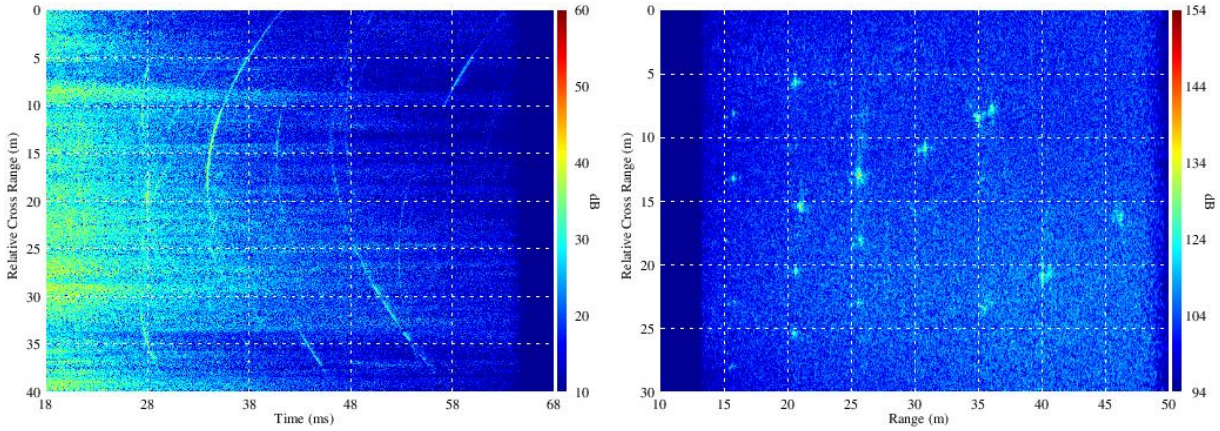


(c) PCB time signals for sequence 68 (d) SAS Image for sequence 68

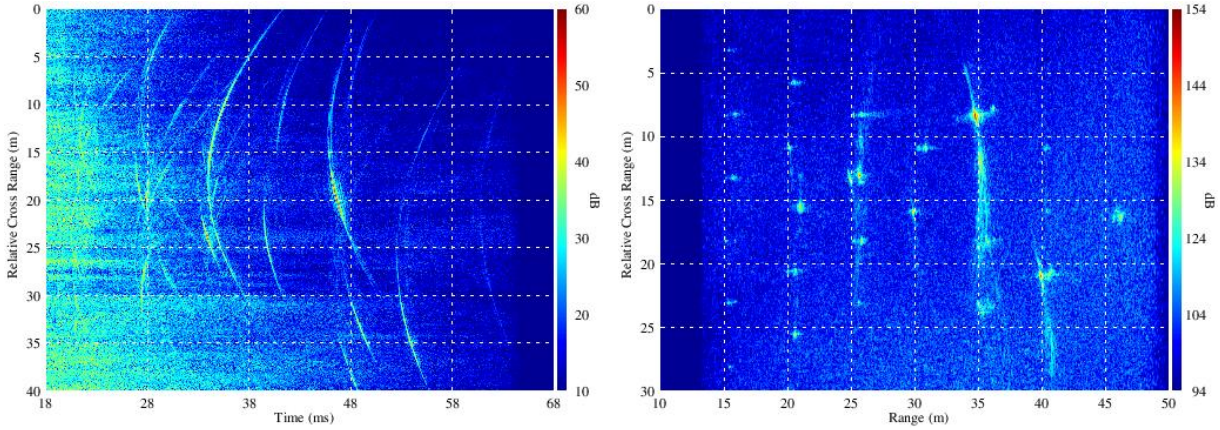


(c) PCB time signals for sequence 70 (d) SAS Image for sequence 70

Figure B7. *Initial processing step produces PCB time signals. Coherent time-domain beamforming of the PCB time signals produces a SAS image.*

| Date | Time | Seq. | Dir. | 15 m (deg) | 20 m (deg) | 25 m (deg) | 30 m (deg) | 35 m (deg) | 40 m (deg) | Notes |
|---|---|---|---|---|---|---|---|---|---|---|
| 4/29 | 1301 | 72 | + | –80 | –80, –80 | –80 | –80 | –80 | –80, –80 | 1 |
| 4/29 | 1316 | 73 | – | –80 | –80, –80 | –80 | –80 | –80 | –80, –80 | |
| 4/29 | 1451 | 74 | + | –60 | –60, –60 | –60 | –60 | –60 | –60, –60 | |
| 4/29 | 1506 | 75 | – | –60 | –60, –60 | –60 | –60 | –60 | –60, –60 | |
| 4/29 | 1643 | 76 | + | –40 | –40, –40 | –40 | –40 | –40 | –40, –40 | |
| 4/29 | 1708 | 77 | – | –40 | –40, –40 | –40 | –40 | –40 | –40, –40 | |
| 4/29 | 1941 | 78 | + | –40 | –40, –40 | –40 | –40 | –40 | –40, –40 | 2 |
| 4/29 | 1955 | 79 | – | –40 | –40, –40 | –40 | –40 | –40 | –40, –40 | 3 |
| 4/30 | 0827 | 80 | + | –20 | –20, –20 | –20 | –20 | –20 | –20, –20 | |
| 4/30 | 0841 | 81 | – | –20 | –20, –20 | –20 | –20 | –20 | –20, –20 | |
| 4/30 | 1059 | 82 | + | 0 | 0, 0 | 0 | 0 | 0 | 0, 0 | |
| 4/30 | 1114 | 83 | – | 0 | 0, 0 | 0 | 0 | 0 | 0, 0 | |
| 4/30 | 1259 | 84 | + | 20 | 20, 20 | 20 | 20 | 20 | 20, 20 | |
| 4/30 | 1314 | 85 | – | 20 | 20, 20 | 20 | 20 | 20 | 20, 20 | |
| 4/30 | 1501 | 86 | + | 40 | 40, 40 | 40 | 40 | 40 | 40, 40 | |
| 4/30 | 1515 | 87 | – | 40 | 40, 40 | 40 | 40 | 40 | 40, 40 | |
| 4/30 | 1704 | 88 | + | 60 | 60, 60 | 60 | 60 | 60 | 60, 60 | |
| 4/30 | 1718 | 89 | – | 60 | 60, 60 | 60 | 60 | 60 | 60, 60 | |
| 5/1 | 0833 | 90 | + | 80 | 80, 80 | 80 | 80 | 80 | 80, 80 | |
| 5/1 | 0848 | 91 | – | 80 | 80, 80 | 80 | 80 | 80 | 80, 80 | |
| 5/1 | 0902 | 92 | + | 80 | 80, 80 | 80 | 80 | 80 | 80, 80 | |
| 5/8 | 1436 | 120 | + | 0 | 0, 0 | 0 | 0 | 0 | 0, 0 | 4 |
| 5/8 | 1451 | 121 | – | 0 | 0, 0 | 0 | 0 | 0 | 0, 0 | 4 |

Table B4. *Notes for TREX13 target configuration 3. The source was aimed down at a 10º depression angle, and the signal amplitude into the power amplifiers was 0.5 $V_{rms}$. All targets were proud.*

1. Aluminum panel (target XX) at 30 m in F0 broadside to rail. Targets 6, 13, and 28 aligned without frame and may not be exactly –80º.
2. Light is ON.
3. Light is OFF.
4. Targets 1, 3, 7, 5, and 15 are rotated to 80º, and everything else is at 0º with tails pointing west. Targets 25 and 29 are not in the field, so location D4 and G4 are empty.

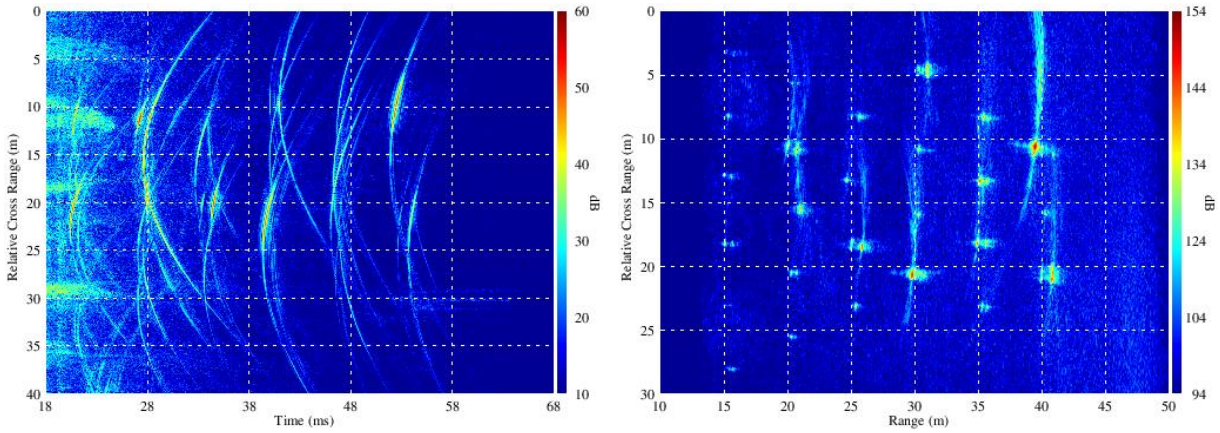


(a) PCB time signals for sequence 72 (b) SAS Image for sequence 72

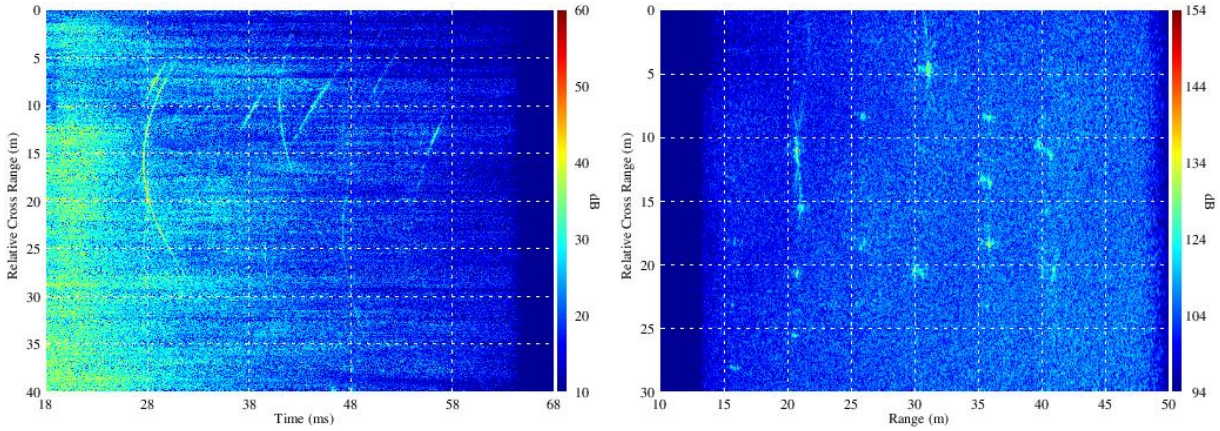


(c) PCB time signals for sequence 74 (d) SAS Image for sequence 74

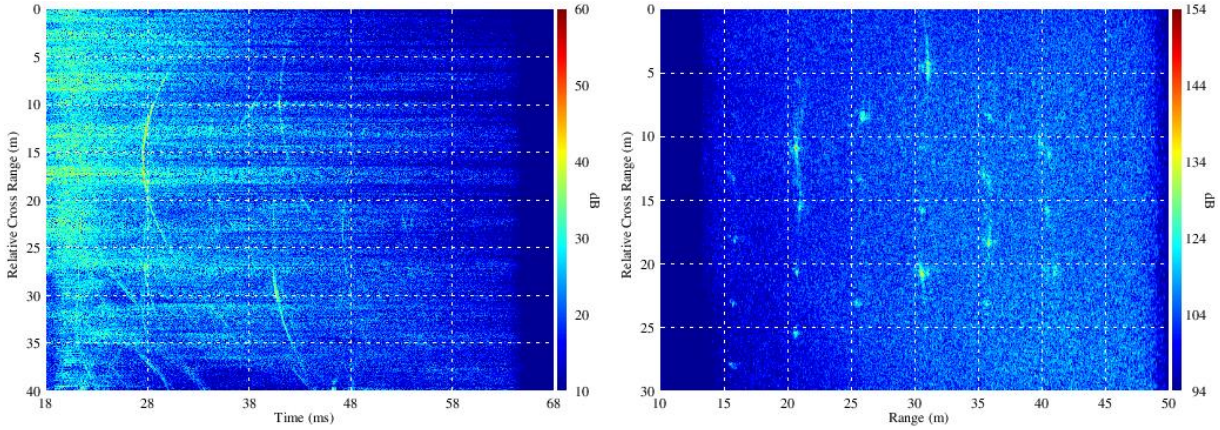


(c) PCB time signals for sequence 76 (d) SAS Image for sequence 76

Figure B8. *Initial processing step produces PCB time signals. Coherent time-domain beamforming of the PCB time signals produces a SAS image.*

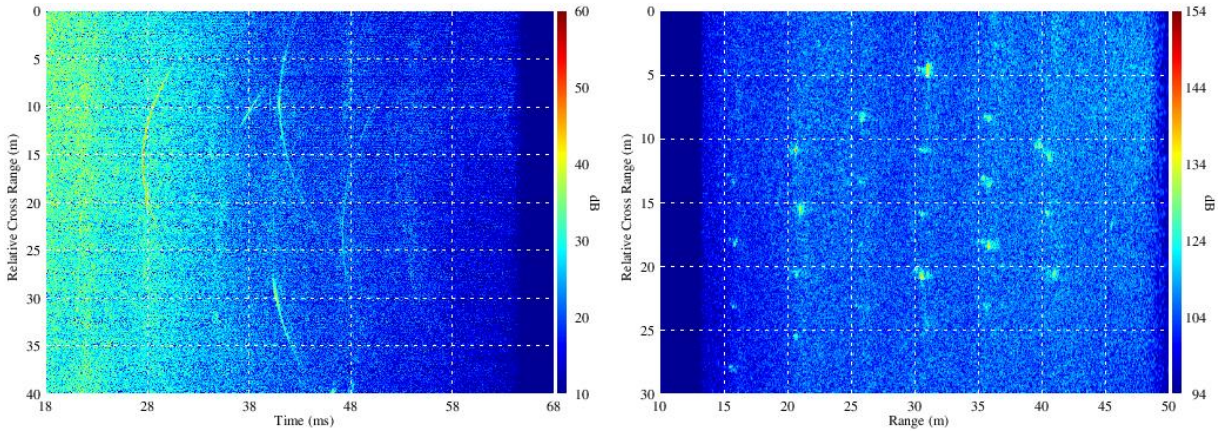


(a) PCB time signals for sequence 78 (b) SAS Image for sequence 78

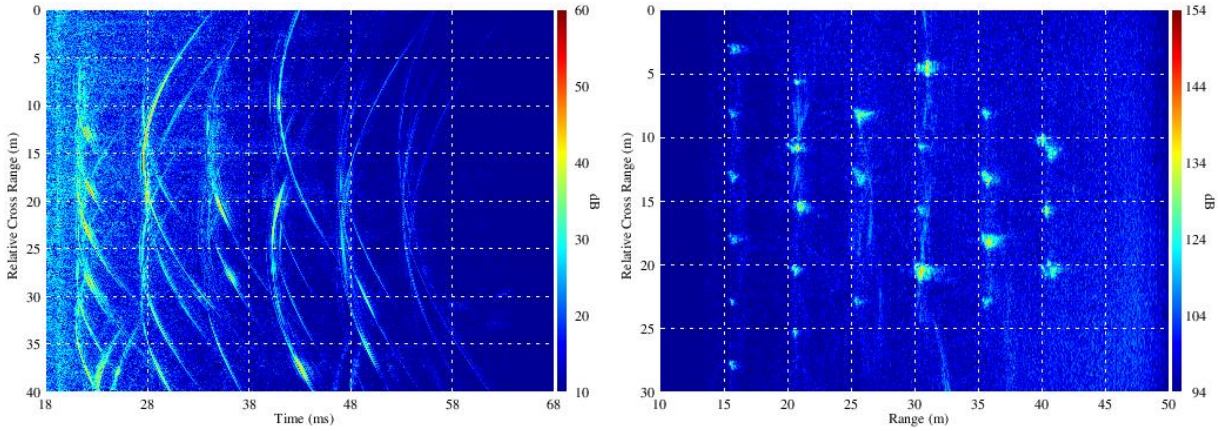


(c) PCB time signals for sequence 80 (d) SAS Image for sequence 80

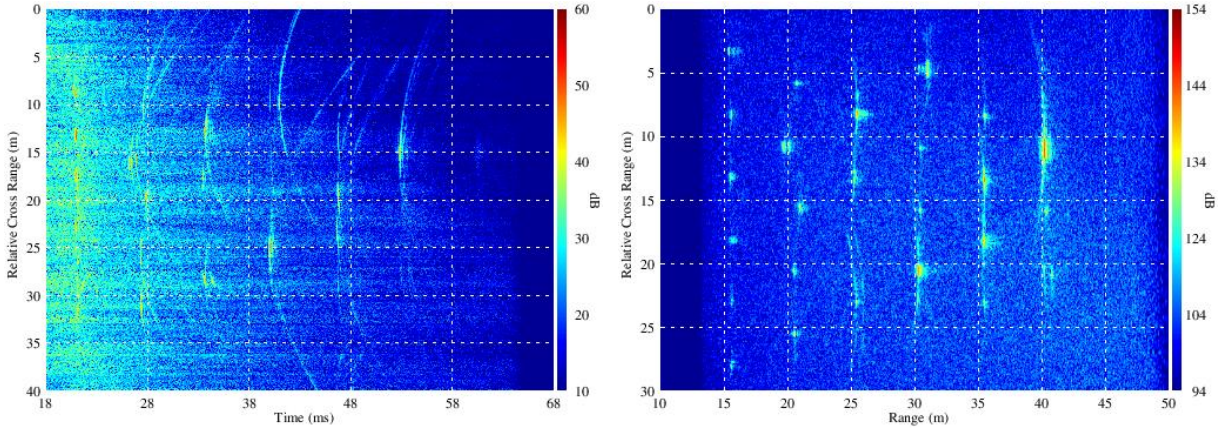


(c) PCB time signals for sequence 82 (d) SAS Image for sequence 82

Figure B9. *Initial processing step produces PCB time signals. Coherent time-domain beamforming of the PCB time signals produces a SAS image.*

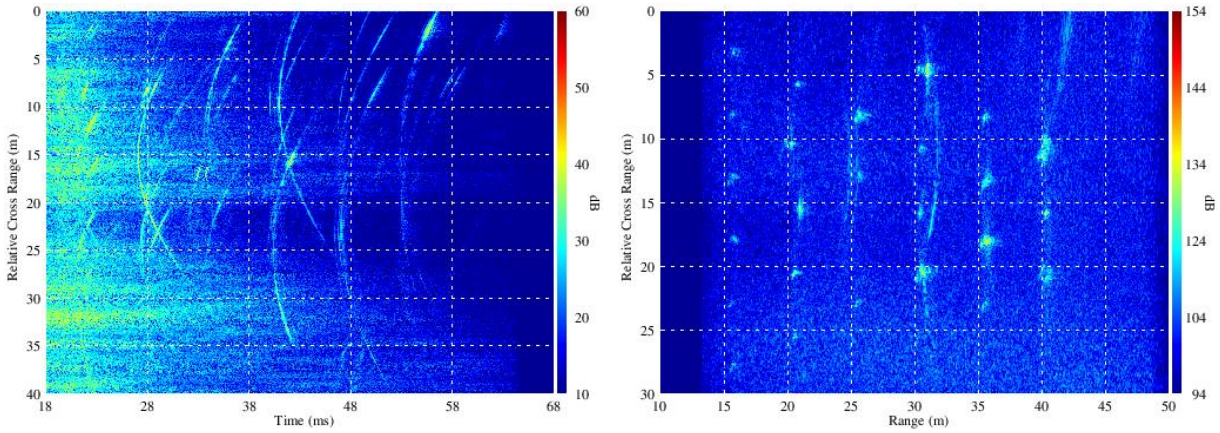


(a) PCB time signals for sequence 84 (b) SAS Image for sequence 84

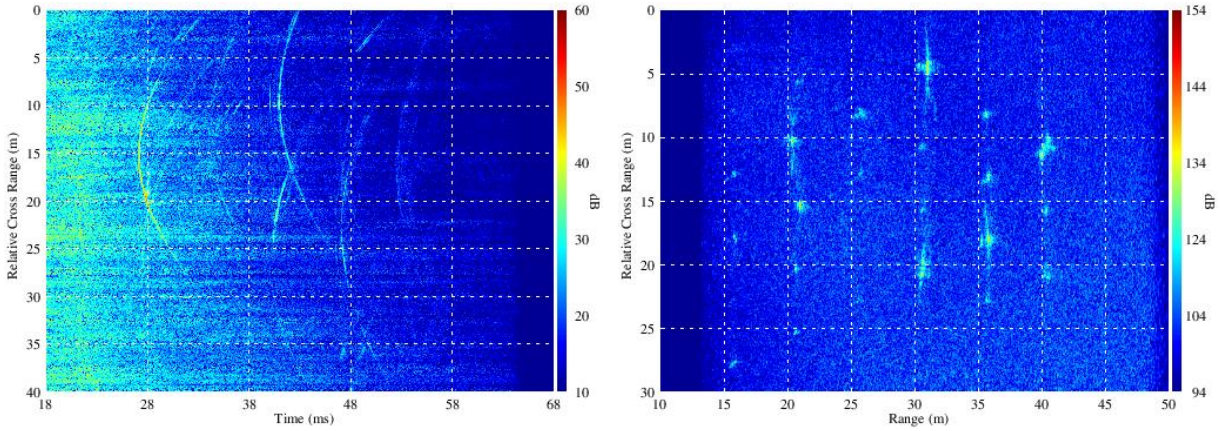


(c) PCB time signals for sequence 86 (d) SAS Image for sequence 86

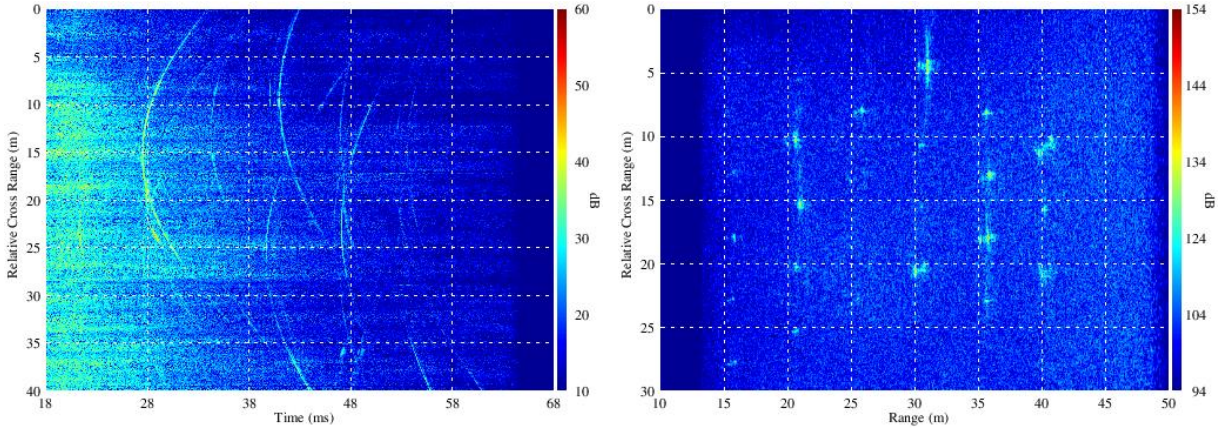


(c) PCB time signals for sequence 88 (d) SAS Image for sequence 88

Figure B10. *Initial processing step produces PCB time signals. Coherent time-domain beamforming of the PCB time signals produces a SAS image.*

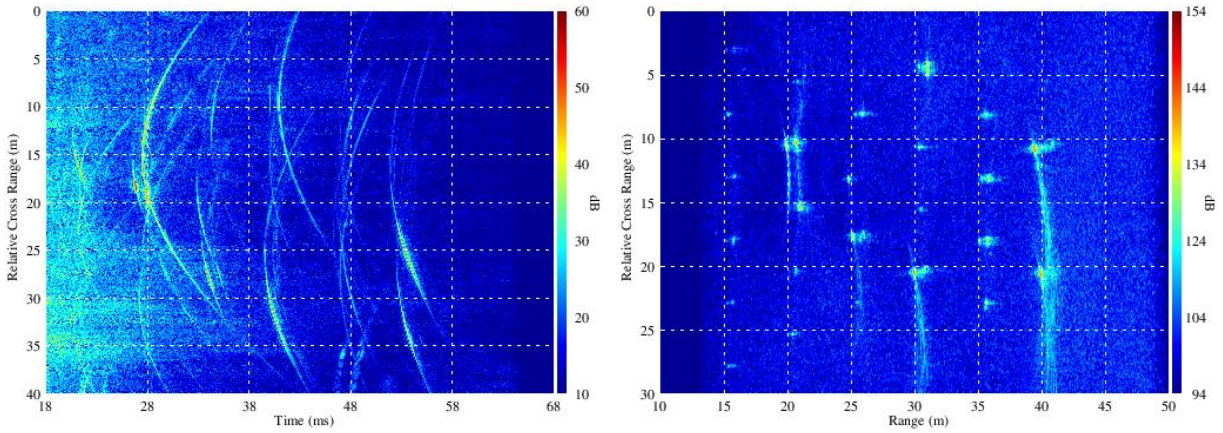


(a) PCB time signals for sequence 90 (b) SAS Image for sequence 90

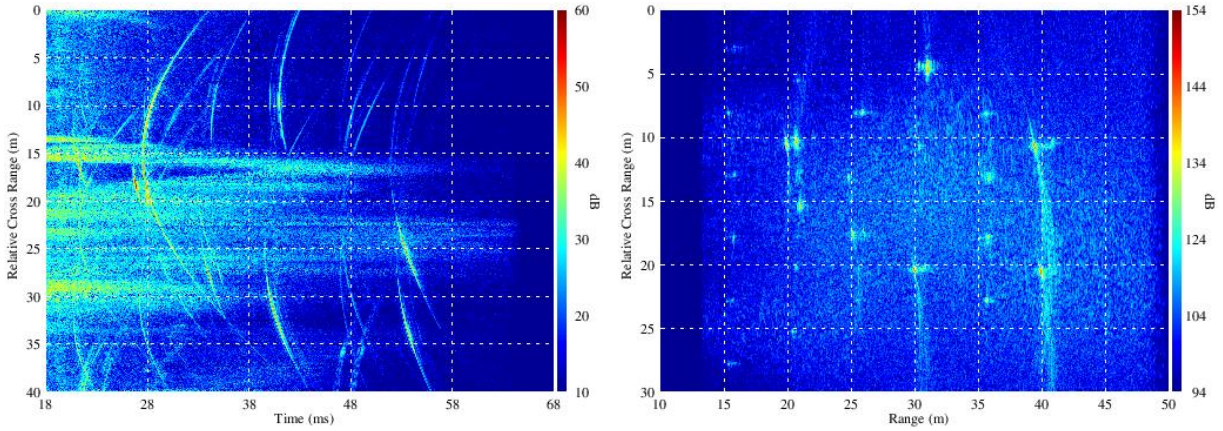


(c) PCB time signals for sequence 92 (d) SAS Image for sequence 92

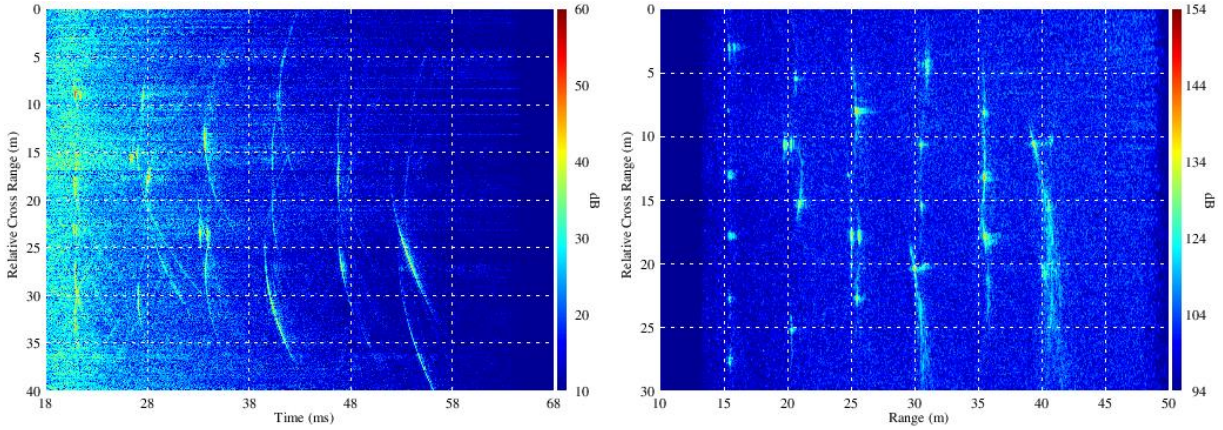


(c) PCB time signals for sequence 120 (d) SAS Image for sequence 120

Figure B11. *Initial processing step produces PCB time signals. Coherent time-domain beamforming of the PCB time signals produces a SAS image.*

| Date | Time | Seq. # | Dir. | 5 m (deg) | 10 m (deg) |
|---|---|---|---|---|---|
| 5/8 | 1749 | 122 | + | 0 | 0 |
| 5/8 | 1804 | 123 | – | 0 | 0 |
| 5/8 | 1818 | 124 | + | 0 | 0 |
| 5/8 | 1902 | 125 | – | 0 | 0 |

Table B5. *Source level check for TREX13 target configuration 4. The source amplitude into the power amplifiers was set to 0.5 $V_{rms}$. All targets are proud. Signals recorded for a 20-ms window.*

| Date | Time | Seq # | Dir. | 5 m (deg) | 10 m (deg) |
|---|---|---|---|---|---|
| 5/9 | 0858 | 126 | + | –80, –80 | –80 |
| 5/9 | 0912 | 127 | – | –80, –80 | –80 |
| 5/9 | 1100 | 128 | + | –60, –60 | –60 |
| 5/9 | 1115 | 129 | – | –60, –60 | –60 |
| 5/9 | 1300 | 130 | + | –40, –40 | –40 |
| 5/9 | 1314 | 131 | – | –40, –40 | –40 |
| 5/9 | 1500 | 132 | + | –20, –20 | –20 |
| 5/9 | 1514 | 133 | – | –20, –20 | –20 |
| 5/9 | 1700 | 134 | + | 0, 0 | 0 |
| 5/9 | 1715 | 135 | – | 0, 0 | 0 |
| 5/10 | 0857 | 136 | + | 20, 20 | 20 |
| 5/10 | 0911 | 137 | – | 20, 20 | 20 |
| 5/10 | 1100 | 138 | + | 40, 40 | 40 |
| 5/10 | 1114 | 139 | – | 40, 40 | 40 |
| 5/10 | 1300 | 140 | + | 60, 60 | 60 |
| 5/10 | 1314 | 141 | – | 60, 60 | 60 |
| 5/10 | 1500 | 142 | + | 80, 80 | 80 |
| 5/10 | 1515 | 143 | – | 80, 80 | 80 |

Table B6. *Notes for TREX13 target configuration 4. All targets are proud. Signals recorded for a 30-ms window. During the recording of sequence 126, the amplifiers were disabled for the first 20 pings.*

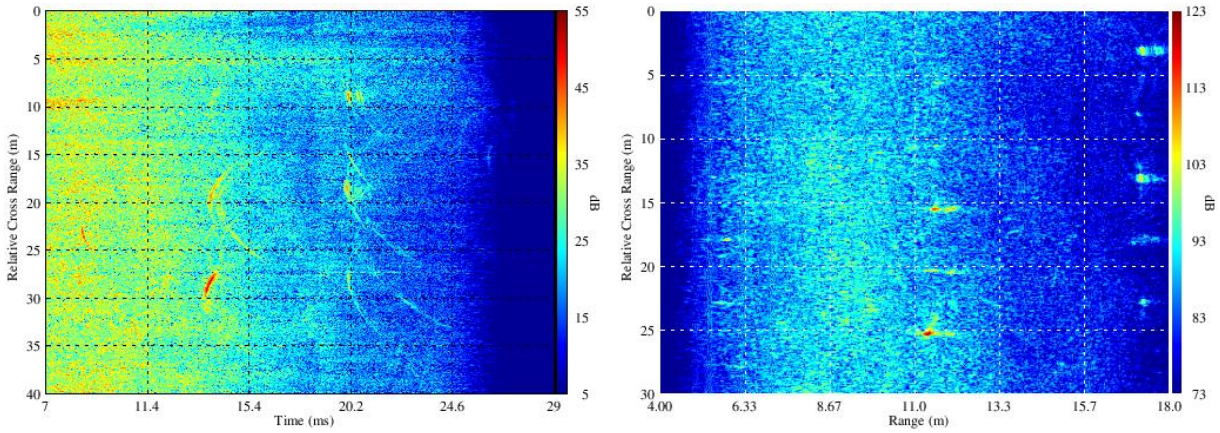


(a) PCB time signals for sequence 126 (b) SAS Image for sequence 126

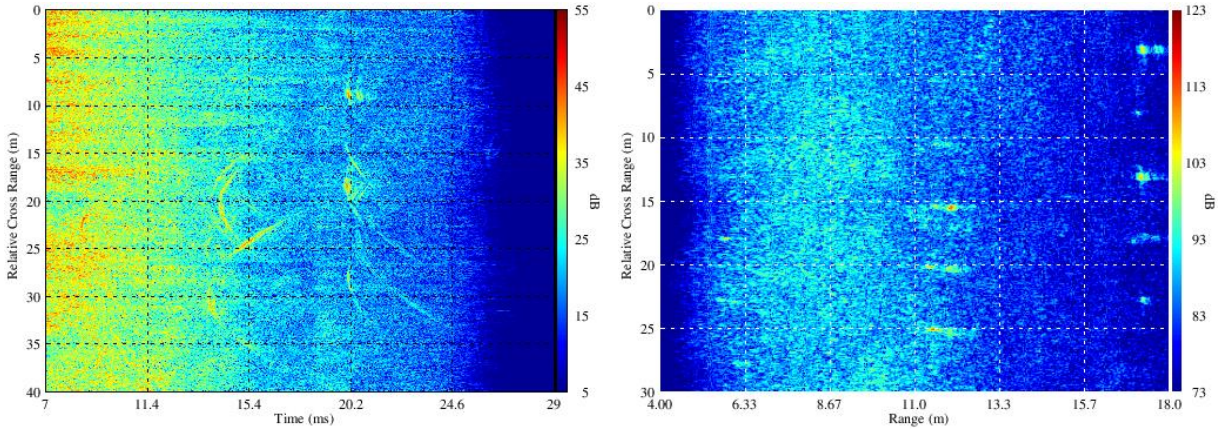


(c) PCB time signals for sequence 128 (d) SAS Image for sequence 128

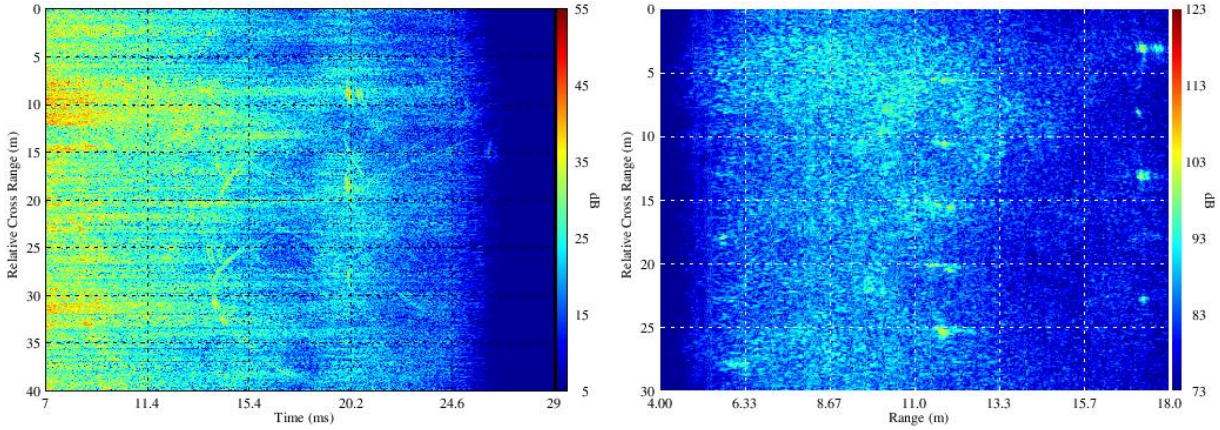


(c) PCB time signals for sequence 130 (d) SAS Image for sequence 130

Figure B12. *Initial processing step produces PCB time signals. Coherent time-domain beamforming of the PCB time signals produces a SAS image.*

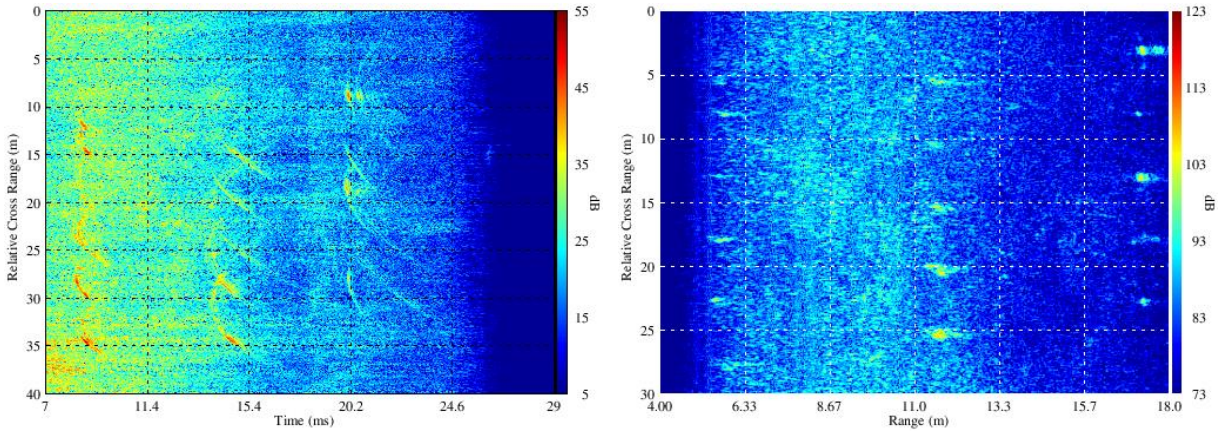


(a) PCB time signals for sequence 132 (b) SAS Image for sequence 132

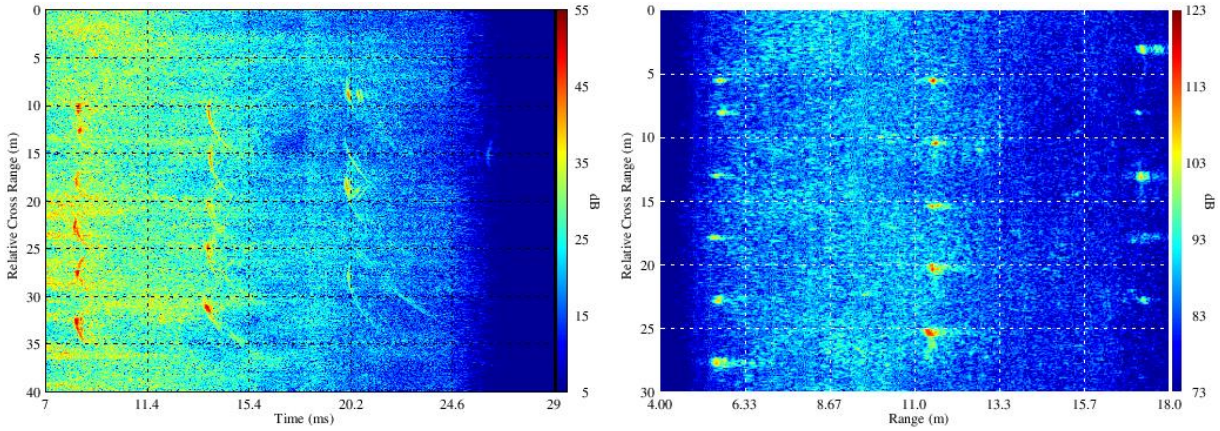


(c) PCB time signals for sequence 134 (d) SAS Image for sequence 134

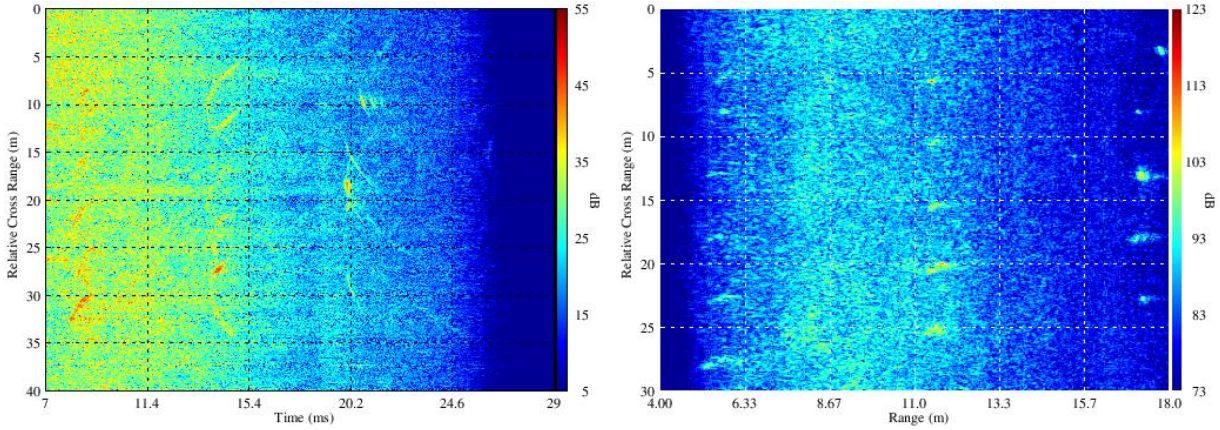


(c) PCB time signals for sequence 136 (d) SAS Image for sequence 136

Figure B13. *Initial processing step produces PCB time signals. Coherent time-domain beamforming of the PCB time signals produces a SAS image.*

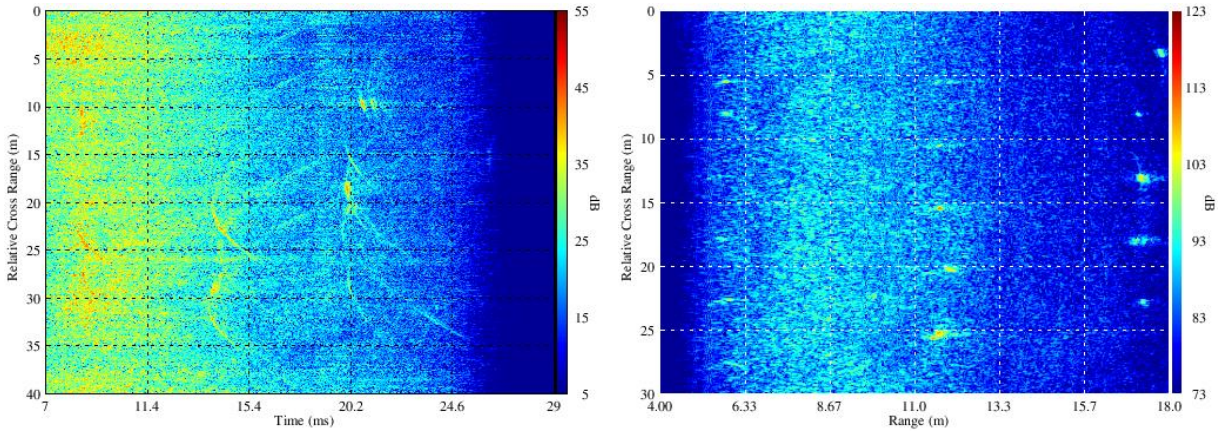


(a) PCB time signals for sequence 138 (b) SAS Image for sequence 138

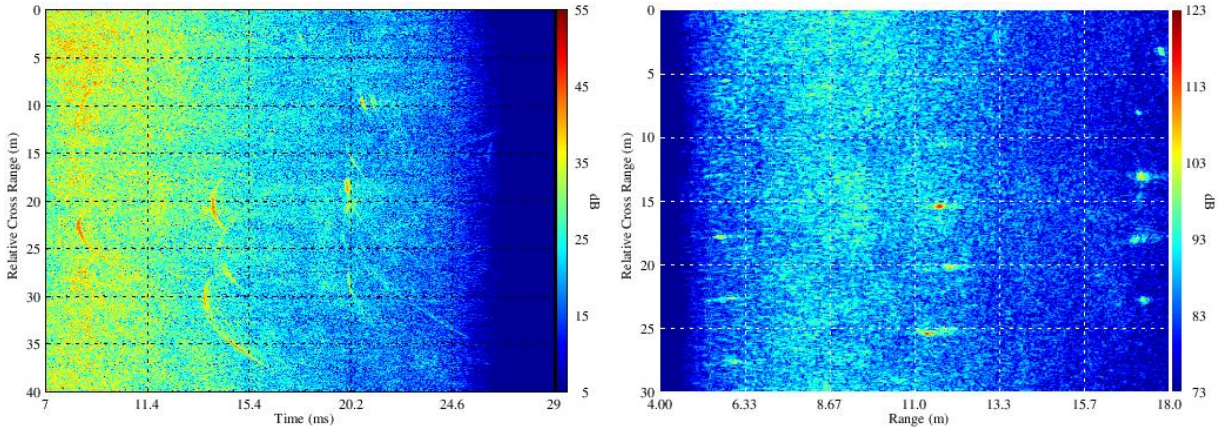


(c) PCB time signals for sequence 140 (d) SAS Image for sequence 140

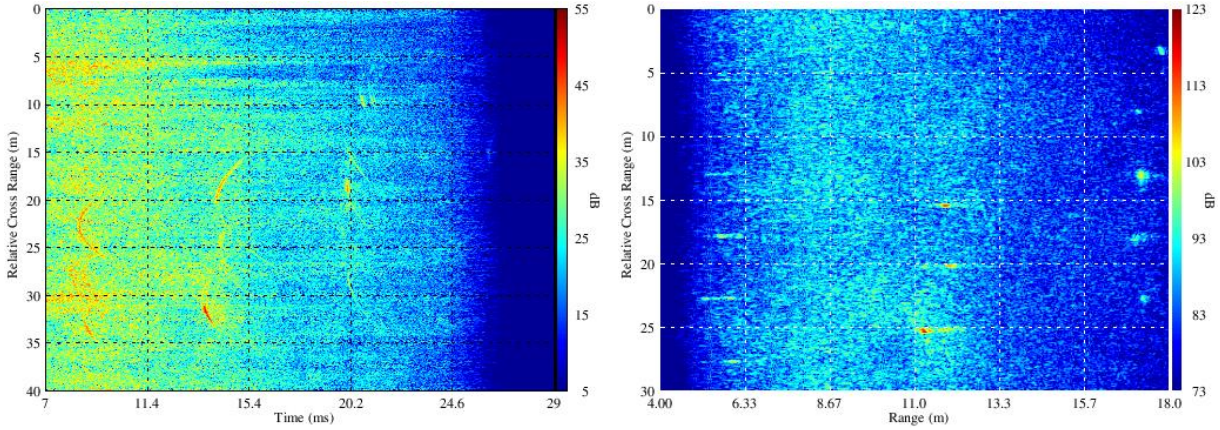


(c) PCB time signals for sequence 142 (d) SAS Image for sequence 142

Figure B14. *Initial processing step produces PCB time signals. Coherent time-domain beamforming of the PCB time signals produces a SAS image.*

| Date | Time | Seq. # | Dir. | 5 m (deg) | 10 m (deg) | Notes |
|---|---|---|---|---|---|---|
| 5/10 | 1700 | 144 | + | –80, 40 | –80 | 1,2 |
| 5/10 | 1714 | 145 | – | –80, 40 | –80 | 1,2 |
| 5/11 | 0857 | 146 | + | –60, 40 | –60 | 2,3 |
| 5/11 | 0911 | 147 | – | –60, 40 | –60 | 2,3 |
| 5/11 | 1100 | 148 | + | –40, 40 | –40 | 2,4,5 |
| 5/11 | 1114 | 149 | – | –40, 40 | –40 | 2,4,5 |
| 5/11 | 1301 | 150 | + | –20, 40 | –20 | 2,6 |
| 5/11 | 1315 | 151 | – | –20, 40 | –20 | 2,6 |
| 5/11 | 1459 | 152 | + | 0, 40 | 0 | 2,7 |
| 5/11 | 1514 | 153 | – | 0, 40 | 0 | 2,7 |
| 5/11 | 1700 | 154 | + | 20, 140 | 20 | 8,9 |
| 5/11 | 1714 | 155 | – | 20, 140 | 20 | 8,9 |
| 5/12 | 0900 | 156 | + | 40, 140 | 40 | 10 |
| 5/12 | 0914 | 157 | – | 40, 140 | 40 | 10 |
| 5/12 | 1100 | 158 | + | 60, 140 | 60 | 11 |
| 5/12 | 1114 | 159 | – | 60, 140 | 60 | 11 |
| 5/12 | 1300 | 160 | + | 80, 140 | 80 | 12 |
| 5/12 | 1314 | 161 | – | 80, 140 | 80 | 12 |

Table B7. *Notes for TREX13 target configuration 4. Targets at the 5-m line are fully buried to a 2-inch depth. The targets at the 10-m line are half buried, and target 17 is proud with a 0º orientation. Signals recorded for a 30-ms window.*

1. Targets 23 and 24 1/4 buried at 40º rotation.
2. Target at A6 flush buried.
3. Targets 23 and 24 1/2 buried at 40º rotation.
4. Targets 23 and 24 3/4 buried at 40º rotation.
5. Fire hose chaffing laying over top of A3.
6. Targets 23 and 24 are flush buried at 40º rotation.
7. Targets 23 and 24 are proud at 140º orientation.
8. Targets 23 and 24 are 1/4 buried at 140º orientation.
9. Target at A6 buried 2 inches, but only rotated to about 5º.
10. Targets 23 and 24 are 1/2 buried at 140º orientation. Target at A6 buried 2 inches.
11. Targets 23 and 24 are 3/4 buried at 140º orientation. Target at A6 buried 2 inches.
12. Targets 23 and 24 buried 2 inches at 140º orientation. Target at A6 buried 2 inches.

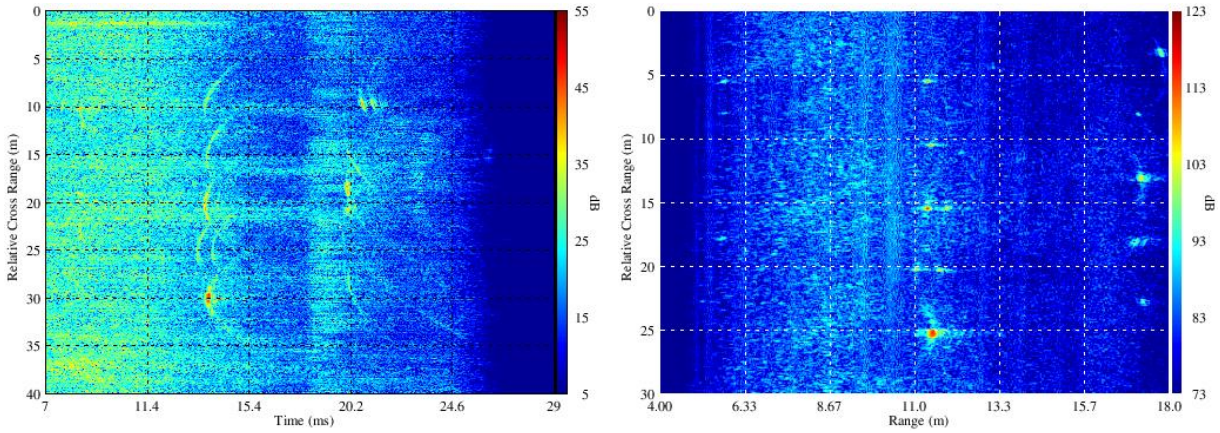


(a) PCB time signals for sequence 144 (b) SAS Image for sequence 144

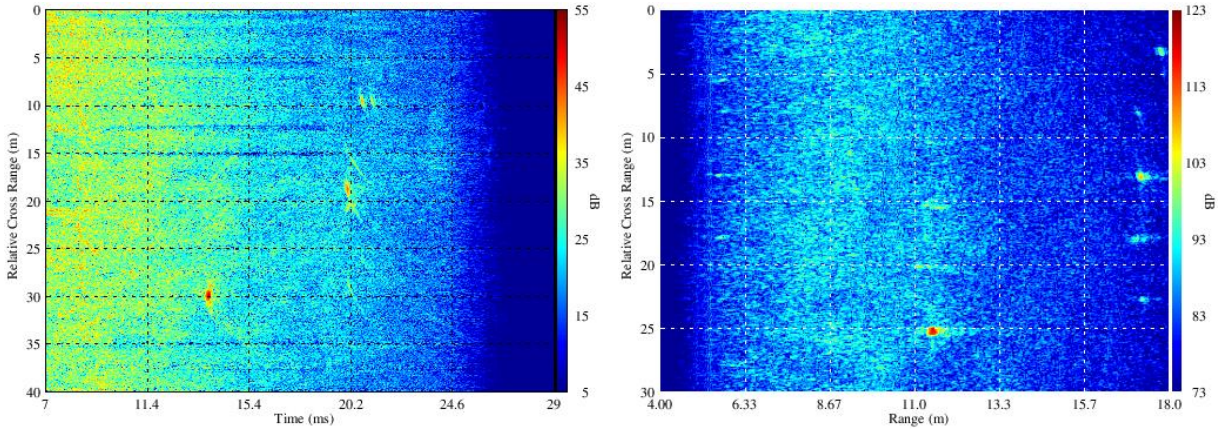


(c) PCB time signals for sequence 146 (d) SAS Image for sequence 146

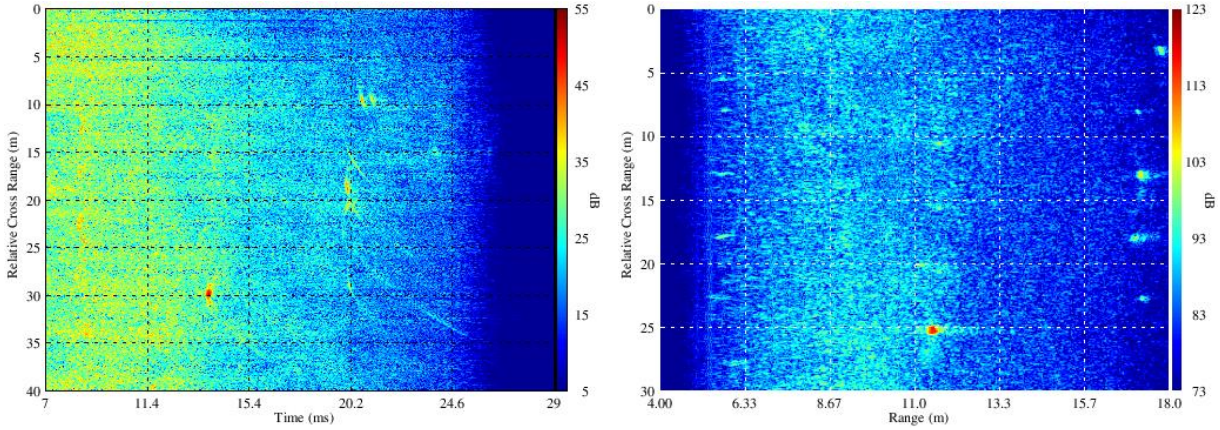


(c) PCB time signals for sequence 148 (d) SAS Image for sequence 148

Figure B15. *Initial processing step produces PCB time signals. Coherent time-domain beamforming of the PCB time signals produces a SAS image.*

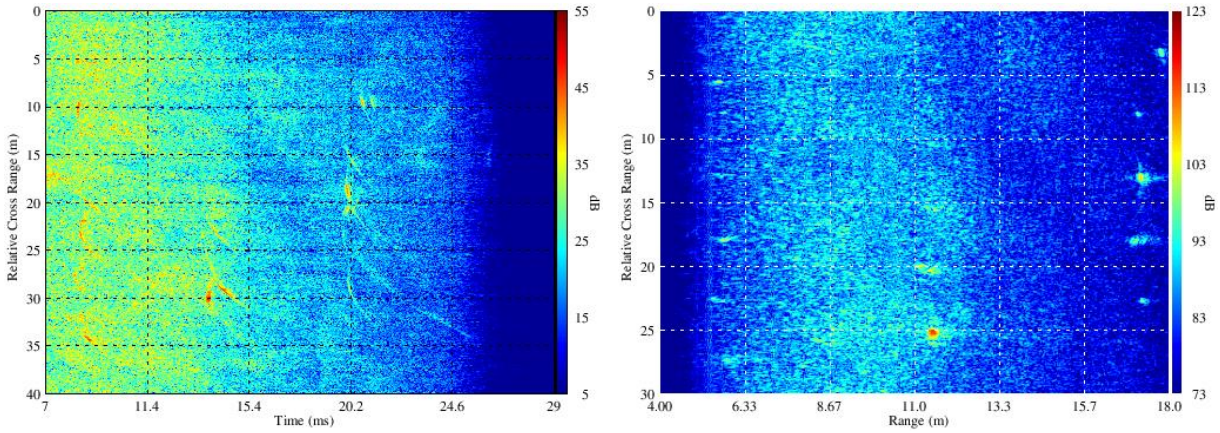


(a) PCB time signals for sequence 150 (b) SAS Image for sequence 150

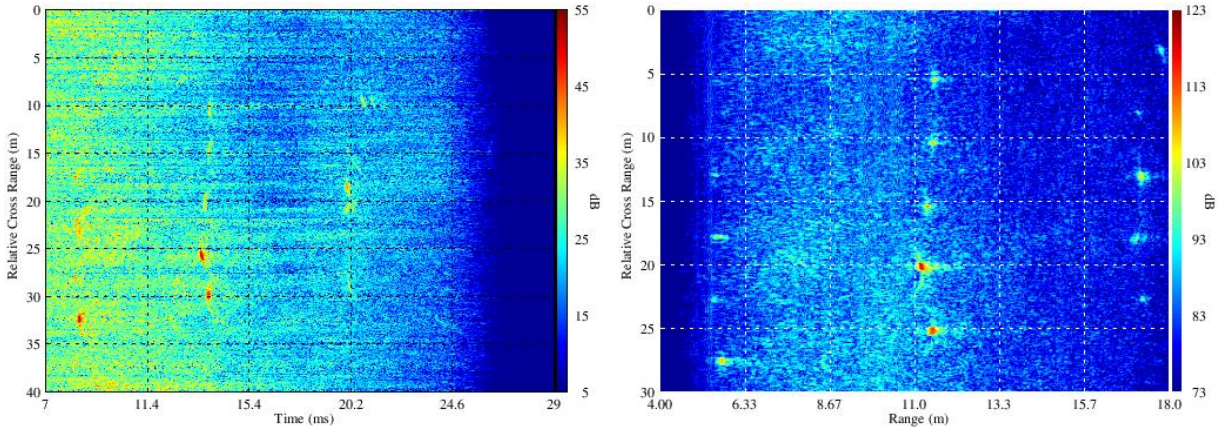


(c) PCB time signals for sequence 152 (d) SAS Image for sequence 152

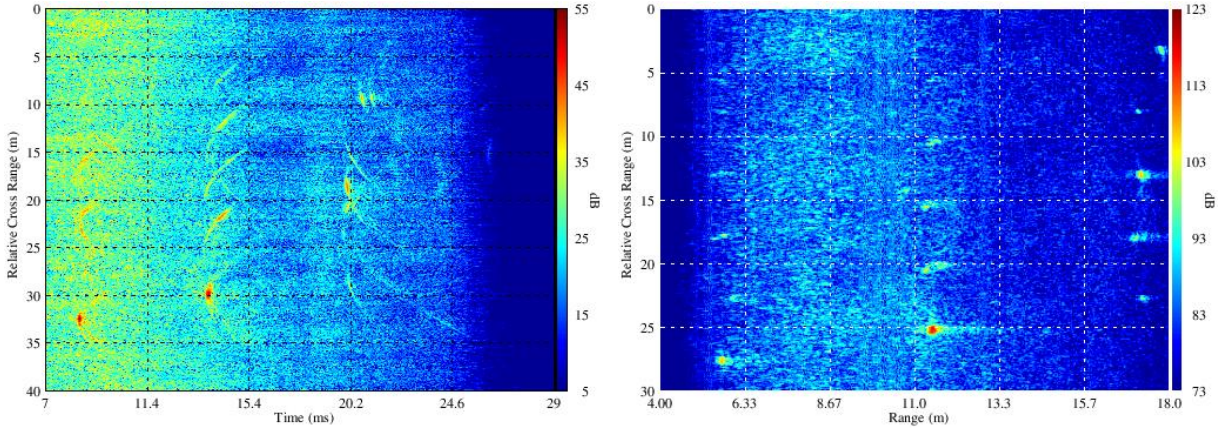


(c) PCB time signals for sequence 154 (d) SAS Image for sequence 154

Figure B16. *Initial processing step produces PCB time signals. Coherent time-domain beamforming of the PCB time signals produces a SAS image.*

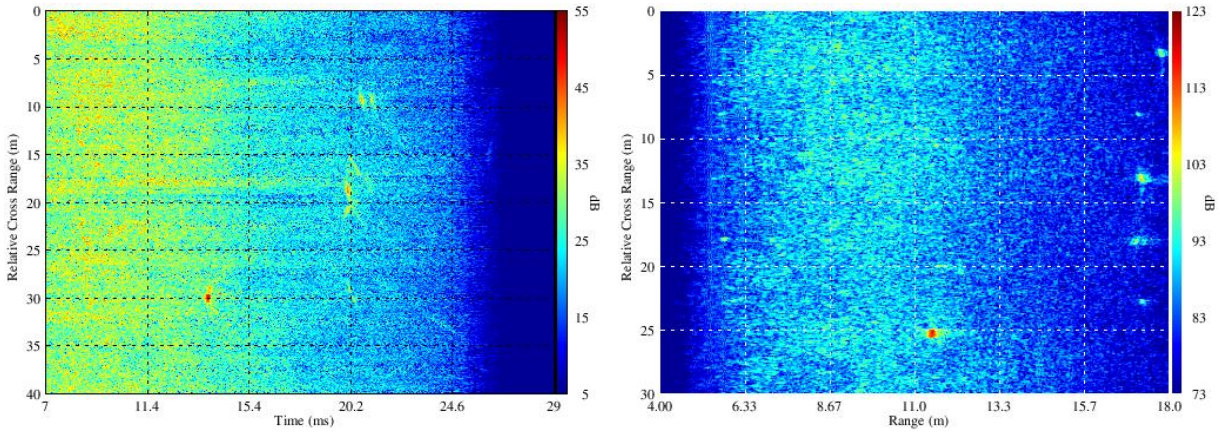


(a) PCB time signals for sequence 156 (b) SAS Image for sequence 156

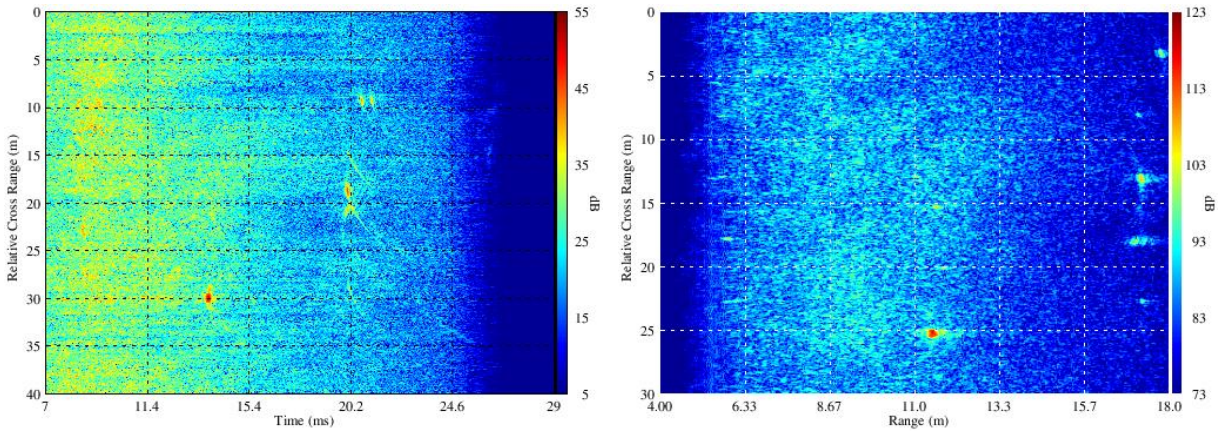


(c) PCB time signals for sequence 158 (d) SAS Image for sequence 158

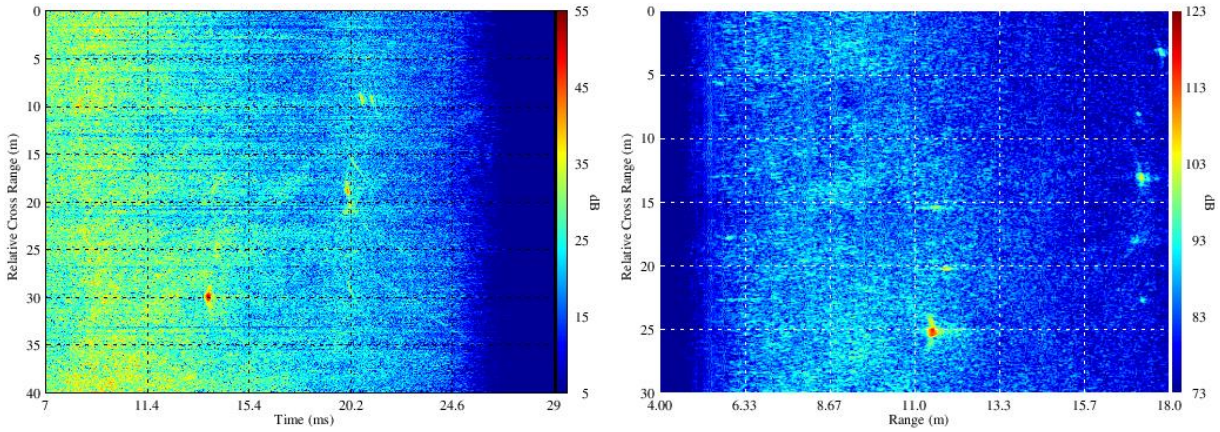


(c) PCB time signals for sequence 160 (d) SAS Image for sequence 160

Figure B17. *Initial processing step produces PCB time signals. Coherent time-domain beamforming of the PCB time signals produces a SAS image.*

| Date | Time | Seq. # | Dir. | 5 m (deg) | 10 m (deg) | 15 m (deg) | Notes |
|---|---|---|---|---|---|---|---|
| 5/12 | 1700 | 162 | + | –80 | –80 | –80, 40 | 1 |
| 5/12 | 1714 | 163 | – | –80 | –80 | –80, 40 | 1 |
| 5/12 | 1729 | 164 | + | –80 | –80 | –80, 40 | 1 |
| 5/12 | 1744 | 165 | – | –80 | –80 | –80, 40 | 1 |
| 5/13 | 0634 | 166 | + | –80 | –80 | –80, 40 | 2 |
| 5/13 | 0900 | 168 | + | –60 | –60 | –60, 40 | 3 |
| 5/13 | 0914 | 169 | – | –60 | –60 | –60, 40 | 3 |
| 5/13 | 1100 | 170 | + | –40 | –40 | –40, 40 | 4 |
| 5/13 | 1114 | 171 | – | –40 | –40 | –40, 40 | 4 |
| 5/13 | 1300 | 172 | + | –20 | –20 | –20, 40 | 5 |
| 5/13 | 1314 | 173 | – | –20 | –20 | –20, 40 | 5 |
| 5/13 | 1500 | 174 | + | 0 | 0 | 0, 40 | 6 |
| 5/13 | 1514 | 175 | – | 0 | 0 | 0, 40 | 6 |
| 5/13 | 1700 | 176 | + | 20 | 20 | 20, 40 | 7,8 |
| 5/13 | 1717 | 177 | – | 20 | 20 | 20, 40 | 8 |
| 5/14 | 0700 | 178 | + | 20 | 20 | 20, 40 | 9,10 |
| 5/14 | 0716 | 179 | – | 20 | 20 | 20, 40 | 20 |
| 5/14 | 0900 | 180 | + | 40 | 40 | 40, 40 | 11 |
| 5/14 | 0914 | 181 | – | 40 | 40 | 40, 40 | 11,12 |
| 5/14 | 1100 | 182 | + | 60 | 60 | 60, 40 | 13 |
| 5/14 | 1114 | 183 | – | 60 | 60 | 60, 40 | 13 |
| 5/14 | 1226 | 184 | + | 80 | 80 | 80, 40 | 14 |
| 5/14 | 1240 | 185 | – | 80 | 80 | 80, 40 | 14 |

Table B8. *Notes for TREX13 target configuration 5. The source was aimed down at a 30º depression angle. The signal amplitude was 0.25 $V_{rms}$ for all sequences. The targets along the 5-m line are buried to a 2-inch depth. Targets at the 10-m line are half buried and the targets at the 15-m line are proud. Target 17 is proud with a 0º orientation. Targets 7 and 28 are slant buried and broadside to the rail (i.e., 0º orientation), and the exposed tails are pointing to the east.*

1. Targets 23 and 24 are proud at 40º, where the paddle plane is exactly vertical and facing the rail. Target 28 is slant buried at 54º. Target 7 is slant buried at 44.3º. Divers later discovered that digital level does not work properly underwater. Target at A6 flush buried.
2. Targets 23 and 24 are proud at 40º, where the paddle plane is exactly vertical and facing the rail. Target 28 slant buried (short edge is 35.6 cm, long edge is 47.6 cm). Target 7 slant buried (short edge is 8.89 cm, long edge is 73.7 cm). There will be no more inclination measurements because the digital level does not work properly underwater. Target at A5 is flush buried, slightly mounded actually.
3. Targets 23 and 24 are proud at 40º with the paddle plane rotated to 22.5º from vertical. Target 28 slant buried (short edge is 34.3 cm, long edge is 47.0 cm). Target 7 slant buried (short edge is 0 cm, long edge is 73.7 cm). Target at A5 is flush buried, slightly mounded actually.

4. Targets 23 and 24 are proud at 40º with the paddle plane rotated to 30º from vertical. Target 28 slant buried (short edge is 30.5 cm, long edge is 48.3 cm). Target 7 slant buried (short edge is 0 cm, long edge is 84.4 cm). Target at A5 is flush buried, slightly mounded actually.
5. Targets 23 and 24 proud at 40º with the paddle plane rotated to 45º from vertical. Target 28 slant buried (short edge is 21.6 cm, long edge is 48.3 cm, bottom corner height above sediment is 12.7 cm). Target 7 slant buried (short edge is 0 cm, long edge is 91.8 cm, top corner height above sediment is 26.7 cm). Target at A5 buried deeper, now 5 cm below sediment.
6. Targets 23 and 24 are proud at 40º with the paddle plane rotated to 67.5º from vertical. Target 28 slant buried (short edge is 17.8 cm, long edge is 35.2 cm, bottom corner height above sediment is 7.62 cm). Target 7 slant buried (long edge is 92.1 cm, bottom corner depth below sediment is 5 cm, top corner height above sediment is 25.4 cm). Target at A5 buried deeper, now 5 cm below sediment.
7. No data acquired on channel 6.
8. Targets 23 and 24 are proud at 40º with the paddle plane rotated to 90º from vertical. Target 28 slant buried (short edge is 26.0 cm, long edge is 52.4 cm, bottom corner height above sediment is 14.0 cm). Target 7 slant buried (exposed end bottom corner height above sediment is 3.81 cm, top corner height above sediment is 34.9 cm, buried end bottom corner height above sediment is 7.30 cm). Target at A5 buried about 2.54 cm below sediment.
9. Dive boat present.
10. Targets 23 and 24 are proud at 40º with the paddle plane rotated to 90º from vertical. Target 28 slant buried (short edge is 25.4 cm, long edge is 53.3 cm, bottom corner height above sediment is 14.0 cm). Target 7 slant buried (exposed end bottom corner height above sediment is 3.18 cm, top corner height above sediment is 33.0 cm, buried end bottom corner height above sediment is 7.62 cm). Target at A5 flush buried.
11. Targets 23 and 24 are proud at 40º with the paddle plane rotated to 112.5º from vertical. Target 28 slant buried (short edge is 25.4 cm, long edge is 53.c cm, bottom corner height above sediment is 14.0 cm). Target 7 slant buried (exposed end bottom corner height above sediment is 3.18 cm, top corner height above sediment is 33.0 cm, buried end bottom corner height above sediment is 7.62 cm). Target at A5 flush buried.
12. Motor slipping.
13. Targets 23 and 24 are proud at 40º with the paddle plane rotated to 135º from vertical. Target 28 slant buried (short edge is 17.8 cm, long edge is 52.1 cm, bottom corner height above sediment is 9.84 cm). Target 7 slant buried (exposed end bottom corner height above sediment is 3.18 cm, top corner height above sediment is 33.0 cm, buried end bottom corner height above sediment is 7.62 cm). Target at A5 buried about 2.54 cm.
14. Dolphin noise present. Targets 23 and 24 are proud at 40º with the paddle plane rotated to 157.º from vertical. Target 28 slant buried (short edge is 7.62 cm, long edge is 65.4 cm, bottom corner height above sediment is 2.22 cm). Target 7 slant buried (exposed end bottom corner height above sediment is 3.18 cm, top corner height above sediment is 33.0 cm, buried end bottom corner height above sediment is 7.62 cm). Target at A5 buried about 2.54 cm.

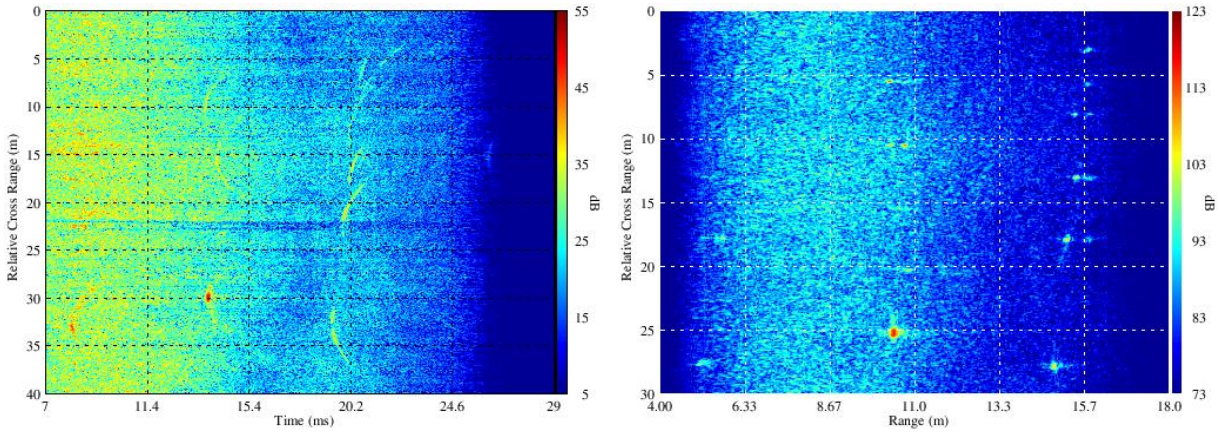


(a) PCB time signals for sequence 166 (b) SAS Image for sequence 166

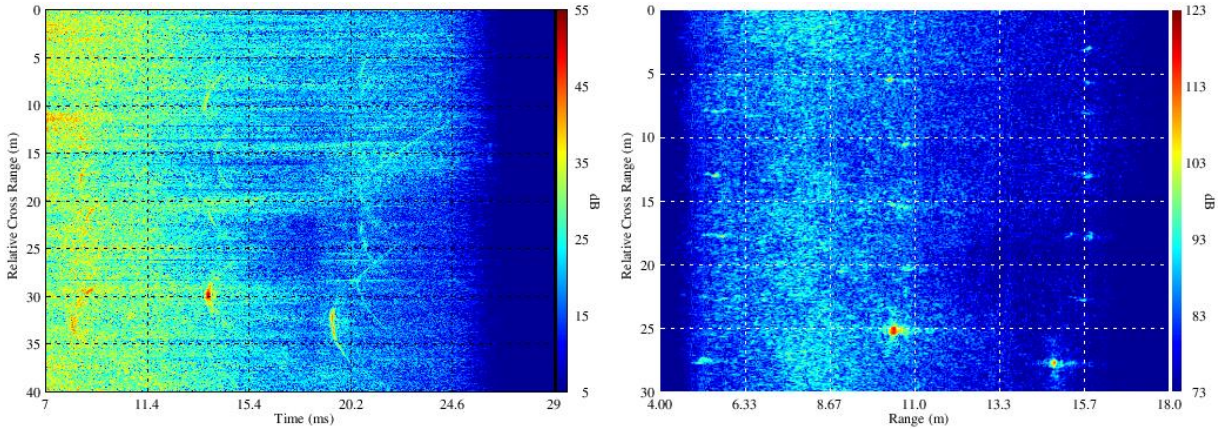


(c) PCB time signals for sequence 168 (d) SAS Image for sequence 168

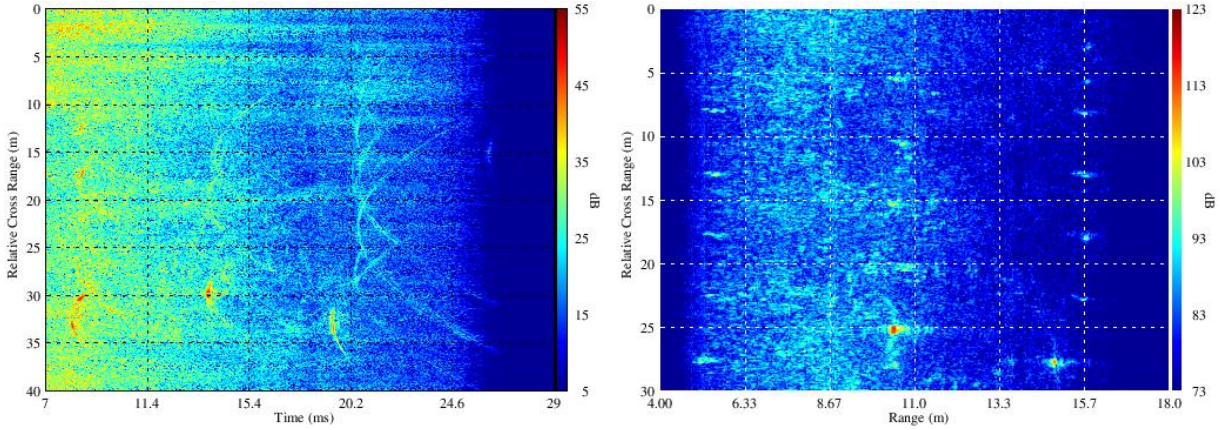


(c) PCB time signals for sequence 170 (d) SAS Image for sequence 170

Figure B18. *Initial processing step produces PCB time signals. Coherent time-domain beamforming of the PCB time signals produces a SAS image.*

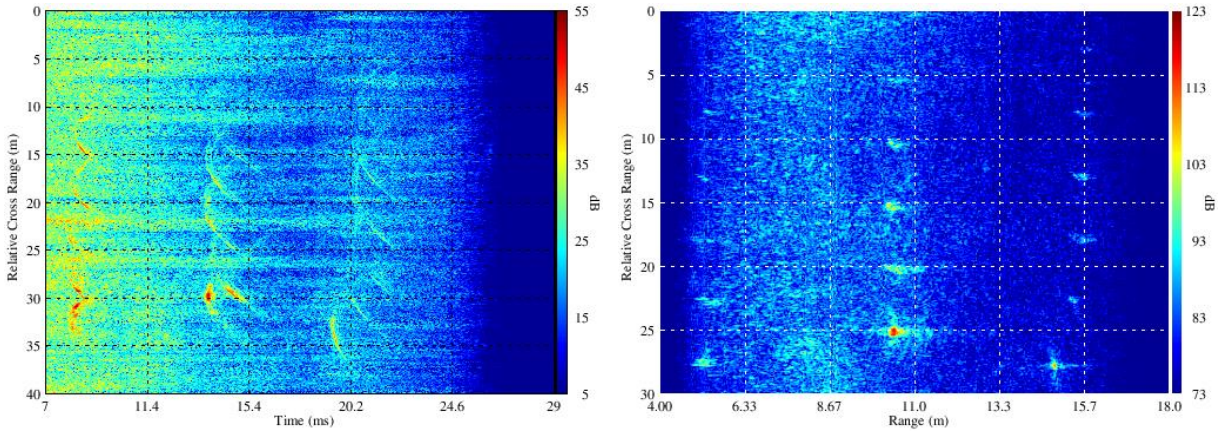


(a) PCB time signals for sequence 172 (b) SAS Image for sequence 172

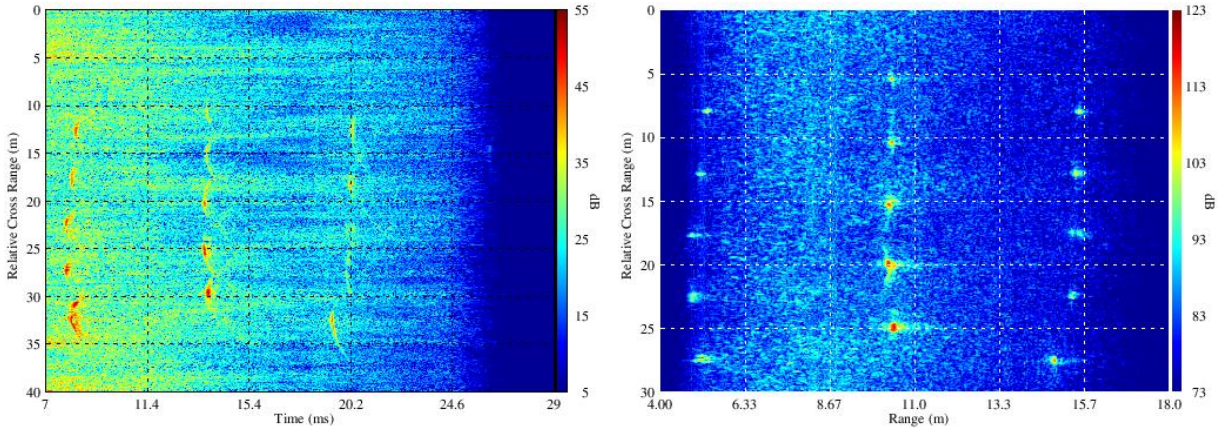


(c) PCB time signals for sequence 174 (d) SAS Image for sequence 174

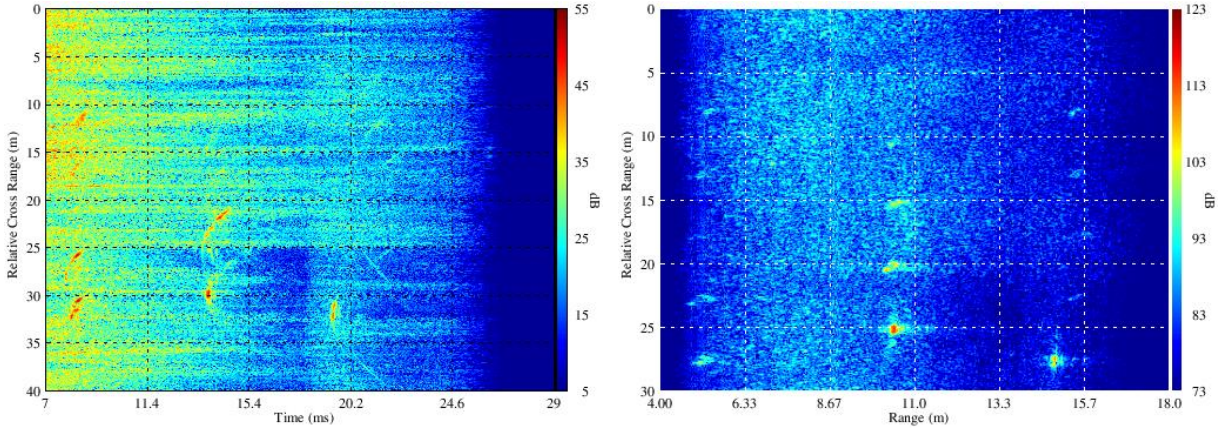


(c) PCB time signals for sequence 176 (d) SAS Image for sequence 176

Figure B19. *Initial processing step produces PCB time signals. Coherent time-domain beamforming of the PCB time signals produces a SAS image.*

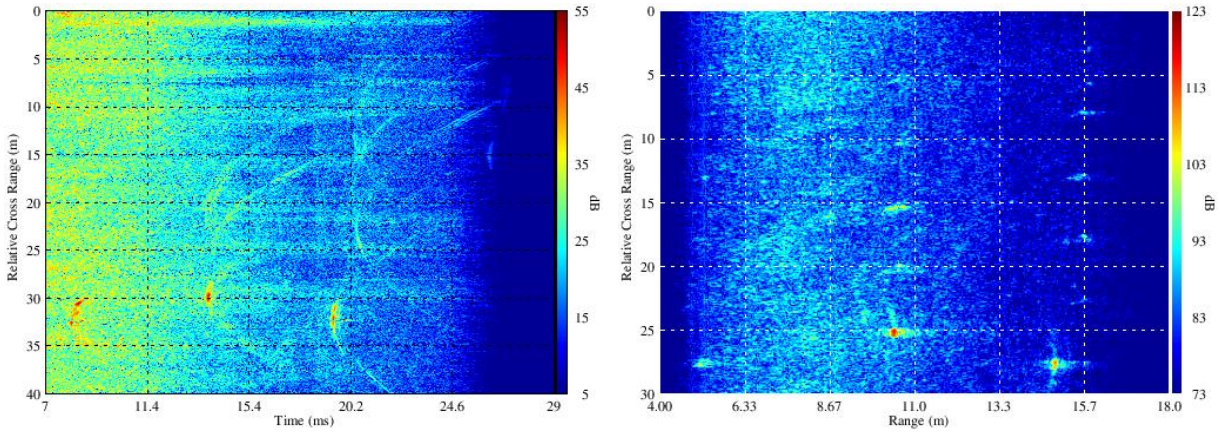


(a) PCB time signals for sequence 180 (b) SAS Image for sequence 180

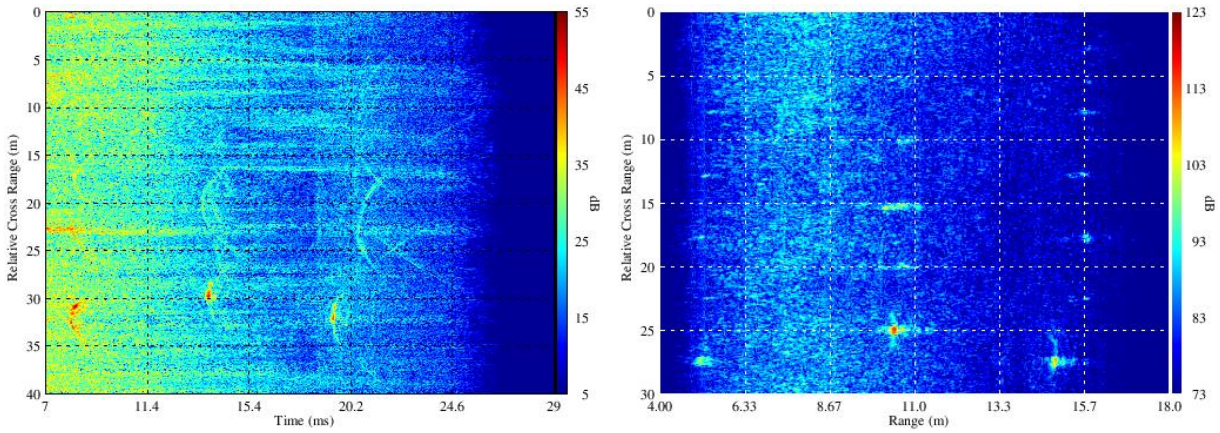


(c) PCB time signals for sequence 182 (d) SAS Image for sequence 182

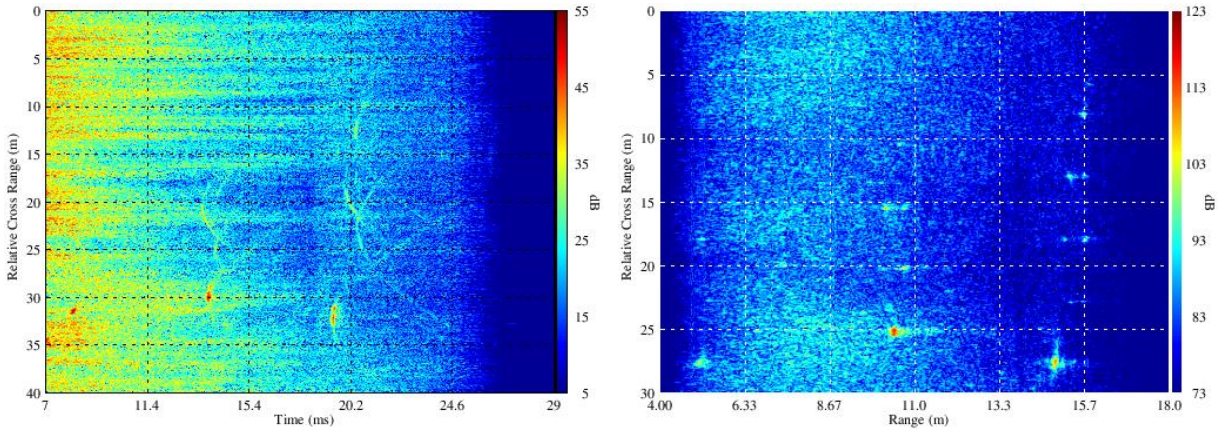


(c) PCB time signals for sequence 184 (d) SAS Image for sequence 184

Figure B20. *Initial processing step produces PCB time signals. Coherent time-domain beamforming of the PCB time signals produces a SAS image.*

| Date | Time | Seq. # | Dir. | Notes |
|---|---|---|---|---|
| 5/15 | 1459 | 220 | + | |
| 5/15 | 1532 | 221 | – | No signal. |
| 5/15 | 1547 | 222 | + | |
| 5/15 | 1603 | 223 | – | Output of L6 flipped. |
| 5/15 | 1617 | 224 | + | Output of L6 flipped. |

Table B9. *Notes for TREX13 target configuration 6. The source was aimed down at a 0º depression angle. The source amplitude into the power amplifiers was 0.5* $V_{rms}$*. All targets were proud and placed at random orientations with respect to the rail.*

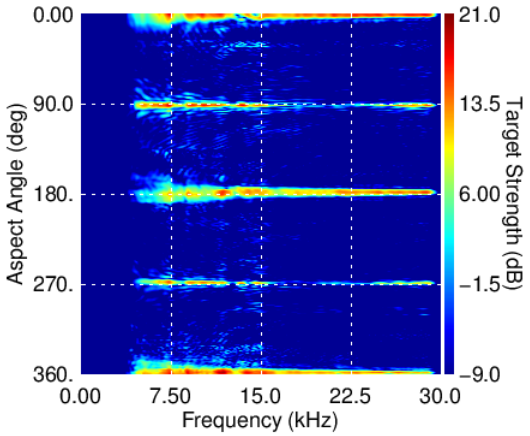


*(a) Target 1 at 35 m horizontal range*

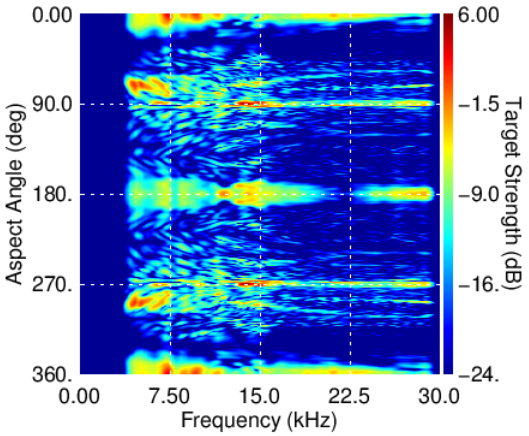


*(b) Target 5 at 25 m horizontal range*

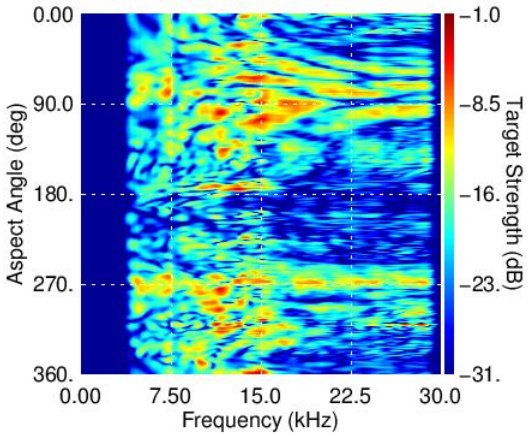


*(c) Target 2 at 35 m horizontal range*

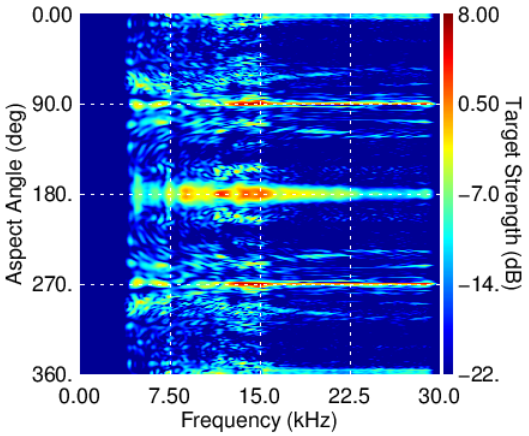


*(d) Target 5 at 30 m horizontal range*

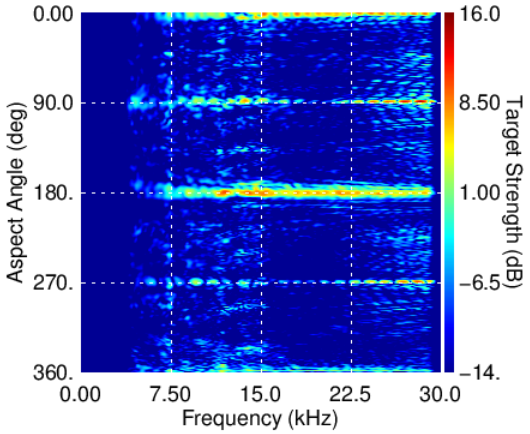


*(e) Target 3 at 35 m horizontal range*

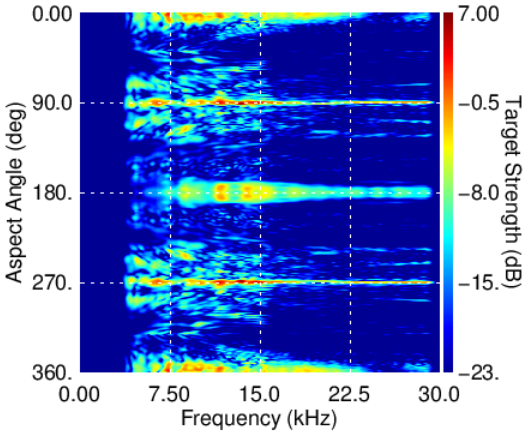


*(f) Target 5 at 40 m horizontal range*

Figure B21. *Full acoustic color templates constructed from TREX13 data. Targets are listed in Table B1.*

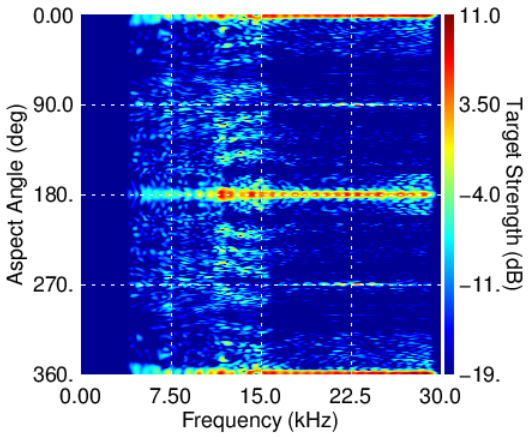


*(a) Target 6 at 25 m horizontal range*

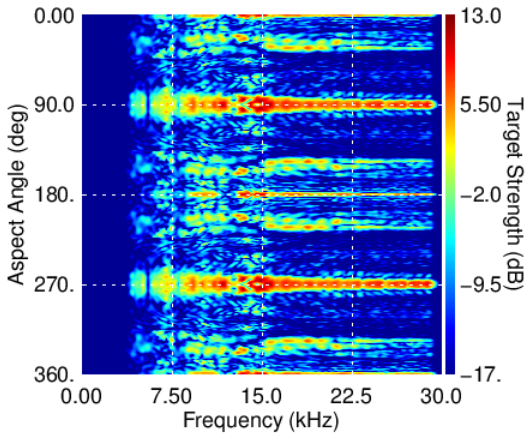


*(b) Target 7 at 30 m horizontal range*

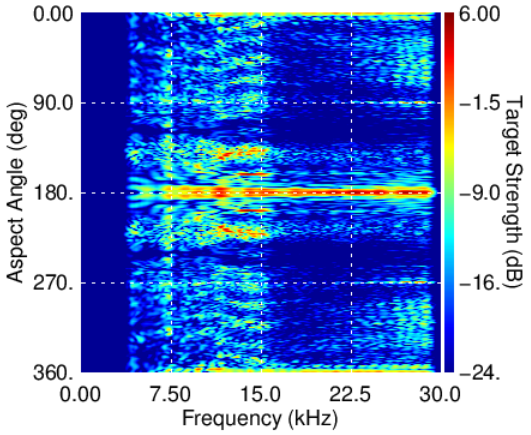


*(c) Target 6 at 35 m horizontal range*

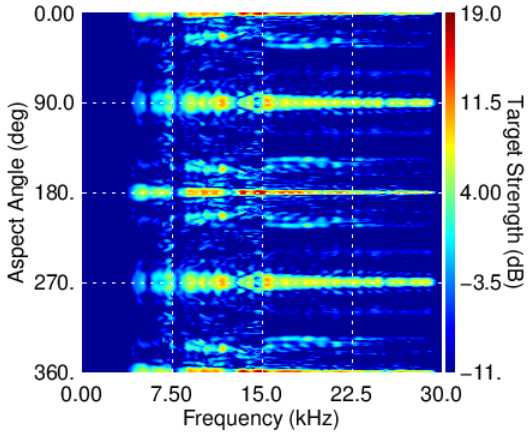


*(d) Target 7 at 35 m horizontal range*

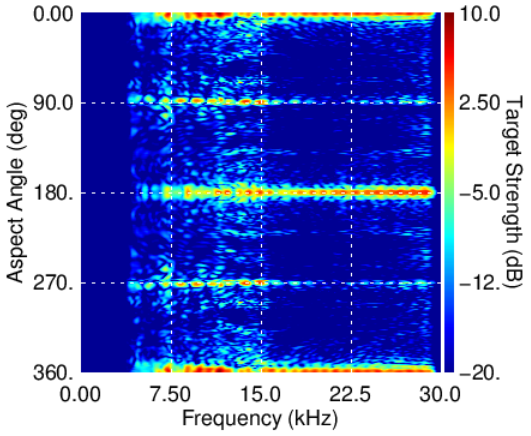


*(e) Target 6 at 40 m horizontal range*

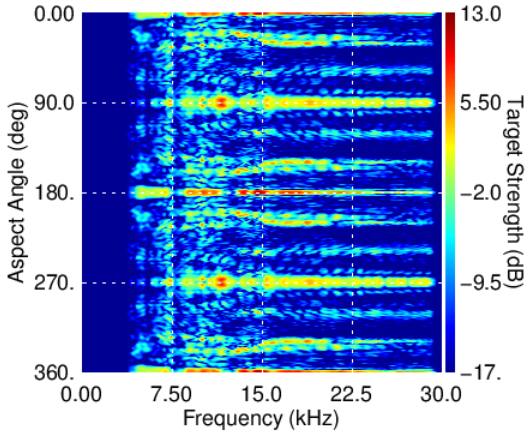


*(f) Target 7 at 40 m horizontal range*

Figure B22. *Full acoustic color templates constructed from TREX13 data. Targets are listed in Table B1.*

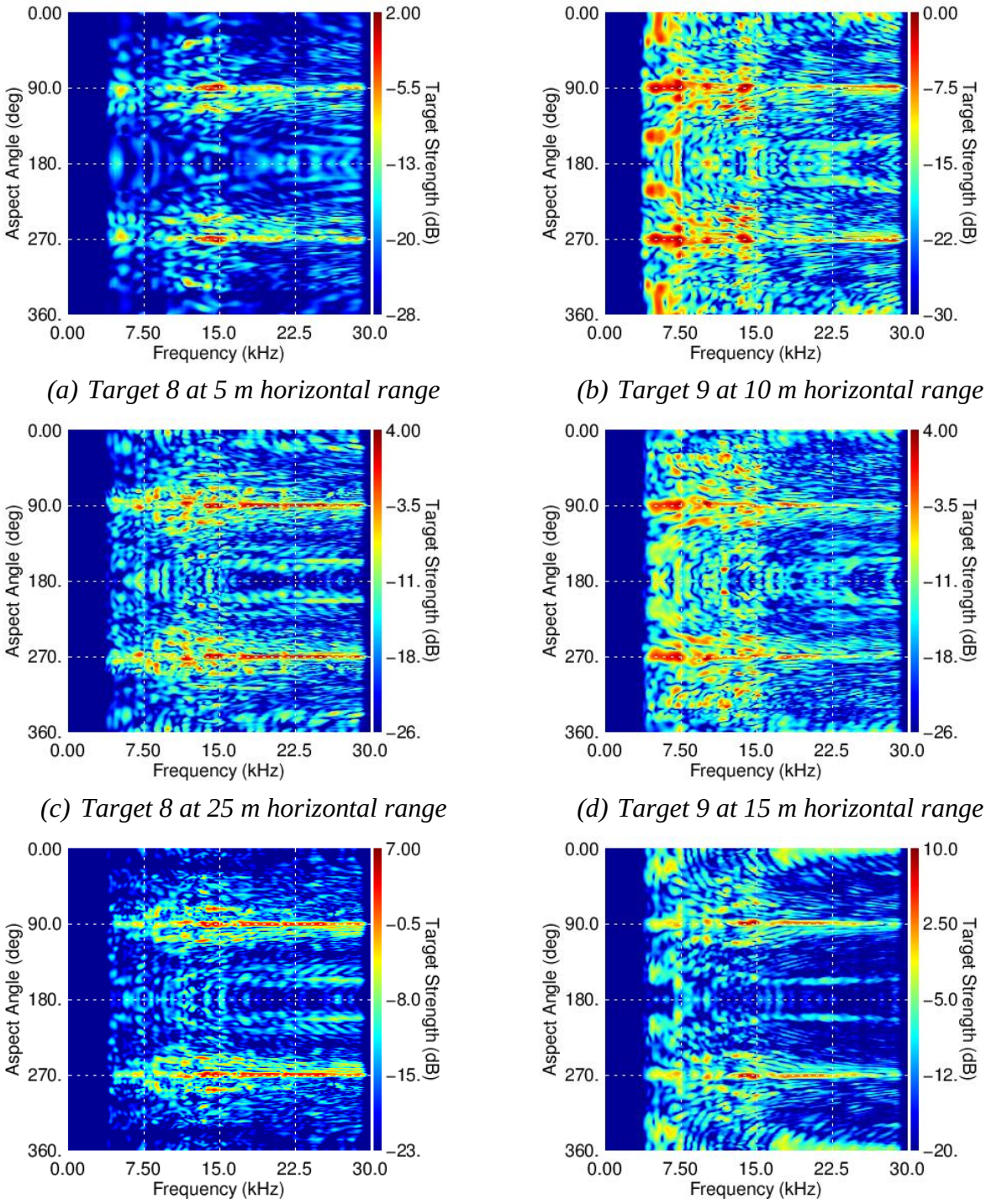


*(a) Target 8 at 5 m horizontal range*

*(b) Target 9 at 10 m horizontal range*

*(c) Target 8 at 25 m horizontal range*

*(d) Target 9 at 15 m horizontal range*

*(e) Target 8 at 30 m horizontal range*

*(f) Target 9 at 20 m horizontal range*

Figure B23. *Full acoustic color templates constructed from TREX13 data. Targets are listed in Table B1.*

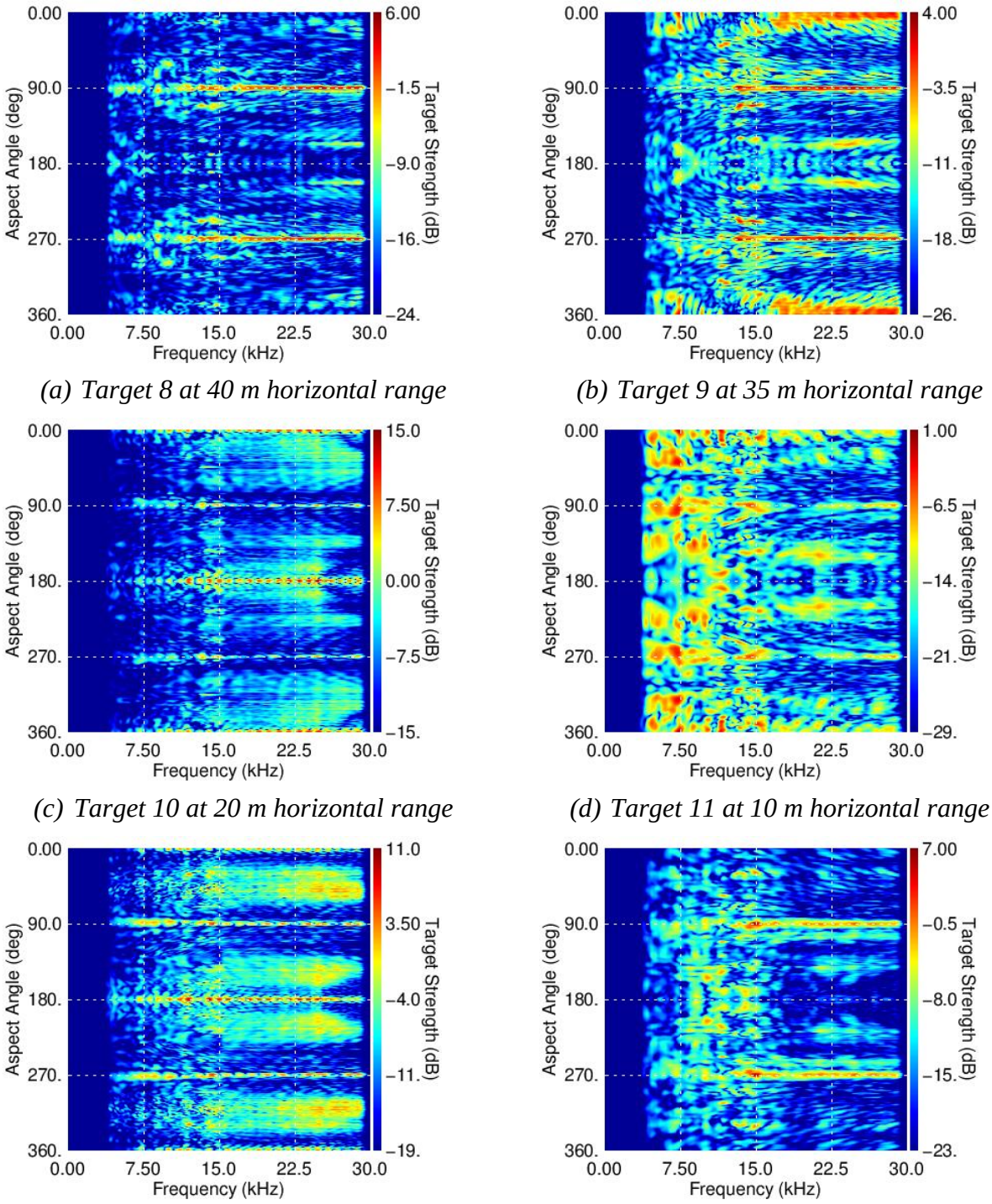


*(a) Target 8 at 40 m horizontal range*

*(b) Target 9 at 35 m horizontal range*

*(c) Target 10 at 20 m horizontal range*

*(d) Target 11 at 10 m horizontal range*

*(e) Target 10 at 25 m horizontal range*

*(f) Target 11 at 20 m horizontal range*

Figure B24. *Full acoustic color templates constructed from TREX13 data. Targets are listed in Table B1.*

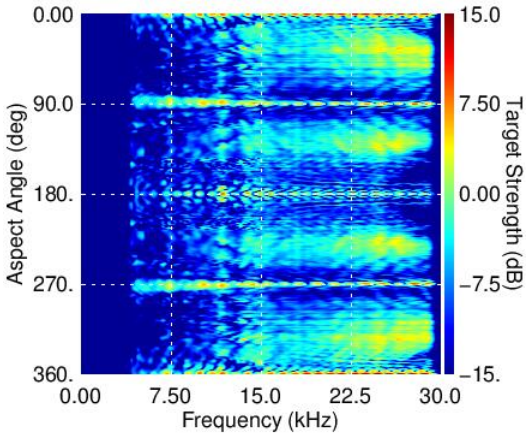


*(a) Target 10 at 30 horizontal range*

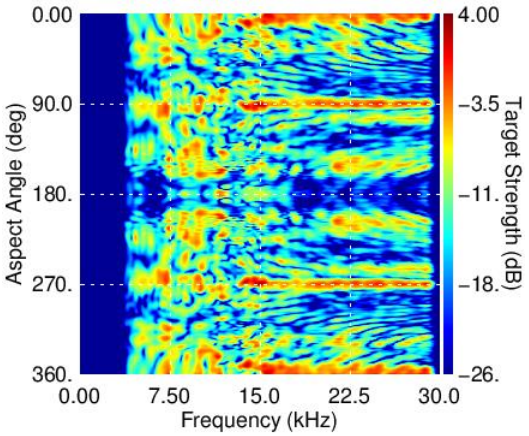


*(b) Target 11 at 25 m horizontal range*

*Intentionally left blank*

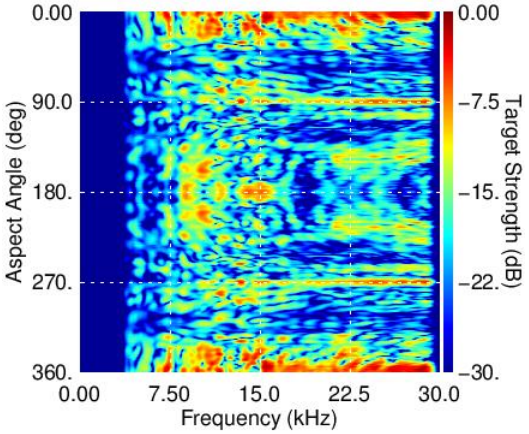


*(c) Target 11 at 35 m horizontal range*

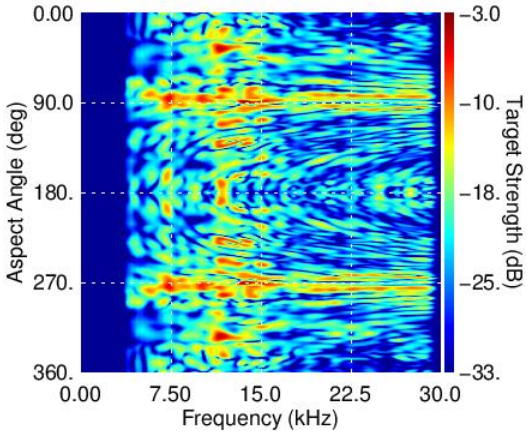


*(d) Target 12 at 15 m horizontal range*

*Intentionally left blank*

Figure B25. *Full acoustic color templates constructed from TREX13 data. Targets are listed in Table B1.*

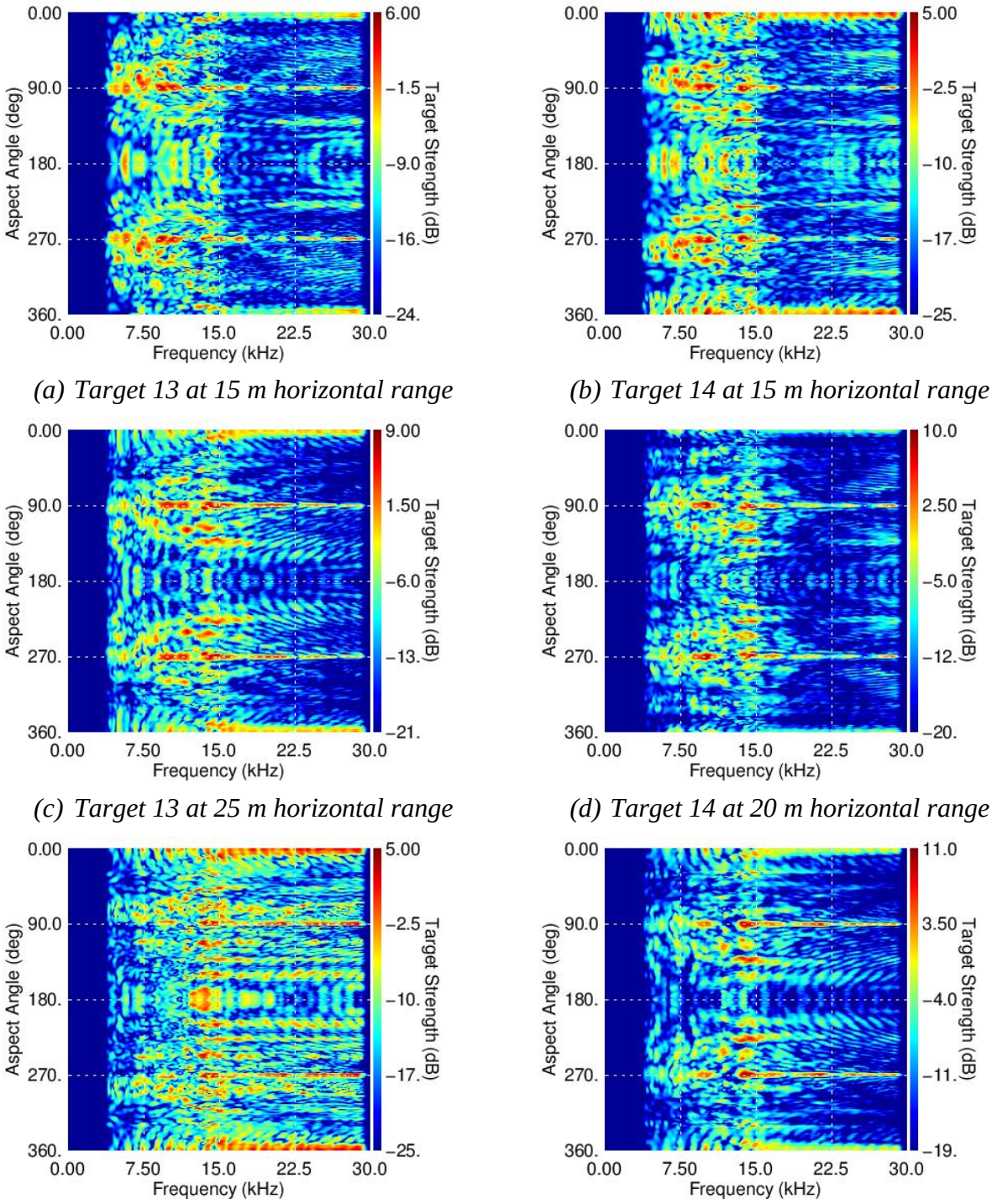


*(a) Target 13 at 15 m horizontal range*

*(b) Target 14 at 15 m horizontal range*

*(c) Target 13 at 25 m horizontal range*

*(d) Target 14 at 20 m horizontal range*

*(e) Target 13 at 35 m horizontal range*

*(f) Target 14 at 25 m horizontal range*

Figure B26. *Full acoustic color templates constructed from TREX13 data. Targets are listed in Table B1.*

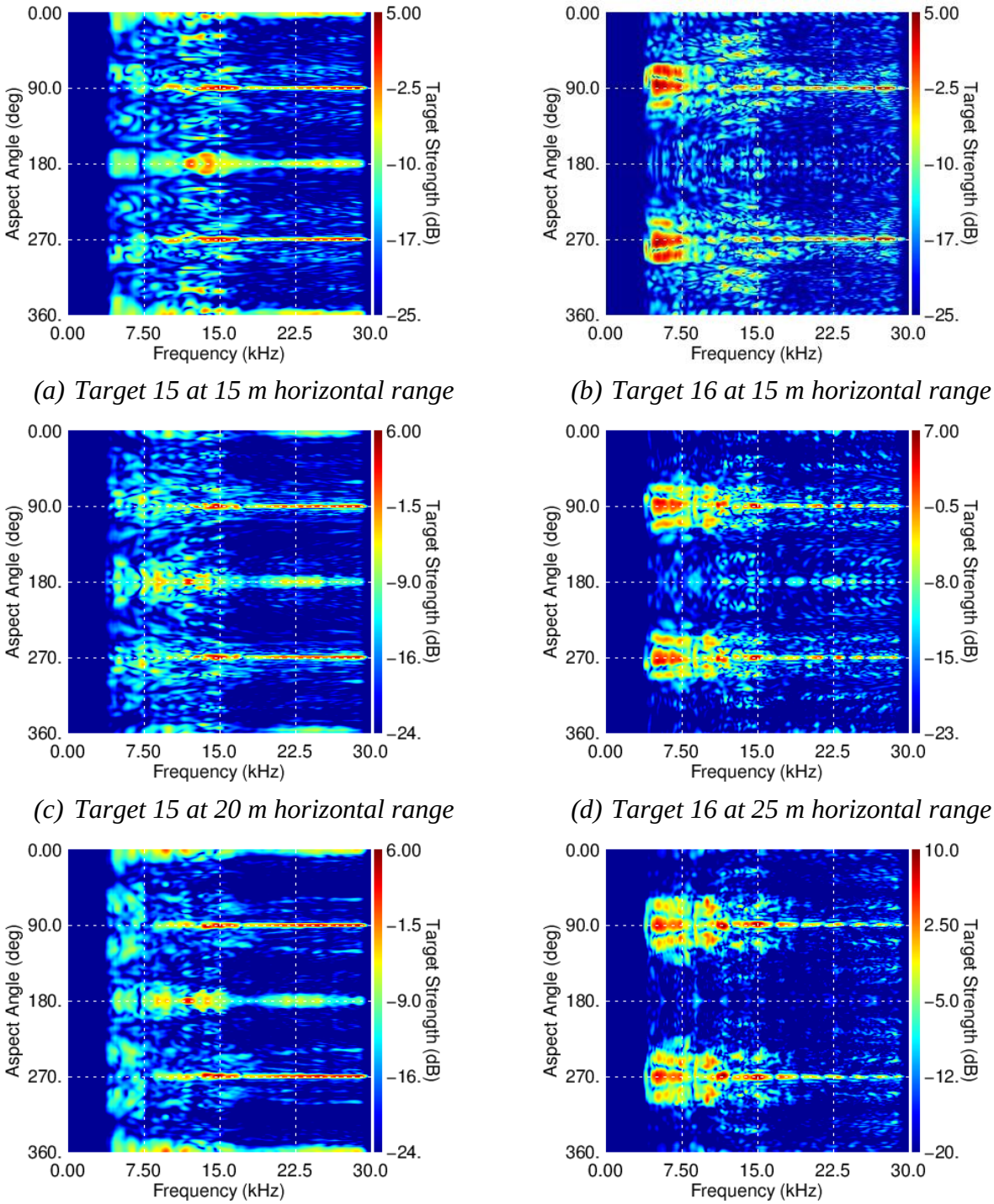


*(a) Target 15 at 15 m horizontal range*

*(b) Target 16 at 15 m horizontal range*

*(c) Target 15 at 20 m horizontal range*

*(d) Target 16 at 25 m horizontal range*

*(e) Target 15 at 25 m horizontal range*

*(f) Target 16 at 30 m horizontal range*

Figure B27. *Full acoustic color templates constructed from TREX13 data. Targets are listed in Table B1.*

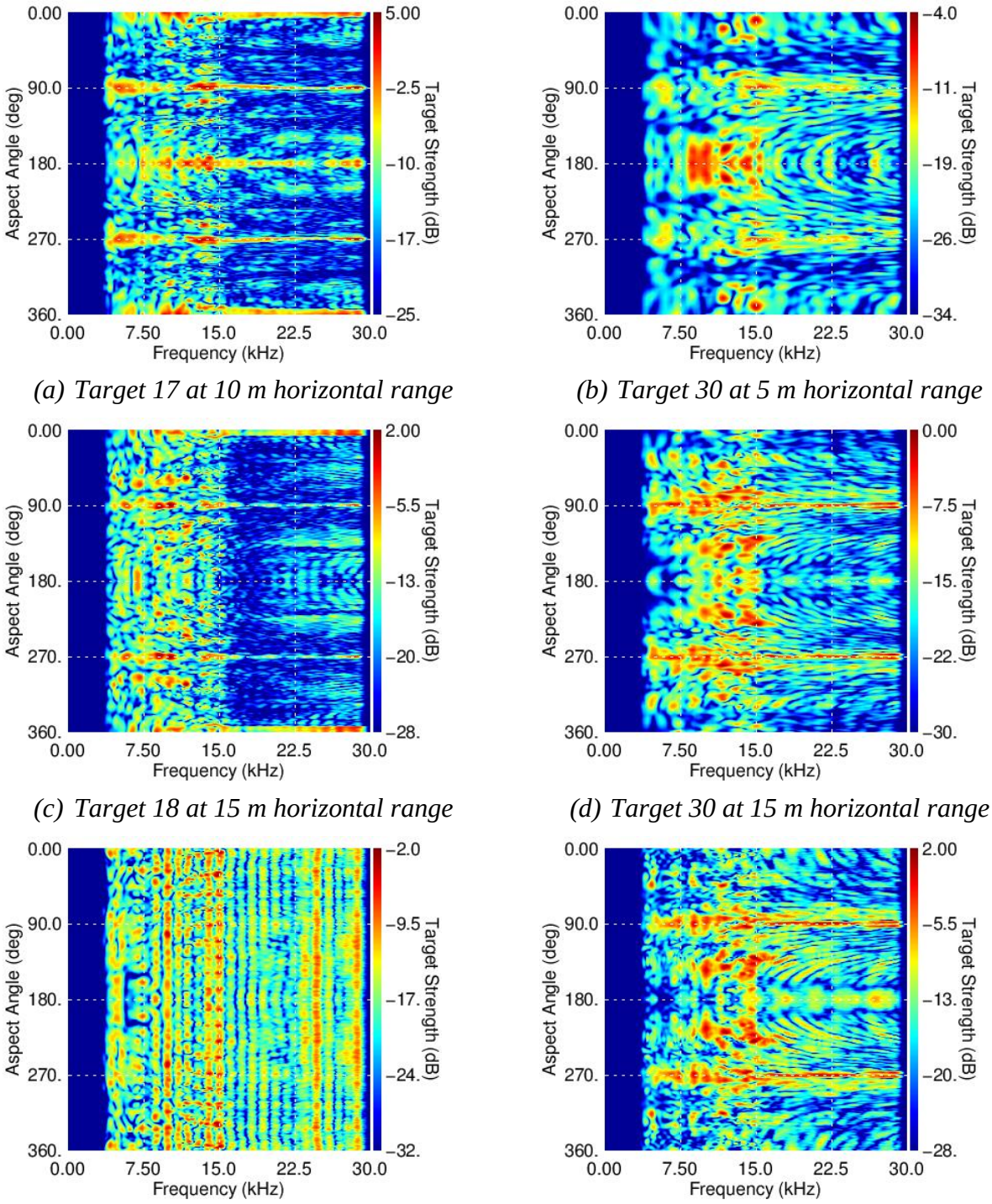


*(a) Target 17 at 10 m horizontal range*

*(b) Target 30 at 5 m horizontal range*

*(c) Target 18 at 15 m horizontal range*

*(d) Target 30 at 15 m horizontal range*

*(e) Target 19 at 20 m horizontal range*

*(f) Target 30 at 20 m horizontal range*

Figure B28. *Full acoustic color templates constructed from TREX13 data. Targets are listed in Table B1.*

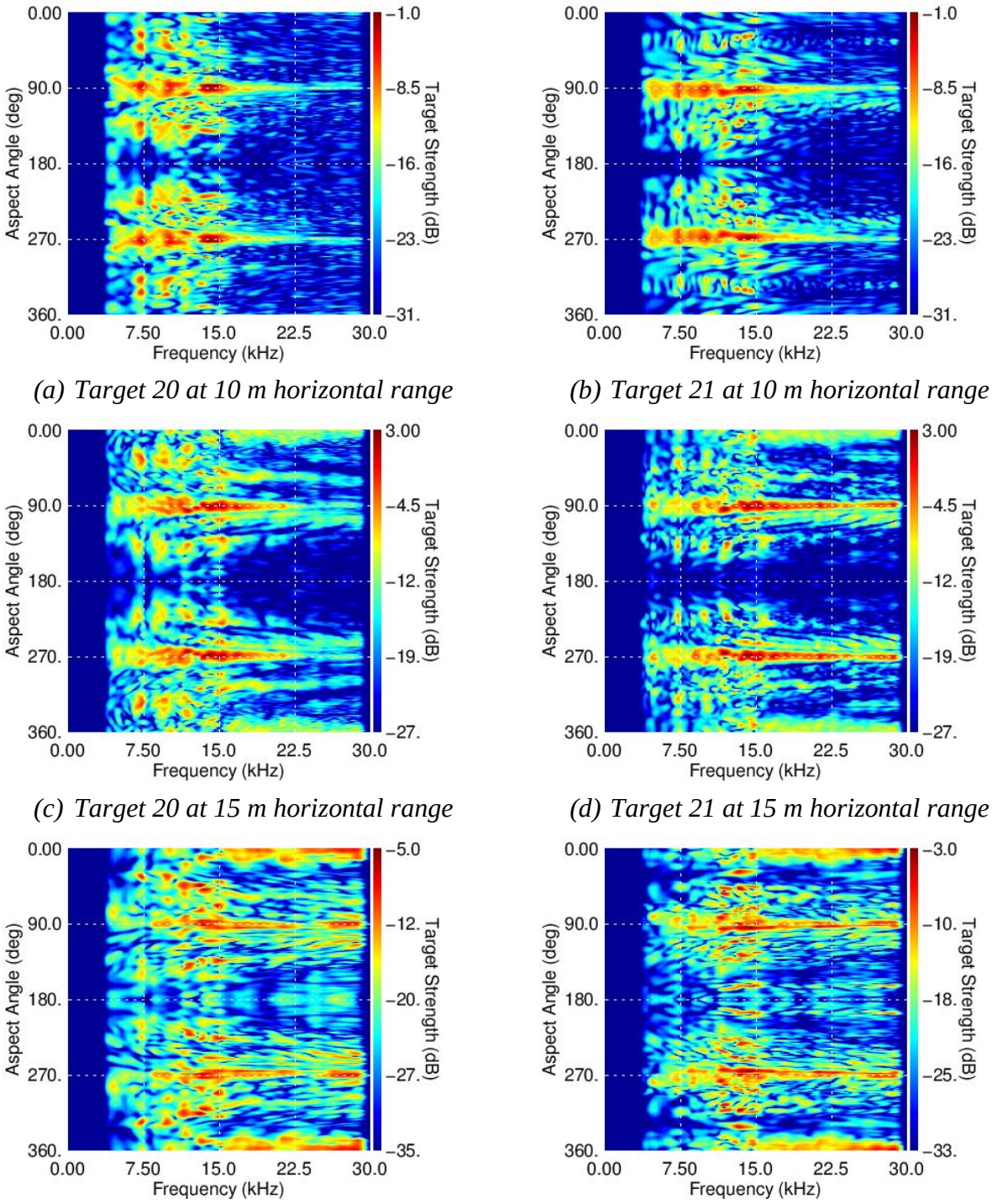


*(a) Target 20 at 10 m horizontal range*

*(b) Target 21 at 10 m horizontal range*

*(c) Target 20 at 15 m horizontal range*

*(d) Target 21 at 15 m horizontal range*

*(e) Target 20 at 30 m horizontal range*

*(f) Target 21 at 25 m horizontal range*

Figure B29. *Full acoustic color templates constructed from TREX13 data. Targets are listed in Table B1.*

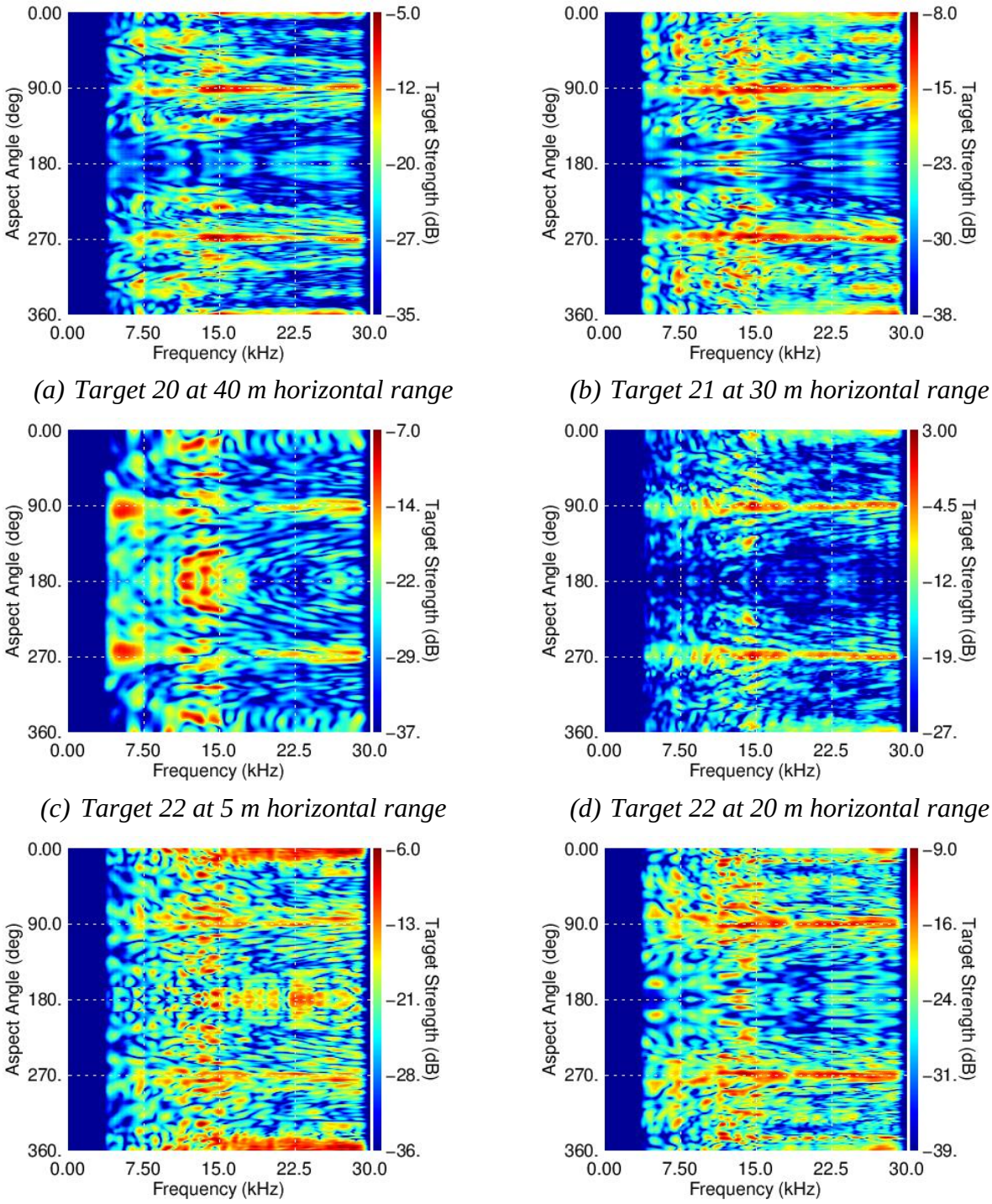


*(a) Target 20 at 40 m horizontal range*

*(b) Target 21 at 30 m horizontal range*

*(c) Target 22 at 5 m horizontal range*

*(d) Target 22 at 20 m horizontal range*

*(e) Target 22 at 30 m horizontal range*

*(f) Target 22 at 40 m horizontal range*

Figure B30. *Full acoustic color templates constructed from TREX13 data. Targets are listed in Table B1.*

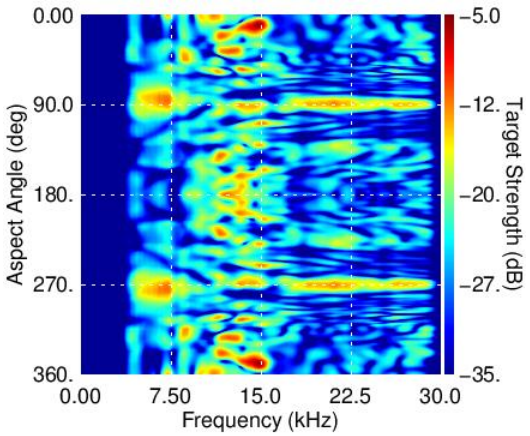


*(a) Target 23 at 5 m horizontal range*

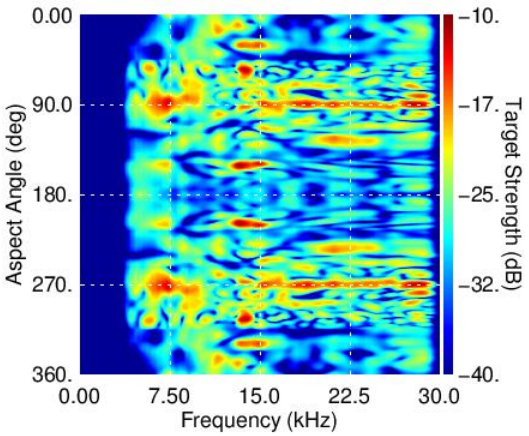


*(b) Target 24 at 5 m horizontal range*

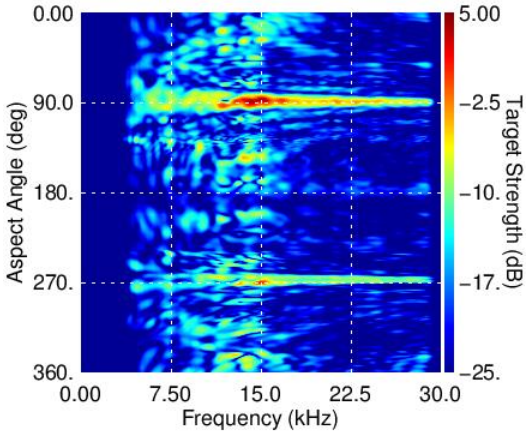


*(c) Target 23 at 15 m horizontal range*

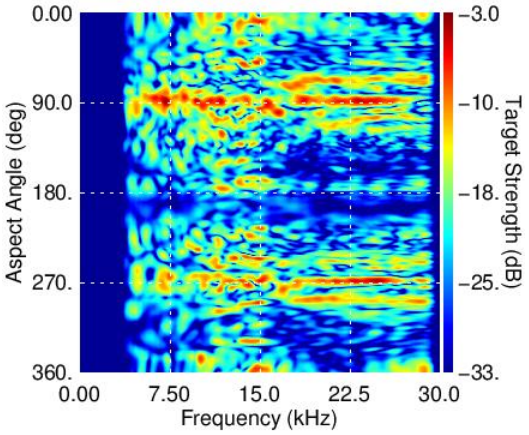


*(d) Target 24 at 15 m horizontal range*

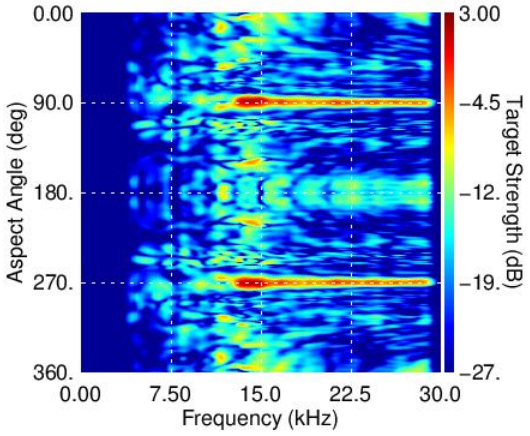


*(e) Target 23 at 20 m horizontal range*

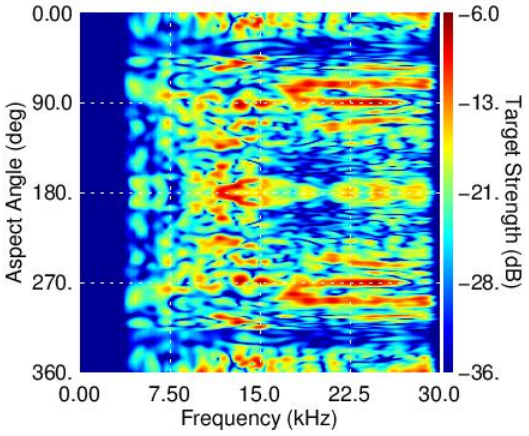


*(f) Target 24 at 20 m horizontal range*

Figure B31. *Full acoustic color templates constructed from TREX13 data. Targets are listed in Table B1.*

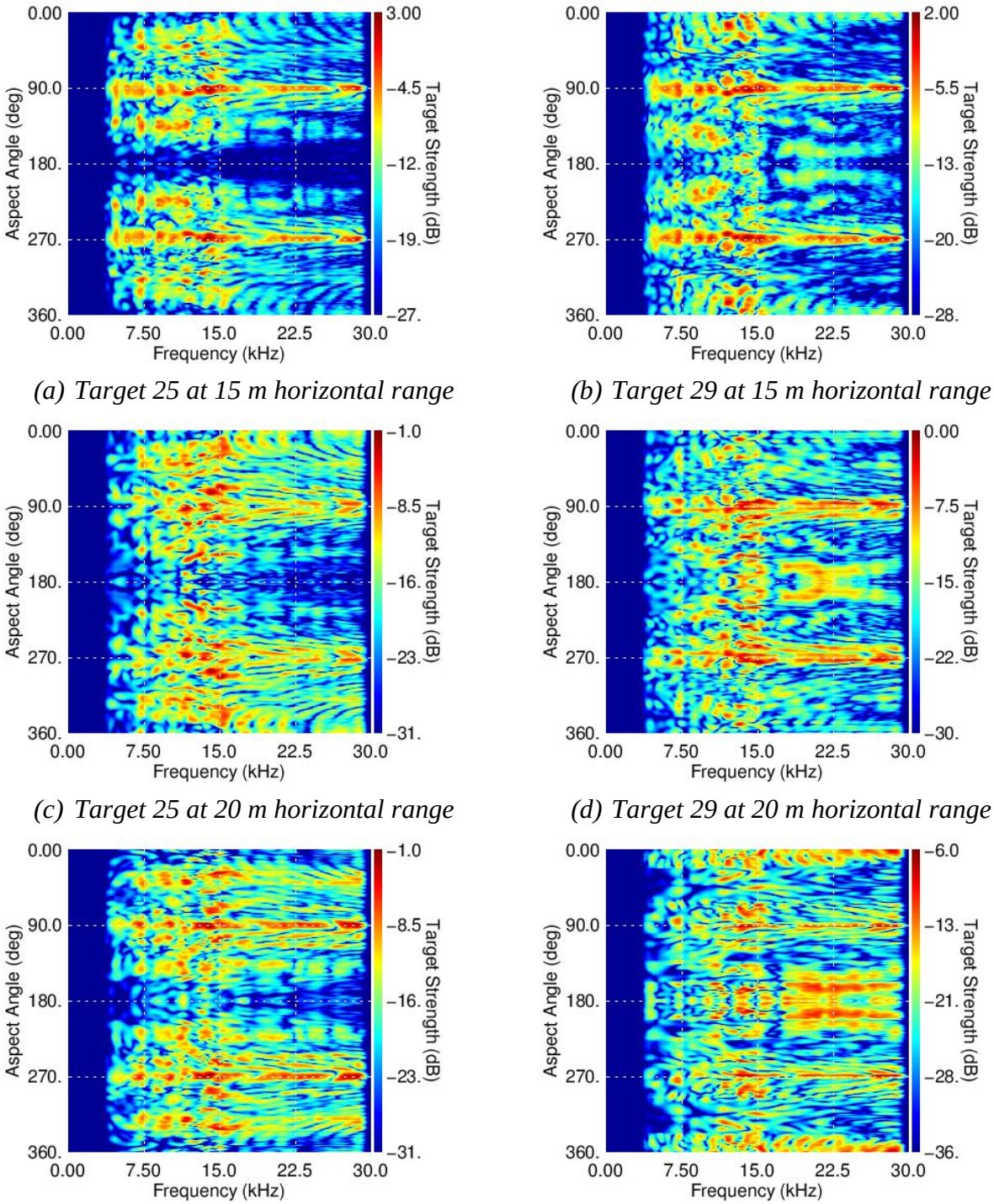


*(a) Target 25 at 15 m horizontal range*

*(b) Target 29 at 15 m horizontal range*

*(c) Target 25 at 20 m horizontal range*

*(d) Target 29 at 20 m horizontal range*

*(e) Target 25 at 25 m horizontal range*

*(f) Target 29 at 35 m horizontal range*

Figure B32. *Full acoustic color templates constructed from TREX13 data. Targets are listed in Table B1.*

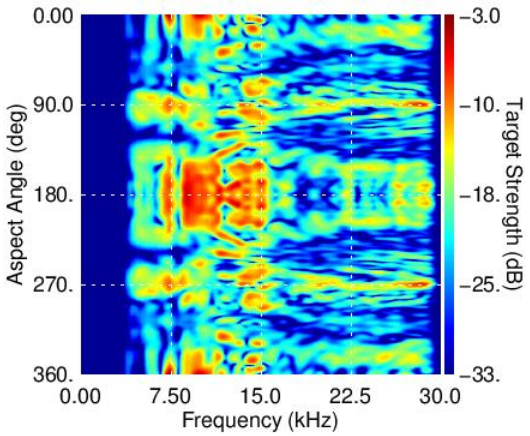


*(a) Target 25 at 5 m horizontal range*

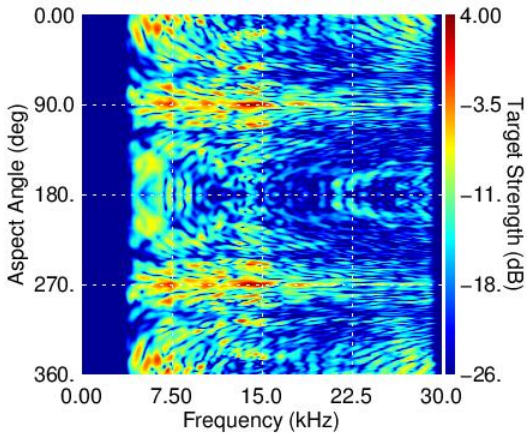


*(b) Target 28 at 15 m horizontal range*

*Intentionally left blank*

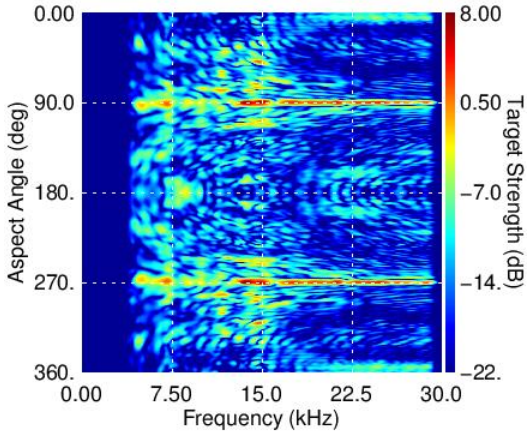


*(c) Target 28 at 25 m horizontal range*

*Intentionally left blank*

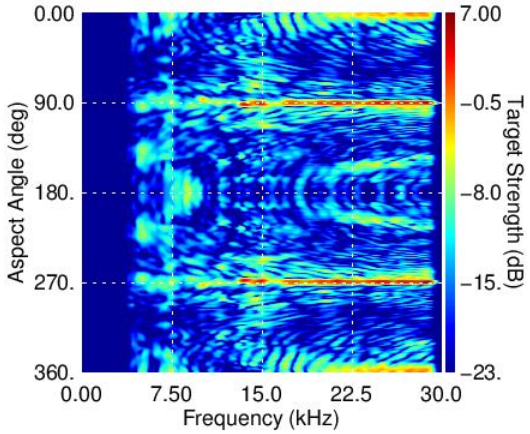


*(d) Target 28 at 30 m horizontal range*

Figure B33. *Full acoustic color templates constructed from TREX13 data. Targets are listed in Table B1.*

## Appendix C: BAYEX14 Target Configurations

Targets were distributed into 11 target configurations. Targets used in TREX13, and listed in Table B1, were deployed during BAYEX14 with only a few minor changes. The BAYEX14 targets and target configurations are given in Tables C1 and C2. The grid locations for the target configurations refer to the grid depicted in Fig. B1. It is noted that due to a strong return from the R/V *Sharp* near and at the time of returns from targets in grid locations C2–C6, the C-line is typically unused. Target field grid entries with a trailing .5 are a location halfway between adjacent locations; for example, H1.5 is the grid location halfway between H1 and H2.

| Target | Target | TF1 | TF2 | TF3 | TF4 | TF5 | TF6 | Notes |
|---|---|---|---|---|---|---|---|---|
| 1 | Diver Evaluation Unit | G1 | G1 | D1 | D1 | D1 | D1 | 1 |
| 2 | Rock | G3 | G3 | | | | | 2 |
| 3 | 55-gallon drum | G2 | G2 | | | | | 3 |
| 4 | 5:1 aluminum cylinder | D4 | A2 | A1 | | | | 4 |
| 6 | 55-gallon drum | F1 | E2 | | | | | 5 |
| 7 | 3:1 aluminum cylinder | H3 | G4 | B5 | B5 | B5 | | |
| 8 | 155-mm howitzer without collar | E1 | H3 | B2 | H2.5 | H2 | G3 | |
| 11 | 152-mm TP-T round | E2 | D2 | B3 | | | | |
| 12 | 81-mm mortar | D5 | A5 | | | | | 4 |
| 13 | Water-filled scuba tank | E3 | A4 | | H1.5 | G1 | F1 | 4,6 |
| 16 | 2:1 aluminum pipe | E4 | F3 | B1 | H2 | H1.5 | G1 | |
| 17 | 2:1 aluminum cylinder | D3 | D3 | D3 | H3 | H2.5 | G4 | |
| 20 | Al replica #1 of target 22 | A3 | D1 | A2 | H1 | G4 | F3 | |
| 21 | Steel replica of target 22 | A2 | E1 | A3 | | | | |
| 22 | 100-mm inert artillery shell | D1 | F1 | A5 | | | | |
| 23 | Solid Al cylinder with notch | A6 | A6 | | | | | 4,7 |
| 24 | Hollow Al cylinder with notch | A1 | A1 | | | | | 4,7 |
| 25 | 105-mm bullet-shaped UXO #1 | A5 | E4 | A4 | | | | |
| 28 | 155-mm howitzer with collar | A4 | D4 | A6 | | | | |
| 29 | 105-mm bullet-shaped UXO #2 | G4 | D5 | B2 | | | | |
| 30 | 105-mm finned shell #1 | D2 | A3 | | | | | 4 |
| 33 | Al replica #2 of target 22 | F3 | E3 | | | | | |
| | Stainless steel spherical shell | | | C1 | C1 | C1 | C1 | 8 |

Table C1. *Enumeration of targets and target field locations during BAYEX14. The first column is the number assigned and painted onto the targets. Targets with assigned numbers, which were not deployed or germane to SERDP MR-2231, are not listed. The second column is the actual target. Columns TF1–TF6 represent the first six target configurations. Target location can be determined from Fig. B1. Last column refers to a note given below.*

In target configuration 1, a small spherical float was anchored beyond the target field with a screw anchor. The spherical float was positioned beyond H2 in Fig. B1 at i1 approximately 42 m from the APL-UW rail for sequences 18–24. The spherical float was then moved to a location above A6 in Fig. B1, but at a ~42-m horizontal range for sequences 25 and above. The small spherical float provided a convenient fiducial, which aided in comparisons of SAS images generated from different sequences.

| Target | Target | TF7 | TF8 | TF9 | TF10 | TF11 | Notes |
|---|---|---|---|---|---|---|---|
| 1 | Diver Evaluation Unit | D1 | | | | | |
| 8 | 155-mm howitzer without collar | F2 | E2.5 | D3 | B3 | A4 | 9 |
| 13 | Water-filled scuba tank | F1 | E1.5 | D13 | B2 | A3 | 9 |
| 16 | 2:1 aluminum pipe | F0.5 | E1 | D0.5 | B1 | A2 | 9 |
| 17 | 2:1 aluminum cylinder | F3.5 | E4 | D5.5 | B5 | A6 | 9 |
| 20 | Al replica #1 of target 22 | F3 | E3 | D4 | B4 | A5 | 9 |

Table C2. *Enumeration of targets and target field locations during BAYEX14. The first column is the number assigned and painted onto the targets. Targets with assigned numbers, which were not deployed or germane to SERDP MR-2231, are not listed. The second column is the actual target. Columns TF7–TF11 represent the last five target configurations. Target location can be determined from Fig. B1. Last column refers to a note given below.*

1. End with zinc anode is tail.
2. Arrow points to nose.
3. Open end of drum is tail and small plumbing fixture was attached to drum.
4. For TF1 and TF2, the targets in A1–A6 are at a 10-m horizontal range (along the B-line in Fig. B1 but below the C-line location.
5. Open end of drum is tail.
6. Stem of scuba tank is the nose.
7. The end with the notch is the tail.
8. The diameter and thickness of the spherical shell are 60 cm and 1.2 cm, respectively. The shell is unnumbered.
9. Targets are in a broadside orientation (axis of symmetry parallel to APL-UW rail).

| Date | Time | Seq. # | Pings | Dir. | Source | Vrms | 5 m (deg) | 15 m (deg) | 45 m (deg) | Angle (deg) | Notes |
|---|---|---|---|---|---|---|---|---|---|---|---|
| 5/10 | 0927 | 0 | 20 | | VLA | 0.5 | | | | | 1 |
| 5/10 | 0931 | 1 | 20 | | VLA | 0.5 | | | | | 1 |
| 5/10 | 0952 | 2 | 20 | | VLA | 0.5 | | | | | 1,2 |
| 5/10 | 1000 | 3 | 20 | | 5494 | 1.0 | | | | | 1 |
| 5/10 | 1006 | 4 | 20 | | VLA/5494 | 0.5/1.0 | | | | | 1,3 |
| 5/10 | 1010 | 5 | 20 | | VLA/5494 | 0.5/1.0 | | | | | 1,4 |
| 5/10 | 1204 | 6 | 20 | | VLA | 0.05 | | | | 0 | 5 |
| 5/10 | 1218 | 7 | 20 | | VLA | 0.5 | | | | 0 | 5 |
| 5/10 | 1222 | 8 | 20 | | VLA | 0.5 | | | | 0 | 5,6 |
| 5/10 | 1226 | 9 | 20 | | 5494 | 1.0 | | | | 0 | 5,6 |
| 5/10 | 1229 | 10 | 20 | | VLA | 0.5 | | | | 0 | 5,7 |
| 5/10 | 1238 | 11 | 20 | | | | | | | 0 | 5,8 |
| 5/10 | 1239 | 12 | 20 | | VLA/5494 | 0.5/1.0 | | | | 0 | 5,9 |
| 5/10 | 1305 | 13 | 20 | | 5494 | 1.0 | | | | 0 | 5,10 |
| 5/10 | 1354 | 14 | 20 | | VLA | 0.5 | | | | 10 | 5 |
| 5/10 | 1356 | 15 | 20 | | VLA/5494 | 0.5/1.0 | | | | 10 | 5 |
| 5/10 | 1357 | 16 | 20 | | 5494 | 1.0 | | | | 10 | 5 |
| 5/11 | 1039 | 17 | 20 | | VLA/5494 | 0.5/1.0 | | | | 10 | |
| 5/11 | 1046 | 18 | 1680 | – | VLA/5494 | 0.5/1.0 | | | 0 | 10 | 11 |
| 5/11 | 1439 | 19 | 20 | | VLA/5494 | 0.5/1.0 | | | 0 | 10 | 12 |
| 5/11 | 1718 | 20 | 1680 | + | VLA/5494 | 0.5/1.0 | 0 | 0 | 0 | 10 | 13 |

Table C3. *Initial tests of APL-UW sources and receiving electronics during BAYEX14.*

1. Mast down. No motion of tower.
2. Polarity of stave 3 in VLA is inverted.
3. Test of dual source operation. Polarity of stave 3 has been flipped back to normal. Listening on 8287 and F41 hydrophones.
4. Test of dual source operation. Listening on 8287, F41, and TC-4013 hydrophones.
5. Mast up. No motion of tower. TC-4013 on tripod at ~6.6 m in front of tower and ~1 m lower in the vertical direction compared to the transducers.
6. Inverted polarity on stave 3.
7. Polarity on stave 3 flipped back to normal.
8. No transmission. Listening to ambient noise on TC-4013.
9. Dual source operation.
10. Mast up. No motion. TC-4013 on tripod at ~6.6 m. Transmitting 150 kHz monotone pulse on 5494.
11. First full run. Spherical float anchored ~6 m behind H2. Nothing in target field except sidelines and the H, G, and F lines.
12. No motion.
13. C-line populated according to target field configuration #1 in broadside orientation.

| Date | Time | Seq. | Dir | 10 m (deg) | 20 m (deg) | 25 m (deg) | 30 m (deg) | 35 m (deg) | 40 m (deg) | 45 m (deg) | Note |
|---|---|---|---|---|---|---|---|---|---|---|---|
| 5/12 | 1419 | 21 | + | 0,0 | 0 | 0 | 0,~0 | 0,~0 | 0,~0 | 0 | 1 |
| 5/12 | 1433 | 22 | – | 0,0 | 0 | 0 | 0,~0 | 0,~0 | 0,~0 | 0 | |
| 5/12 | 1558 | 23 | + | 0,0 | 0 | 0 | 0,~0 | 0,~0 | 0,~0 | 0 | 2 |
| 5/12 | 1712 | 24 | – | 0,0 | 0 | 0 | 0,~0 | 0,~0 | 0,~0 | 0 | 3 |
| 5/13 | 1128 | 25 | | –80, –80 | –80 | –80 | –80, ~0 | –80, ~0 | ~0, ~0 | 0 | 4 |
| 5/13 | 1129 | 26 | + | –80, –80 | –80 | –80 | –80, ~0 | –80, ~0 | ~0, ~0 | 0 | 5 |
| 5/13 | 1144 | 27 | – | –80, –80 | –80 | –80 | –80, ~0 | –80, ~0 | ~0, ~0 | 0 | 6 |
| 5/13 | 1457 | 28 | + | –60, –60 | –60 | –60 | –60, ~0 | –60, ~0 | ~0, ~0 | 0 | 7 |
| 5/13 | 1512 | 29 | – | –60, –60 | –60 | –60 | –60, ~0 | –60, ~0 | ~0, ~0 | 0 | 7 |
| 5/14 | 0918 | 30 | + | –40, –40 | –40 | –40 | –40, ~0 | –40, ~0 | ~0, ~0 | 0 | 8 |
| 5/14 | 0933 | 31 | – | –40, –40 | –40 | –40 | –40, ~0 | –40, ~0 | ~0, ~0 | 0 | 9 |
| 5/14 | 1120 | 32 | + | –20, –20 | –20 | –20 | –20, ~0 | –20, ~0 | ~0, ~0 | 0 | 10 |
| 5/14 | 1134 | 33 | – | –20, –20 | –20 | –20 | –20, ~0 | –20, ~0 | ~0, ~0 | 0 | 11 |
| 5/14 | 1501 | 34 | + | 0,0 | 0 | 0 | 0,0 | 0,0 | 0,0 | 0 | 12 |
| 5/14 | 1515 | 35 | – | 0,0 | 0 | 0 | 0,0 | 0,0 | 0,0 | 0 | |
| 5/15 | 0629 | 36 | + | 0,0 | 0 | 0 | 0,0 | 0,0 | 0,0 | 0 | 13 |
| 5/15 | 0653 | 37 | – | 0,0 | 0 | 0 | 0,0 | 0,0 | 0,0 | 0 | 14 |
| 5/15 | 1058 | 38 | + | 20,20 | 20 | 20 | 20,30 | 20,30 | 30,30 | 0 | 15 |
| 5/15 | 1205 | 39 | – | 20,20 | 20 | 20 | 20,30 | 20,30 | 30,30 | 0 | 16 |
| 5/15 | 1431 | 40 | + | 40,40 | 40 | 40 | 40,30 | 40,30 | 30,30 | 0 | 17 |
| 5/15 | 1449 | 41 | | 40,40 | 40 | 40 | 40,30 | 40,30 | 30,30 | 0 | |
| 5/16 | | 42 | | | | | | | | | 18 |
| 5/16 | 0907 | 43 | + | 60,60 | 60 | 60 | 60,60 | 60,60 | 50,60 | 0 | 19 |
| 5/16 | 0922 | 44 | – | 60,60 | 60 | 60 | 60,60 | 60,60 | 50,60 | 0 | |
| 5/16 | 1119 | 45 | + | 80,80 | 80 | 80 | 80,90 | 80,90 | 70,90 | 0 | 20 |
| 5/16 | 1134 | 46 | – | 80,80 | 80 | 80 | 80,90 | 80,90 | 70,90 | 0 | 21 |
| 5/16 | 1417 | 47 | + | 80,80 | 80 | 80 | 80,90 | 80,90 | 90,90 | 0 | 22 |
| 5/16 | 1431 | 48 | – | 80,80 | 80 | 80 | 80,90 | 80,90 | 90,90 | 0 | 23 |

*Table C4. Notes for BAYEX14 target configuration 1. The signal amplitudes for the LF and HF sources were 0.5 and 1.0 $V_{rms}$, respectively. Angles listed in black are for 180º symmetric targets, while red indicates targets with 360º of symmetry. The tower faceplate was set to a 10º depression angle. All sequences contain 1680 pings except sequence 2, which contains only 20 pings.*

1. All targets originally deployed along the C-line (see Table C3, sequence 20) were moved to the 10-m line. This line is shown in Fig. B1 as the B-line, but for target configurations 1 and 2 the 10-m line is labeled as the "A-line" in Tables C2 and C3. Small targets are partially buried.
2. Small targets pushed into mud. Exact depth unknown.
3. Channels 7–12 of the low-frequency receiving array have an 18 dB gain setting.
4. The gain has been reset to 12 dB on channels 7–12. No motion. Acoustic test only. Divers later discovered that target 12 was at 80º (nose-to-rail).
5. Spherical float, which was above H2 in Fig. B1, was moved to the east edge of field on H-line (above A6). Big targets were not rotating. Target 2 is being rotated through the same angles as 180º symmetric targets. Divers later discovered that target 12 was at 80º.

6. Target 12 still has an 80º rotation.
7. Target 2 exposed 5–8 cm. Targets 16 and 17 were buried 20.3 cm. Target 6 was buried 17.8 cm. Target 29 was deeply buried by ~20–25 cm. Target 13 was flush buried. All other targets were buried to some indeterminate depth.
8. Divers could not locate target 29, so it remained at –60º. All other targets were completely buried with their top approximately level with the mud/water interface.
9. Target 29 still at –60º.
10. Target 29 was located and rotated to –20º. Bottom edge on the east end of target 7 was 7.62 cm above the hard layer while the bottom edge on the west end of target 7 is 27.9 cm above hard layer.
11. Target 29 was rotated to –20º.
12. Targets 1 and 31 moved to a broadside orientation. Target 32 moved more towards center of box. Target 7 moved 60–100 cm towards the R/V Sharp. It was leveled and set in a broadside orientation. Targets 3 and 27 were not move as the divers found the targets were already nearly broadside
13. Dive boat arrived towards the end of the run. The tower did not reach $X_{max}$ and was found to be ~5 cm short. Divers report target 29 appeared to be nose-down slightly.
14. Target 29 nose down slightly.
15. Tower was fighting strong water current. The run ended a little more than 60 cm short of $X_{max}$. Targets 31, 32, 7, 1, 3, 27 rotated blindly by ~30º. HF SAS images provided estimates of 5º, 20º, 28º, 25º, and 28º for targets 31, 1, 3, 6, and 7, respectively. HF sources used in bistatic scattering measurements from the mud were rotated up to 15º by divers during target manipulations.
16. No problems with tower movement.
17. Tower did not reach $X_{max}$ (11 cm from end). Targets 31, 32, 7, 1, 3, and 27 not rotated and have the same nominal angle as before.
18. Ambient noise recording. No transmission
19. Tower made it all the way to $X_{max}$. Big targets (31, 32, 1, 3, 27) rotated blindly by an additional 30º. Target 7 rotated by about 20º (should be at 50º now). HF SAS images provided estimates of 25º, 40º, and 50º for targets 31, 1, and 3, respectively. LF SAS image gave a very rough estimate of 6º rotation for target 7.
20. Big targets (31, 32, 1, 3, 27) have tails away from the ship. Target 7 is nominally at 70º. LF SAS image gave a very rough estimate of 60º for target 7.
21. Tower did not reach home 5–10 cm short of end of rail.
22. TC-4013 hydrophone was place by the HF source. The F41 hydrophone was placed in a lower position. Target 7 moved to 90º; all other targets were left as-is.
23. LF source stopped transmitted at ping 792 and started transmitting again at 1000.

| Date | Time | Seq. | Dir | 10 m (deg) | 20 m (deg) | 25 m (deg) | 30 m (deg) | 35 m (deg) | 40 m (deg) | 45 m (deg) | Note |
|---|---|---|---|---|---|---|---|---|---|---|---|
| 5/17 | 1115 | 76 | + | –80,100 | –80 | –80 | –80,120 | –80,120 | –80,120 | 0 | 1 |
| 5/17 | 1130 | 77 | – | –80,100 | –80 | –80 | –80,120 | –80,120 | –80,120 | 0 | 2 |
| 5/17 | 1634 | 78 | + | –60,120 | –60 | –60 | –60,150 | –60,150 | –60,150 | 0 | 3 |
| 5/17 | 1649 | 79 | – | –60,120 | –60 | –60 | –60,150 | –60,150 | –60,150 | 0 | |
| 5/18 | 0707 | 131 | + | –60,120 | –60 | –60 | –60,150 | –60,150 | –60,150 | 0 | 4 |
| 5/18 | 0721 | 132 | – | –60,120 | –60 | –60 | –60,150 | –60,150 | –60,150 | 0 | |
| 5/18 | 0914 | 133 | + | –40, 140 | –40 | –40 | –40, 150 | –40, 150 | –40,150 | 0 | 5 |
| 5/18 | 0928 | 134 | – | –40, 140 | –40 | –40 | –40, 150 | –40, 150 | –40, 150 | 0 | 6 |
| 5/18 | 1102 | 135 | | –20, 160 | –20 | –20 | –20, 180 | –20, 180 | –20, 180 | 0 | 7 |
| 5/18 | 1104 | 136 | + | –20, 160 | –20 | –20 | –20, 180 | –20, 180 | –20, 180 | 0 | 8 |
| 5/18 | 1118 | 137 | – | –20, 160 | –20 | –20 | –20, 180 | –20, 180 | –20, 180 | 0 | |
| 5/18 | 1608 | 138 | + | 0, 180 | 0 | 0 | 0, 210 | 0, 210 | 0, 210 | 0 | 9 |
| 5/18 | 1622 | 139 | – | 0, 180 | 0 | 0 | 0, 210 | 0, 210 | 0, 210 | 0 | |
| 5/19 | 0909 | 190 | + | 20, 200 | 20 | 20 | 20, 240 | 20, 240 | 20, 240 | 0 | 10 |
| 5/19 | 0924 | 191 | – | 20, 200 | 20 | 20 | 40, 240 | 20, 240 | 20, 240 | 0 | 11 |
| 5/19 | 1106 | 192 | | 40, 220 | 40 | 40 | 40, 270 | 40, 270 | 40, 270 | 0 | 7 |
| 5/19 | 1107 | 193 | | 40, 220 | 40 | 40 | 40, 270 | 40, 270 | 40, 270 | 0 | 7 |
| 5/19 | 1108 | 194 | | 40, 220 | 40 | 40 | 40, 270 | 40, 270 | 40, 270 | 0 | 7 |
| 5/19 | 1109 | 195 | + | 40, 220 | 40 | 40 | 40, 270 | 40, 270 | 40, 270 | 0 | 12 |
| 5/19 | 1124 | 196 | – | 40, 220 | 40 | 40 | 40, 270 | 40, 270 | 40, 270 | 0 | |
| 5/19 | 1400 | 197 | | | | | | | | | |
| 5/19 | 1401 | 198 | + | 60, 240 | 60 | 60 | 60, 300 | 60, 300 | 60, 300 | 0 | 13 |
| 5/19 | 1415 | 199 | – | 60, 240 | 60 | 60 | 60, 300 | 60, 300 | 60, 300 | 0 | 14 |
| 5/19 | 1603 | 200 | + | 80, 260 | 80 | 80 | 80, 330 | 80, 330 | 80, 330 | 0 | 15 |
| 5/19 | 1618 | 201 | – | 80, 260 | 80 | 80 | 80, 330 | 80, 330 | 80, 330 | 0 | |
| 5/20 | 0906 | 252 | + | 80, 260 | 80 | 80 | 80, 330 | 80, 330 | 80, 330 | 0 | 16 |
| 5/20 | 0922 | 253 | – | 80, 260 | 80 | 80 | 80, 330 | 80, 330 | 80, 330 | 0 | |
| 5/20 | 1654 | 304 | + | | 0 | | | | | 0 | 17 |
| 5/20 | 1710 | 305 | – | | 0 | | | | | 0 | 18 |
| 5/21 | 1802 | 356 | – | | 0,0 | | | | | 0 | 17 |

*Table C5. Notes for BAYEX14 target configuration 2. The signal amplitudes for the LF and HF sources were 0.5 and 1.0 $V_{rms}$, respectively. Angles listed in black are for 180º symmetric targets; while red indicates targets with 360º of symmetry. The tower faceplate was set to a 10º depression angle except for sequences 304, 305, and 356 where the angle is 5º. All sequences contain 1680 pings except sequences 135, 192–194, and 197, which contains only 20 pings.*

1. Target 2 was erroneously at –80º. It should have been at 100º. Target 7 was at ~20º. Targets 30 and 21 where aligned by eye. Data shows these targets were at –60º. HF SAS images reveal that targets 31, 1, and 3 were at 110º, 115º, and 121º, respectively.
2. Tower did not reach home. It stopped 10 to 15 cm short.
3. Target 2 now at 120º (nose towards rail). Target 7 is nominally at 40º. Targets 30 and 21 are at –80º. HF SAS images reveal targets 31, 1, 3, and 7 are at 145º, 145º, 139º, and 43º.
4. Targets were not manipulated before data collection, so same orientations as previous night.

5. The F41 is in the lower position with a 0º depression angle. Small targets pushed down a little further into mud. Mud smoothed over top of targets and any craters were filled. Targets 21 and 30 are now tracking the planned rotations at –40º.
6. Transmission stopped at ping 150 and started again at ping 260, then stopped transmitting at ping 710 and again restarted at ping 860.
7. Stationary test of acoustics, no movement.
8. Targets 31, 32, 1, 3, and 27 were rotated blindly and should have been broadside with tails pointing east (180º). Target 7 was at ~60º. HF SAS images showed that target 31, 1, 7, and 3 have 180º, 180º, 70º, and 200º orientations. Divers observed that target 27 and 32 were at 195º and 190º, respectively.
9. Targets 31, 32, 1, 27 were rotated by ~30º. Target 3 was rotated back to broadside with its tail east (180º). Target 7 was rotated back to ~55º.
10. Targets 31, 32, 1, and 27 were rotated by ~30º to bring them to 240º. Target 3 was rotated by ~60º to bring it to 240º. Target 7 was rotated to end-on.
11. MatLab crashed. Transmission stopped at ping 400, resumed at ping 535, stopped at ping 600, and then resumed at ping 725.
12. Target 31, 32, 1, 27, and 3 were turned to have their tails to rail. Target 7 was broadside.
13. Tower stopped short of $X_{max}$ by 2 to 3cm. Divers report targets on D-line did not have to be rotated by much. Target 6 was not touched. LF SAS images later revealed target 6 was at 45º. Target 16 may be at 40º, but hard to tell from data. Target 7 left at broadside and sand was flattened around it.
14. Tower stopped short of end by 1 m.
15. Target 7 placed broadside at an oblique angle with respect to the mud/water interface. East end completely out of mud with its face exactly proud on interface. West end completely buried in mud, with its top edge just under the interface.
16. Target 2 moved to 100º (nose-to-rail). Target 6 moved to 60º. All other targets in same position as last night. Measurement on target 7 showed west end 7.62 cm exposed and east end 27.9 cm exposed.
17. Sphere at west end of target field and 50 m from rail. Target 7 is at the east end and placed at a 50 m horizontal range. Target 1 and 17 were placed at D1 and D3, respectively. Data were collected for 100 ms on channel 32 of STMS-2.
18. Data collected only on the LF receiving array.

| Date | Time | Seq. | Dir. | $V_{rms}$ | 5 m (deg) | 10 m (deg) | 20 m (deg) | Angle | Note |
|---|---|---|---|---|---|---|---|---|---|
| 5/22 | 1139 | 357 | + | 0.25/1.0 | | | 0,~0 | 15 | 1,2 |
| 5/22 | 1213 | 358 | – | 0.25/1.0 | | | 0,~0 | 35 | 1 |
| 5/22 | 1637 | 359 | + | 0.5/1.0 | –80 | –80 | 0,0 | 35 | 3 |
| 5/22 | 1705 | 360 | – | 0.5/1.0 | –80 | –80 | 0,0 | 15 | |
| 5/23 | 0742 | 361 | + | 0.25/0.5 | –80 | –80 | 0,0 | 35 | |
| 5/23 | 0757 | 362 | – | 0.125/0.5 | –80 | –80 | 0,0 | 35 | |
| 5/23 | 1000 | 363 | + | 0.125/0.25 | –60 | –60 | 0,30 | 35 | 4 |
| 5/23 | 1029 | 364 | – | 0.5/1.0 | –60 | –60 | 0,30 | 15 | |
| 5/23 | 1142 | 365 | + | 0.5/1.0 | –40 | –40 | 0,60 | 15 | 5 |
| 5/23 | 1225 | 366 | – | 0.125/0.25 | –40 | –40 | 0,60 | 35 | |
| 5/23 | 1447 | 367 | + | 0.125/0.25 | –20 | –20 | 0,90 | 35 | 6 |
| 5/23 | 1512 | 368 | – | 0.5/1.0 | –20 | –20 | 0,90 | 15 | |
| 5/23 | 1627 | 369 | + | 0.5/1.0 | 0 | 0 | 0,120 | 15 | 7 |
| 5/23 | 1706 | 370 | – | 0.125/0.25 | 0 | 0 | 0,120 | 35 | |
| 5/24 | 0936 | 371 | + | 0.125/0.25 | 20 | 20 | 0,210 | 35 | 8 |
| 5/24 | 1000 | 372 | – | 0.5/1.0 | 20 | 20 | 0,210 | 15 | |
| 5/24 | 1104 | 373 | + | 0.5/1.0 | 40 | 40 | 0,180 | 15 | 9 |
| 5/24 | 1126 | 374 | – | 0.125/0.25 | 40 | 40 | 0,180 | 35 | |
| 5/24 | 1406 | 375 | + | 0.125/0.25 | 60 | 60 | 0,155 | 35 | 10 |
| 5/24 | 1427 | 376 | – | 0.5/1.0 | 60 | 60 | 0,155 | 15 | |
| 5/24 | 1546 | 377 | + | 0.5/1.0 | 80 | 80 | 0,240 | 15 | 11 |
| 5/24 | 1609 | 378 | – | 0.125/0.25 | 80 | 80 | 0,240 | 35 | |

Table C6. *Notes for BAYEX14 target configuration 3. The signal amplitudes for the LF and HF sources are given in the column labeled $V_{rms}$. Angles listed in black are for 180º symmetric targets; while red indicates targets with 360º of symmetry. All sequences contain 1680 pings.*

1. Target located at the 45-m line.
2. D-line populated according to Table C1 with targets broadside and tails pointing west. B-line was populated, but targets were not aligned. Target 7 at B5 had its west end 27.9 cm exposed and its east end was 11.4 cm exposed. Spherical float placed on the A-line between A5 and A6.
3. All targets were aligned. Target 7 at B5 had its west end 27.9 cm exposed and its east end was 11.4 cm exposed. Spherical float removed from A5.5. D-line re-aligned to broadside (previous runs were slightly off).
4. Target 7 oblique angle changed. West end completely out of mud with bottom edge 15.2 cm above mud/water interface. East end exactly flush buried. HF SAS image showed that targets 1 and 31 on the D-line were oriented at 30º and 28º.
5. Target 7 oblique angle changed. Measurement on dive revealed that the west end was completely out of mud with its bottom edge 17.8 cm above the mud/water interface. Top edge of east end was 5.2 cm below the mud/water interface. HF SAS image showed that targets 1 and 31 were now at 57 º and 44º, respectively.

6. Target 7 picked up and moved slightly west, then placed down level on mud and broadside to rail.
7. Targets on A-line picked up and moved slightly east of tag-lines to undisturbed mud, then placed down broadside with tails pointing west. Target 7 did not move. D-line rotated to ~120º. This was a blind rotation, so there were errors associated with this rotation. HF SAS images revealed that target 1 and 31 were oriented at137º and 124º.
8. Target 7 at B5 rotated by eye to 20º. This aligned target 7 with other targets on the B-line. HF SAS images found that targets 7, 1, and 31 were rotated to 22º, 201º, and 210º, respectively.
9. Target 7 rotated to ~45 deg. HF SAS images found target 7 at a 42º rotation. Target 28 at A6 is about a meter or more off the target line towards the rail. Targets on the D-line were rotated to broadside tails to the east (180º)
10. Target 7 rotated to ~68 deg. Divers report targets on the A-line and B-line were covered by mud, so the craters have been filled. D-line targets moved back to ~155º. HF SAS images found that target 7, 1, and 31 were rotated to 62º, 145º, and 166º.
11. Target #rotated to 90º. Poor visibility during D-line rotation, targets rotated to ~240º. HF SAS image showed that targets 1 and 31 were at 227º and 222º.

| Date | Time | Seq. | Dir. | TF# | 20 m (deg) | 25 m (deg) | 30 m (deg) | 35 m (deg) | 40 m (deg) | Note |
|---|---|---|---|---|---|---|---|---|---|---|
| 5/25 | 0935 | 379 | + | 4 | 270 | | | | 0 | |
| 5/25 | 0957 | 380 | – | 4 | 270 | | | | 0 | |
| 5/25 | 1044 | 381 | + | 5 | 300 | | | 0 | 0 | |
| 5/25 | 1059 | 382 | – | 5 | 300 | | | 0 | 0 | |
| 5/25 | 1246 | 383 | + | 6 | 330 | | 0 | 0 | | |
| 5/25 | 1300 | 384 | – | 6 | 330 | | 0 | 0 | | |
| 5/25 | 1455 | 385 | + | 7 | 115,245 | | 0 | | | 1 |
| 5/25 | 1510 | 386 | – | 7 | 115,245 | | 0 | | | |
| 5/25 | 1615 | 387 | + | 8 | | 0 | | | | |
| 5/25 | 1629 | 388 | – | 8 | | 0 | | | | |
| 5/26 | 0912 | 389 | + | 9 | 0 | | | | | 2 |
| 5/26 | 1013 | 390 | – | 9 | 0 | | | | | 3 |

Table C7. *Notes for special target configurations 4–9 during BAYEX14. The amplitudes of the LF and HF sources were 0.5 and 1.0 $V_{rms}$. The faceplate of the APL-UW was set to a 10º depression angle. Each sequence contains 1680 pings except as stated in Note 3.*

1. Clean-up run to get two missing angles on D-line. Target 1 was set 115º and target 31 was set to 245º. Targets 32 and 27 were not rotated.
2. Sediment attenuation measurement using the PASS apparatus occurred during this time.
3. Missed the first 20 seconds of pings after motor started moving the tower along the rail.

| Date | Time | Seq. # | Dir. | TF# | 5 m (deg) | 10 m (deg) | Angle (deg) |
|---|---|---|---|---|---|---|---|
| 5/26 | 1153 | 391 | + | 10 | | 0 | 20 |
| 5/26 | 1208 | 392 | – | 10 | | 0 | 20 |
| 5/26 | 1341 | 393 | + | 11 | 0 | | 35 |
| 5/26 | 1355 | 393 | – | 11 | 0 | | 35 |

Table C8. *Notes for special target configurations 10 and 11 during BAYEX14. The amplitudes of the LF and HF sources sources were 0.125 and 0.25 $V_{rms}$. Each sequence contains 1680 ping. The IMP was located on the C-line (at 15 m horizontal). IMP is an apparatus used for the measurement of interface roughness and sediment conductivity.*